NUMERICAL AND ANALYTICAL INVESTIGATION OF AEROSOL ACOUSTICS THROUGH DUCTS

A THESIS SUBMITTED TO
THE GRADUATE SCHOOL OF NATURAL AND APPLIED SCIENCES
OF
MIDDLE EAST TECHNICAL UNIVERSITY

BY

ERSEN ARSLAN

IN PARTIAL FULFILMENT OF THE REQUIREMENTS
FOR
THE DEGREE OF DOCTOR OF PHILOSOPHY
IN
MECHANICAL ENGINEERING

JUNE 2017

Approval of the thesis:

NUMERICAL AND ANALYTICAL INVESTIGATION OF AEROSOL ACOUSTICS THROUGH DUCTS

submitted by **ERSEN ARSLAN** in partial fulfillment of the requirements for the degree of **Doctor of Philosophy in Mechanical Engineering Department, Middle East Technical University** by,

Prof. Dr. Gülbin Dural Ünver _____
Dean, Graduate School of **Natural and Applied Sciences**

Prof. Dr. R. Tuna Balkan _____
Head of Department, **Mechanical Engineering**

Prof. Dr. Mehmet Çalışkan _____
Supervisor, **Mechanical Engineering Dept., METU**

Examining Committee Members:

Assoc. Prof. Dr. Yiğit Yazıcıoğlu _____
Mechanical Engineering Dept., METU

Prof. Dr. Mehmet Çalışkan _____
Mechanical Engineering Dept., METU

Prof. Dr. Yusuf Özyörük _____
Aerospace Engineering Dept., METU

Assoc. Prof. Dr. Selin Aradağ _____
Mechanical Engineering Dept., TOBB ETU

Assist. Prof. Dr. Bülent Özer _____
Mechanical Engineering Dept., TOBB ETU

Date: 19.06.2017

I hereby declare that all information in this document has been obtained and presented in accordance with academic rules and ethical conduct. I also declare that, as required by these rules and conduct, I have fully cited and referenced all material and results that are not original to this work.

Name, Last Name : Ersen ARSLAN

Signature :

ABSTRACT

NUMERICAL AND ANALYTICAL INVESTIGATION OF AEROSOL ACOUSTICS THROUGH DUCTS

Arslan, Ersen

Ph.D., Department of Mechanical Engineering
Supervisor: Prof. Dr. Mehmet Çalışkan

June 2017, 188 pages

The aim of this thesis is to develop a numerical approach which can solve the sound propagation problem in air-filled circular duct containing water droplets (regarded as an aerosol) in order to obtain acoustic absorption and dispersion characteristics of the system. There exist several analytical approaches in literature for treatment of basic aerosol problems with certain limitations; however; in order to solve rather complex cases, these limitations must be handled and worked out. In this study, a coupled phase approach is chosen due to its superiority for aerosol acoustics among others. The developed codes in 1-D and 3-D (axisymmetric) forms are based on finite difference method in frequency domain. Perfectly Matched Layers (PML) equations are adopted for inlet and outlet boundaries. The codes have been validated with the corresponding analytical results, while existing analytical solutions are extended to cover the cases of mean flow and 3-D (axisymmetric) cases.

Results of 1-D solutions have shown that the effect of finite mass loading on attenuation is not linearly proportional. Furthermore; the effect of mean flow has relatively different behavior on attenuation with respect to concentration level and flow direction. The dependency of dispersion on the mean flow and the concentration

level is not similar for all frequencies. On the other hand, the 3-D solution has been analyzed for higher order duct modes and impedance wall conditions, emphasizing on the discrepancies between 1-D cases. Last but not the least, 3-D results show that aerosol parameters interestingly have significant effect on the cut-off frequencies of the duct.

Keywords: Aerosol Acoustics, Finite Difference Method in Frequency Domain (FDFD), Duct Acoustics, Perfectly Matched Layers (PML)

ÖZ

KANALLARDAKİ AEROSOL AKUSTİĞİNİN SAYISAL VE ANALİTİK İNCELENMESİ

Arslan, Ersen

Doktora, Makine Mühendisliği Bölümü
Tez Yöneticisi: Prof. Dr. Mehmet Çalışkan

Haziran 2017, 188 sayfa

Bu tezin amacı, içinde hava ve su damlacıkları (aerosol olarak nitelenen) olan silindirik kesitli bir kanaldaki ses yayılım problemini, sistemin akustik sönümleme ve saçınım parametrelerini bulmak amacı ile çözebilecek sayısal bir kod geliştirmektir. Literatürde temel aerosol problemlerinin sınırlı çözümleri için çeşitli analitik yaklaşımlar mevcuttur; fakat daha karmaşık problemleri çözmek için bu sınırlamaların kaldırılması gerekir. Bu çalışmada, çift fazlı yaklaşım aerosol akustiğindeki üstünlüğünü sebebiyle diğerleri arasından referans teori olarak seçilmiştir. Bu tez kapsamında geliştirilmiş olan 1-B ve 3-B (eksenel simetrik) kodlar, frekans uzayında sonlu farklar yöntemine dayanmaktadır ve *Perfectly Matched Layers* (PML) denklemleri giriş ve çıkış sınırlarını tanımlamak için kullanılmıştır. Kodlar, ilgili analitik sonuçlar ile doğrulanırken mevcut teorik çözümler, ortalama akış ve 3-B (eksenel simetrik) durumları için genişletilmiştir.

1-B çözümlerinin sonuçlarına göre sonlu kütle yüklemesinin sönümleme üzerindeki etkisi doğrusal ilişkili değildir. Dahası; ortalama akışın etkisi, konsantrasyon

seviyesine ve akış yönüne göre sönümleme üzerinde nispeten farklı davranışlara sahiptir ve akustik dağılımın (*dispersion*) ortalama akış ve konsantrasyon seviyesine bağımlılığı, tüm frekanslar için benzer değildir. Öte yandan 3-B çözüm, 1-B karşılıkları ile aralarındaki farklılıklar vurgulanarak yüksek dereceli kanal modları ve empedans duvar koşulları için analiz edilmiştir. Son olarak, 3-B sonuçlar aerosol parametrelerinin kanalın kesme (*cut-off*) frekansları üzerinde ilginç bir şekilde önemli etkiye sahip olduğunu göstermektedir.

Anahtar kelimeler: Aerosol Akustiği, Frekans Uzayında Sonlu Farklar Yöntemi, Kanal Akustiği, Mükemmel Eşleşen Katmanlar (PML)

To My Beautiful Family.

ACKNOWLEDGEMENTS

Firstly, I would like to express my sincere thanks and appreciation to my supervisor Dr. Mehmet Çalışkan for his guidance, support, empathy and encouragement. I must admit that his wide perspective and huge experience on any kind of problem is impressive and he is my idol for many aspects.

I would also like to express my sincere appreciation to Dr. Yusuf Özyörük, for his priceless contributions and supports in this thesis.

I want to thank Dr. Yiğit Yazıcıoğlu for his supportive advices and criticism as a member of my thesis advisory committee.

I would like to extend my gratitude to my company, FİGES. Dr. Tarık Öğüt deserves a special thanks for his sincere support.

I want to express my special thanks to my parents Hatice Arslan and Nuri Arslan and my brother Eren Arslan for their everlasting support and confidence in me. Indeed, without my mum Hatice Arslan's moral support, I could not even make it. I also want to thank Baydar and Çil family for all their help and understanding.

Last but not least, but most important of all, I owe my deepest gratitude to my beloved wife Elçin. Thanks to her being in my life, this success has become much more meaningful.

TABLE OF CONTENTS

ABSTRACT v

ÖZ vii

ACKNOWLEDGEMENTS x

TABLE OF CONTENTS xi

LIST OF TABLES xv

LIST OF FIGURES xvi

LIST OF SYMBOLS AND ABBREVIATIONS xxiv

CHAPTERS

1 INTRODUCTION 1

1.1 Introduction 1

1.2 Motivation 2

1.2.1 Noise Suppression with Aerosols 3

1.2.2 Acoustic Agglomeration of Aerosols 7

1.2.3 Particle Characterization 8

1.3 Scope, Objective and Contribution of Work 8

1.4 Outline of the Dissertation 9

2 LITERATURE SURVEY 11

2.1 History and Evolution of Suspension Acoustics 11

2.2 Literature Survey on Application Areas 21

2.2.1 Acoustic Agglomeration 21

2.2.2 Jet Noise Suppression 23
2.2.3 Suspension Characterizations 25
2.3 Summary and Discussions 26
3 COUPLED PHASE THEORY 29
3.1 Introduction to Coupled-Phase Model 29
3.2 Preliminaries of the Theory 31
3.2.1 Concentration Parameters 31
3.2.2 Force Acting on a Spherical Particle 33
3.2.3 Heat Transfer to a Spherical Particle 37
3.3 Conservation Equations 39
3.3.1 Conservation of Mass 39
3.3.2 Conservation of Linear Momentum 41
3.3.3 Conservation of Energy 43
3.3.4 Equation of State 44
3.4 System of Equations 46
3.4.1 Sound Propagation with Only Momentum Exchange 46
3.4.2 Sound Propagation with Momentum and Heat Exchange 51
3.5 Summary and Comments 56
4 ONE DIMENSIONAL SOLUTIONS 59
4.1 Numerical Approach 59
4.1.1 Model Development 59
4.1.2 Governing Equations 62
4.1.3 Boundary Conditions and Acoustic Source Definitions 65
4.1.4 Numerical Schemes 68
4.1.5 Verification of the Code 69

4.2 Extensions to the Theoretical Solution for Mean Flow 75
4.2.1 Sound Propagation with Momentum Exchange under Mean Flow . 75
4.2.2 Sound Propagation with Momentum and Thermal Exchange under Mean Flow 77
5 ONE DIMENSIONAL RESULTS AND COMPARISONS..... 79
5.1 Sound Propagation with Only Momentum Exchange..... 81
5.1.1 Comparisons with Analytical Results 81
5.1.2 Additional Numerical Results 84
5.2 Sound Propagation with Only Heat Exchange..... 88
5.3 Sound Propagation with Only Momentum Exchange under Mean Flow 90
5.4 Sound Propagation with Momentum and Heat Exchange under Mean Flow 94
5.5 Summary 98
6 THREE DIMENSIONAL (AXISYMMETRIC) SOLUTIONS..... 101
6.1 Numerical Approach 101
6.1.1 Model Development..... 101
6.1.2 Governing Equations..... 105
6.1.3 Boundary Conditions and Acoustic Source Definitions 109
6.1.4 Numerical Scheme 114
6.2 Extension of the 1-D Analytical Solution to 3-D..... 124
7 THREE DIMENSIONAL (AXISYMMETRIC) RESULTS AND COMPARISONS 133
7.1 Hard Boundary..... 133
7.1.1 Comparisons with Analytical Results 133
7.1.2 Additional Results..... 142

7.2 Impedance Boundary 147
7.2.1 Comparisons with a Commercial Code: Purely Air 147
7.2.2 Aerosol Medium: Water Droplets in an Air 151
7.3 Summary 155
8 SUMMARY AND CONCLUSION 157
8.1 Summary 157
8.1.1 One Dimensional Results 158
8.1.2 Three Dimensional Results 160
8.2 Conclusions 161
8.3 Recommendations for future work 165
REFERENCES 167
APPENDICES
A. MATERIAL PROPERTIES 177
B. SOLUTION OF WAVE EQUATION IN CIRCULAR DUCTS 179
C. ACOUSTIC MODEL DEFINITIONS IN ANSYS MECHANICAL 183
CURRICULUM VITAE 187

LIST OF TABLES

TABLES

Table 1.1 Maximum pass-by noise limits set by RCD 94/25/EC 6

Table 4.1 Finite difference coefficients used for 1-D spatial discretization 69

Table 5.1 System parameters used in the numerical solution. 81

Table 5.2 System parameters used in the numerical solution with mean flow. 90

Table 5.3 The effects of the system parameters on attenuation 99

Table 5.4 The effects of the system parameters on dispersion 99

Table 6.1 Hard wall boundary conditions on the axis and on the wall. 111

Table 6.2 Weighting coefficients for axial derivative terms of finite difference scheme. 115

Table 6.3 Weighting coefficients for radial derivative terms of finite difference scheme. 115

Table 7.1 Impedance boundary conditions on the wall..... 148

Table 7.2 Attenuation per meter for different media and boundary conditions.. 155

LIST OF FIGURES

FIGURES

Figure 1.1 Example of a wet type exhaust system(Axces) [47] 4

Figure 1.2 Representation of sound propagation problem in duct filled with air and water droplets 5

Figure 1.3 Schematic view of acoustic agglomeration. 7

Figure 2.1. Measurement results of Knudsen et al.: Decay curves in a reverberation chamber for a frequency of 6,000 Hz, with no fog in the room (upper curve), and with a fairly dense artificial fog in the room (lower curve). [6] 12

Figure.2.2 Attenuation(left) and dispersion (right) results of coupled phase theory and measurements of Temkin and Dobbins's. [13] 15

Figure 2.3 Schematic diagram of the cloud chamber and the optical system used by Cole and Dobbins. [19] 16

Figure 2.4 High-frequency (10 kHz) acoustic agglomeration of a trimodal aerosol.[53] 22

Figure 2.5 Influence of sound frequency on agglomeration.[60] 23

Figure 2.6 Water jet injection to nozzle exit for noise suppression.[44] 24

Figure 2.7 Predicted (Kandula's) and measured (Norum's) SPL reduction values for different mass flow rates.[81] 24

Figure 2.8 Measurement of particle concentration in horizontal, multiphase pipe flow using ultrasonic signals.[83] 25
Figure 3.1 Schematic view of the problem and two phase representation of the control volume. 30
Figure 3.2 Drag coefficient with respect to Reynolds number[100] 34
Figure 3.3 Schematic representation of a flow problem over a spherical particle 36
Figure 3.4 Schematic representation of a heat transfer problem onto a spherical particle 38
Figure 3.5 Attenuation results scaled to mass loading in air with water droplets. 50
Figure 3.6 Attenuation results per wavelength due to viscous and thermal losses scaled to mass loading in air with water droplets. 54
Figure 3.7 Attenuation results per meter due to viscous and thermal losses scaled to mass loading in air with water droplets. 55
Figure 3.8 Dispersion ratio for viscous and thermal effects scaled to unit mass loading in air with water droplets. 56
Figure 4.1 Representation of plane wave propagation in a circular-sectioned duct with full reflective walls. 60
Figure 4.2 Illustration of the numerical problem with PML boundary definitions. 61
Figure 4.3 The illustration of the numerical discretization for 1-D solution. 69
Figure 4.4 Variation of the damping factor σx w.r.t axial distance at f = 500 Hz. 71
Figure 4.5 Comparison of the computed pressure perturbations with exact solution at f = 500 Hz. 72
Figure 4.6 The computed dispersion $co2c\omega 2$ results versus frequency. 72

Figure 4.7 Comparison of the computed pressure perturbations at u_o=100 m/s with exact solution at f = 500 Hz. 73

Figure 4.8 Comparison of the computed pressure perturbations at u_o=-100 m/s with exact solution at f = 500 Hz. 73

Figure 4.9 The computed dispersion $co2c\omega2$ results with respect to frequency, u_o=100 m/s. 74

Figure 4.10 The computed dispersion $co2c\omega2$ results with respect to frequency, u_o=-100 m/s. 75

Figure 5.1 Representation of the 1-D problem and the definition of the incident acoustic wave. 79

Figure 5.2 Variation of the damping factor σx for calculations 80

Figure 5.3 Comparison of the computed scaled attenuation $\alpha = \alpha\, co\omega$ with theoretical (analytical) solution which is valid for low mass loading σm solid line is the theoretical (analytical) and dashed line is the numerical. 82

Figure 5.4 Comparison of the computed scaled attenuation $\alpha = \alpha\, co\omega$ with theoretical (analytical) solution which is valid for finite mass loading σm, solid line is the theoretical (analytical) and dashed with line is the numerical. 82

Figure 5.5 Comparison of the computed dispersion $co2c\omega2$with theoretical (analytical) solution which is valid for low mass loading σm, solid line is the theoretical (analytical) and dashed with line is the numerical. 83

Figure 5.6 Acoustic pressure amplitudes for particle volume concentration levels of 0.001%, 0.01% and 0.1%. 85

Figure 5.7 Acoustic pressure levels in dB scale for particle volume concentration levels of 0.001%, 0.01% and 0.1%..... 85

Figure 5.8 Acoustic pressure levels in dB scale for particle size of 1μm, 2μm, 4μm, 8μm and 16μm, at frequency of 1,000 Hz..... 86

Figure 5.9 Attenuation per meter versus frequency for particle size of 2μm, 4μm, 8μm and 16μm 87

Figure 5.10 Scaled attenuation $\alpha = \alpha co\omega$ versus frequency for particle size of 2μm, 4μm, 8μm and 16μm. 87

Figure 5.11 Comparison of the computed scaled attenuation $\alpha = \alpha co\omega$ with theoretical (analytical) solution which is valid for low mass loading σm, solid line is the theoretical and dashed with line is the numerical. 89

Figure 5.12 Comparison of the computed dispersion $\alpha = \alpha co\omega$ with theoretical (analytical) solution which is valid for low mass loading σm solid line is the theoretical and dashed with line is the numerical..... 90

Figure 5.13 Numerical and analytical attenuation for three different volume concentration levels. 91

Figure 5.14 Numerical and analytical scaled attenuation $\alpha = \alpha co\omega$ for three different volume concentration levels. 92

Figure 5.15 Analytically obtained scaled attenuations, parameter sets of M=0, M=0.1 and M=-0.1 for three different concentration level. 93

Figure 5.16 Numerical and analytical dispersion ratio $co\ 2c\omega 2$ for three different volume concentration levels. 94

Figure 5.17 Numerical and analytical attenuation for three different volume concentration levels. 95

Figure 5.18 Numerical and analytical scaled attenuation $\alpha = \alpha co\omega$ for three different volume concentration levels. 96

Figure 5.19 Analytically obtained scaled attenuations, parameter sets of M=0, M=0.1 and M=-0.1 for three different concentration level. 97

Figure 5.20 Numerical and analytical dispersion $co\ 2c\omega 2$ for three different volume concentration levels. 98

Figure 6.1 Representation of the axisymmetric problem 102

Figure 6.2 Acoustic duct modes and the corresponding wavenumbers of a circular duct 104

Figure 6.3 Bessel functions of the first kind for m=0, 1, 2, 3, 4. 105

Figure 6.4 Discretized domain and the bottom left stencil for 4th order finite difference scheme. 114

Figure 6.5 Mode number (0, 0) – acoustic pressure plot (f_{ax}=1,500 Hz). 116

Figure 6.6 Comparison of the pressure perturbations for mode number (0, 0), f_{ax}=1,500 Hz. 117

Figure 6.7 Mode number (1, 0) – acoustic pressure plot (f_{ax}=1,500 Hz). 118

Figure 6.8 Comparison of the pressure perturbations for mode number (1, 0), f_{ax}=1,500 Hz. 118

Figure 6.9 Mode number (0, 1) – acoustic pressure plot (f_{ax} =1,500 Hz). 119

Figure 6.10 Comparison of the pressure perturbations for mode number (0, 1), f_{ax} =1,500 Hz. 120

Figure 6.11 Mode (1, 1) – acoustic pressure plot (f_{ax}=1,500 Hz). 120

Figure 6.12 Comparison of the pressure perturbations for mode number (1, 1), f_{ax}=1,500 Hz. 121

Figure 6.13 Mode number (2, 0) – acoustic pressure plot (f_{ax} =1,500 Hz). 122

Figure 6.14 Comparison of the pressure perturbations for mode number (0, 2), f_{ax} =1,500 Hz. 122

Figure 6.15 Mode number (0, 2) – acoustic pressure plot (f_{ax} =1,500 Hz). 123

Figure 6.16 Comparison of the pressure perturbations for mode number (0, 2), f_{ax} =1,500 Hz. 123

Figure 6.17 Modified wave number versus reference wave number in axial direction for three different volume concentrations: Duct mode (1, 0). 127

Figure 6.18 Modified wave number versus reference wave number in axial direction for three different volume concentrations: Duct mode (0, 1). 128

Figure 6.19 Modified wave number versus reference wave number in axial direction for three different volume concentrations: Duct mode (1, 1). 128

Figure 6.20 Modified wave number versus reference wave number in axial direction for three different particle size: Duct mode (1, 0). 129

Figure 6.21 Modified wave number versus reference wave number in axial direction for three different particle sizes: Duct mode (0, 1). 130

Figure 6.22 Modified wave number versus reference wave number in axial direction for three different particle sizes: Duct mode (1, 1). 130

Figure 7.1 Analytical and numerical attenuation results of mode (0, 0). 134

Figure 7.2 Analytical and numerical dispersion results of mode (0, 0). 134

Figure 7.3 Numerical pressure results of mode (0, 0) at 1,000 Hz for volume concentrations: a) 0.001%, b) 0.01% and c) 0.1%. 135
Figure 7.4 Analytical and numerical attenuation results of mode (1, 0). 136
Figure 7.5 Analytical and numerical dispersion results of mode (1, 0). 137
Figure 7.6 Numerical pressure results of mode (1, 0) at 1,000 Hz for volume concentrations: a) 0.001%, b) 0.01% and c) 0.1%. 138
Figure 7.7 Analytical and numerical attenuation results of mode (0, 1). 139
Figure 7.8 Analytical and numerical dispersion results of mode (0, 1). 139
Figure 7.9 Numerical pressure results of mode (0, 1) at 1,000 Hz for volume concentrations: a) 0.001%, b) 0.01% and c) 0.1%. 140
Figure 7.10 Analytical and numerical attenuation results of mode (1, 1). 141
Figure 7.11 Analytical and numerical dispersion results of mode (1, 1). 141
Figure 7.12 Numerical pressure results of mode (1, 1) at 1,000 Hz for volume concentrations: a) 0.001%, b) 0.01% and c) 0.1%. 142
Figure 7.13 The change in the cut-off frequency for different volume concentrations versus axial frequency, linear axis. 144
Figure 7.14 The change in the cut-off frequency for different volume concentrations versus axial frequency, logarithmic axis. 145
Figure 7.15 The change in the cut-off frequency for different particle radius parameters versus axial frequency, linear axis. 146
Figure 7.16 The change in the cut-off frequency for different particle radius parameters versus axial frequency, logarithmic axis. 146
Figure 7.17 Acoustic absorption surface and the location of the incident wave 149

Figure 7.18 Acoustic pressure results in X-R plane of a) ANSYS Mechanical, b) developed code for duct mode (0, 0). 149
Figure 7.19 Acoustic pressure results in X-R plane of a) ANSYS Mechanical, b) developed code, for the duct mode (1, 0). 150
Figure 7.20 Acoustic pressure results in X-R plane of a) ANSYS Mechanical, b) developed code, for the duct mode (0, 1). 150
Figure 7.21 Acoustic pressure results in X-R plane of a) ANSYS Mechanical, b) developed code, for the duct mode (1, 1). 151
Figure 7.22 Acoustic pressure results in X-R plane of the mode (0, 0) with a)α_{su}=0.25, b) α_{su} =0.50 and α_{su} =0.75. 152
Figure 7.23 Acoustic pressure results in X-R plane of the mode (1, 0) with a)α_{su}=0.25, b) α_{su} =0.50 and c) α_{su} =0.75. 153
Figure 7.24 Acoustic pressure results in X-R plane of the mode (0, 1) with a)α_{su}=0.25, b) α_{su} =0.50 and c) α_{su} =0.75. 153
Figure 7.25 Acoustic pressure results in X-R plane of mode (1, 1) with a)α_{su}=0.25, b) α_{su} =0.50 and c) α_{su} =0.75. 154

LIST OF SYMBOLS AND ABBREVIATIONS

RCD Recreational Craft Directive

LEE Linearized Euler Equations

PML Perfectly Matched Layers

NPPW Number of Point per Wavelength

VC Volume Concentration

RHS Right Hand Side

LHS Left Hand Side

a Particle radius

$\bar{a}$ Arithmetic mean of particle radius

N_o Total number of particles in a control volume

ΔV Total volume of the control volume

ΔV_p Total volume of the particles in a control volume

$\emptyset_v$ Particle volume concentration

$\emptyset_m$ Particle mass concentration

σ_m Mass loading

σ_x Damping factor

ρ_{eq} Equivalent suspension density

Re Reynolds number

u_o Mean flow velocity

M Mach number

u	Velocity of flow
u_p	Velocity of particle
u_g	Velocity of gas
ρ	Density of flow
ρ_p	Density of particle
ρ_g	Density of gas
ρ_{go}	Density of gas (static condition)
p	Pressure of flow
p_p	Pressure of particle
p_g	Pressure of particle
μ	Dynamic viscosity of flow
μ_g	Dynamic viscosity of gas
F_n	Normal component of drag force
F_t	Tangential component of drag force
F_D	Stoke's drag force
Q_c	Newtons' heat conduction
m_p	Mass of a single particle
τ_d	Dynamic relaxation time
τ_T	Thermal relaxation time
$\dot{Q}_p$	Heat transfer rate to a single particle
$\dot{Q}_g$	Heat transfer rate to gas
k_g	Thermal conductivity of gas
c_{pp}	Specific heat capacity of particle at constant pressure

c_{pg} Specific heat capacity of gas at constant pressure

c_{vg} Specific heat capacity of gas at constant volume

T_p Temperature of particle

T_g Temperature of gas

E_g Internal energy of gas phase

$\dot{W}_g$ The rate of work done on gas phase

P_{og} Static pressure of gas

c_o Speed of sound

R Thermodynamic gas constant

k Wave number

k_{xmn} Axial wave number of mode(m,n)

k_{rmn} Radial wave number mode(m,n)

α Attenuation per meter

$\bar{\alpha}$ Scaled attenuation

CHAPTER 1

INTRODUCTION

1.1 Introduction

Multi-phase environments which consists of combinations of gas, fluid or solid phases are called suspensions. They can be categorized according to their composition as; aerosols (solid and liquid particles in gas), emulsions (liquid particles in liquid), hydrosols (solid particles in liquids) and bubbly liquids. Generally, host phase is called fluid while minority phase is called particles (even they are bubbles). How an acoustic wave propagates in such media depends on many parameters like particle concentration, particle size, particle rigidity, frequency of interest, etc. in addition to the other physical parameters of the system.

Analysis of the propagation of the acoustic wave in a suspension is important in many aspects and for applications. Some of these can be listed as ; analysis and measurement of cloud and humidity parameters (atmospheric sciences), controlling the parameters of chemical processes (chemical engineering), agglomeration of dust and particles in air (environmental engineering), filtration of particles in fluids (water sciences), ultrasonic imaging in tissues (biomedical engineering), reducing instabilities in combustion chambers (propulsion applications), stealth and exploration (underwater applications), and noise reduction (aerospace and marine applications).

For the last 60 years, several theoretical and experimental studies have been carried out related to suspension acoustics and the corresponding results have

been shared in the literature[1]–[46]. It is necessary to make some simplifying assumptions when examining the acoustics of the suspensions, as in other engineering problems. For example; each phase is supposed to have its own separate volume so that the physical mechanisms are associated with the corresponding parameters of each phase and the total number of the particles must be sufficiently large in a unit element to justify continuum approach. Although these assumptions make things easier, the acoustics of such environments are more complicated than the single-phase environments where the linear acoustic wave equation is valid. One can obtain the attenuation and dispersion characteristics of such media from the developed analytical theories only with additional simplifying assumptions which will be explained in the following chapters. Even though such simplifications yield satisfactory results in the field of atmospheric acoustics, these assumptions must be abandoned as much as possible to meet the new demands coming from industry. This can be achieved through numerical solutions which can account for effects of complex geometries, varying system parameters of finite value, convection effects due to moving environment and some other additional system parameters.

Nevertheless; existing numerical tools of acoustics usually do not provide a sufficient solution when the medium is suspension. Besides; the calculations made indirectly by using Computational Fluid Dynamics (CFD) tools are neither useful in terms of solution time nor they are serving precisely in terms of outputs. Consequently; specialized numerical codes for suspension acoustics are needed to investigate such problems more accurately and widely.

1.2 Motivation

Acoustical investigation of sound propagation in an aerosol is very important in many engineering applications such as noise suppression in wet exhaust systems, acoustic agglomeration of fine particle in exhaust lines, suspension (particle) characterization in flow pipes and thermal-acoustic instability control of

combustion chambers of jets. While most of the related works in those fields are made experimentally, there exists analytical solution methods which can provide quite satisfactory results within the constraint limits of those corresponding theory. However, more advanced solution methods are necessary so as to investigate the acoustic effects of different parameters (geometric, physical, and operational) of the problem specific.

On the other hand, commercial acoustic software packages which are able to solve sound propagation problems by means of wave equation and are commonly based on various numerical methods like finite element, boundary element or statistical energy analysis, do not provide any solution when the sound propagation is in suspension like media (aerosol in this case).

Consequently, it is aimed to develop a numerical method which makes it possible to investigate sound propagation problems in aerosol in detail so that one can consider the effects of problem specific parameters such as mean flow condition, higher order duct modes in the frequency range of interest, or the effect of surface type of the duct (hard or soft wall).

1.2.1 Noise Suppression with Aerosols

The power needs in the naval industry are often achieved through the use of diesel engines. The biggest problems associated with the use of diesel engines are particulate emissions and high level exhaust noise. It is necessary to have an exhaust system to overcome these issues. In addition to safely carry away and filter the byproducts of combustion, another purpose of the exhaust system is to suppress the high levels of exhaust noise resulting in combustions in the engine.

Unlike automotive industry, two types of exhaust systems are used in naval industry; namely, dry type and wet type exhaust systems. Dry type exhaust systems are like the conventional exhaust systems used in the automotive industry. Wet type exhaust systems are called wet because seawater is mixed into the exhaust line [47]. As a result of this application, temperature of the exhaust gas dramatically decreases. And, exhaust noise level gets lower mostly because

the injected water turns into steam which can be regarded as an aerosol with acoustically damping properties. In addition, special mufflers called water locks, which are special for wet type of exhaust systems, are used together with conventional mufflers to further suppress the exhaust noise.



Figure 1.1 Example of a wet type exhaust system(Axces) [47] .

Because of their advantages in terms of temperature and noise reduction, wet-type exhaust systems are preferred in the yacht and marine industries, including war ships (for stealth purposes). However; the design of wet type exhaust systems is still based on general application know-how. There is no engineering calculation method in technical literature, specifically for the acoustic design of such systems and the acoustical effect of the steam in the exhaust system is not clearly known. The scarcity of the existing literature on wet exhaust systems may be due to several reasons: a) The wet type of exhaust system is only used in marine industry together with dry exhaust systems, b) The coupled physics of this system (fluid dynamics, thermodynamics, and acoustics) is rather difficult to study theoretically or numerically. The system manufacturers mostly adopt in principle design–test procedure. c) The noise regulations and standards for marine industry are not stiff and actively controlled as the corresponding ones in automotive industry.

Consequently, it is very important to solve the sound propagation problem in a duct as shown in Figure 1.2 which consists of gas and particles, e.g. water droplets while designing a wet type exhaust system in order to predict the attenuation performance values correctly.

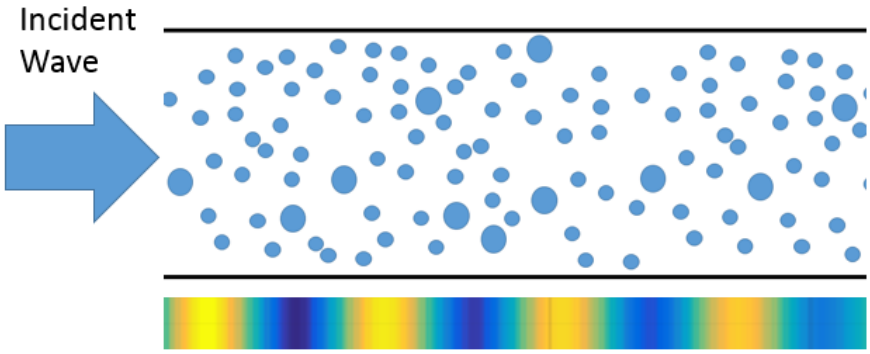


Figure 1.2 Representation of sound propagation problem in duct filled with air and water droplets

1.2.1.1 Limiting Standards on Ship Noise

There have been many concerns over the sailors' noise exposure who spend the majority of their lives on the ships. While the level of loudness may change significantly according to the location of the ship, accommodation spaces are usually subjected to considerably high noise levels. On the other hand; ships in harbors may cause disturbing noise in nearby coastal areas. The increased demand for planning settlements on the coast results in the need for quietness. To address these concerns and needs, some legislative precautions are taken in order to keep the ship noise under control. There are several well-recognized standards, already being enforced in the naval industry. It would be more meaningful to first specify the major sources of external noise from ships before passing on the information about the standards.

The first legislative document is the European directive 94/25/EC, Recreational Craft Directive (RCD). The RCD lays down safety requirements for vessel design and it puts limits on the exhaust and noise emissions that must be met by shipbuilders before they sell their products within the European Union (EU). In addition to safety standards and an exhaust emission standard, the RCD requires that the ships comply with noise emission levels. ISO 14509, titled "Small craft-Measurement of airborne sound emitted by powered recreational craft," is recognized in this directive. According to this directive, pass-by noise tests are made at 25 m. distance from the ship and maximum noise limits are given for some types of ships and engines as listed in Table 1.1 below.

Table 1.1 Maximum pass-by noise limits set by RCD 94/25/EC

Single Engine Power, P_n In kW	**Maximum Sound Pressure Level = L_{pASmax} In dB**
$P_n \leq 10$ kW	67
10 kW < $P_n \leq 40$ kW	72
$P_n > 40$ kW	75

The second widely used standard is referred to as the Model Noise Act (MNA) and is recognized in the United States. In this code there is also a limit on the stationary sound level of ship. The MNA references two noise measurement procedures; namely, SAE J2005 'Stationary Sound Level Measurement Procedure for Pleasure Motorboats' and SAE J1970 'Shoreline Sound Level Measurement Procedure'. The limits on the maximum allowable noise is almost the same as the RCD 94/25/EC.

In addition to these, the International Maritime Organization (IMO) adopted the resolution A.468(XII) which lays out a 'Code on Noise Levels on Board Ships' in order to put maximum noise levels and exposure limits to sailors. Other than these, organizations like NATO, Lloyd's, ABYC have also their own limits and test specifications for ship noise and procedures for exhaust system design.

1.2.2 Acoustic Agglomeration of Aerosols

The possibility of using sound waves to increase the efficiency of the particle filtering in exhaust ducts can be investigated. As an undoubted truth, particulate pollution is very dangerous to human health, and is a key contributor to air pollution. Conventional particle filtering systems have drawbacks in collecting very fine particles in micron sizes. A new methodology called acoustic agglomeration has emerged, in which fine particles are forced to agglomerate and form into comparatively larger particles by means of sound waves (Figure 1.3). This makes it possible to filter those fine particles which are not captured by the conventional particulate filtering systems.

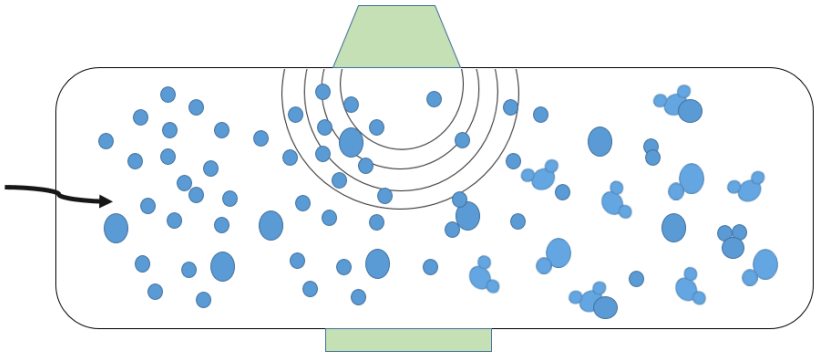


Figure 1.3 Schematic view of acoustic agglomeration.

There are several physical explanations that are supposed to be true in acoustic agglomeration. One of the most pronounced mechanism is the so called orthokinetic effect which tells that the particles with dissimilar dimensions happen to oscillate with different frequencies, phases and amplitudes and cause an increase of probability of collisions. As the size distributions are not expected to be too wide in exhaust systems, there will be an optimum acoustic frequency for agglomeration corresponding to the mean diameter of the particles. Thus, the knowledge of sound propagation in such environment with considering

operational and geometrical effects will be of great value in finding the optimum acoustic frequency for better acoustic agglomeration.

1.2.3 Particle Characterization

The identification of acoustic properties of suspension-like media in terms of the size or concentration of particles have been of interest in numerous applications, such as active control of ingredients in the chemical process and the nuclear power generation industries. Similar to the cases of sonar applications in underwater acoustics or ultrasonic applications in biomedical engineering, by means of the reflected acoustic signal received by sensors, particle parameters can be estimated with inversed methodologies. The idea is to predict particle size and concentration parameters through attenuation and dispersion parameters. The accuracy of this method is highly dependent on the mathematical model which relates the particle parameters with the acoustical outputs. Coupled phase theory, scattering theory and Biot theory are the ones which are adopted for such purposes. As these theories have their own limitations and only applicable to 1-D problems, they do not fulfill the accuracy requirements for problems with complex geometries and operational conditions like background flow. Thus, there is a necessity for an advanced numerical method which can provide a solution with more parameters.

1.3 Scope, Objective and Contribution of Work

In the scope of this thesis, numerical codes have been developed which can solve the problem of propagation of an acoustic wave in a channel filled with an aerosol. Acoustical design principles of wet type exhaust systems in particular are to be established. First of all, taking into consideration the general conditions and parameters in the applications, the numerical approach is designed to have the capability to meet the requirements given below:

- Circular sectional channel geometries are taken into account as the tubes in exhaust systems are circular in cross section,
- The suspension being considered is in the aerosol category, as the water droplets (steam) together with the exhaust gas constitute the medium of interest,
- It is necessary to include momentum, heat and flow (convection) effects in the solution, given the physical nature of the application.
- The solution must be a one-dimensional solution that can solve both the plane wave and a three-dimensional solution that can solve complex waveforms considering higher order duct modes, when the noise spectrum and the geometric parameters of the exhaust system are considered,
- Boundary conditions, that are, hard walled and impedance definitions can be specified as surface boundary conditions.

The accuracy of the developed approach results has been checked by experimental results and existing limited theoretical results in the literature. In addition, for some cases where theoretical results do not exist in the literature, existing theories have been extended and compared with the numerical results produced in this study.

1.4 Outline of the Dissertation

In chapter 2, background and literature surveys on topics relevant to the study are presented.

In chapter 3, details of the coupled phase theory which the reference theoretical solution (verified with experimental results) chosen to be used in this thesis is given. Firstly, preliminaries of aerosol acoustics and the theory is shared, then the system of equations are derived starting from the very beginning of conservation equations. Finally, the theoretical (analytical) solution for attenuation and

dispersion parameters are presented and comments on the analytical solutions is made.

In chapter 4, 1-D numerical approach based on finite difference method in frequency domain is briefly explained. The code has the capability of solving the wave propagation in an aerosol with thermal and mean flow effects, in addition to viscous drag between the phases. The verification of the developed code is firstly made by comparing the solutions for the case of pure air. In this chapter, the existing analytical solution is also extended to include the mean flow effects.

In chapter 5, results of numerical solution is presented and comparisons made between with analytical solutions for two cases; namely, sound propagation with only momentum exchange and sound propagation with only heat exchange. In addition, the results for the mean flow cases are shared both from numerical solution and the extended analytical solution.

In chapter 6, 3-D numerical approach for the axisymmetric problem with isothermal condition is given in detail. Firstly, the solutions are obtained for the medium which is pure air and the results are checked for several duct modes with the exact results. In this chapter, the existing 1-D analytical solution is also extended to 3-D axisymmetric case with hard wall boundary condition.

In chapter 7, results of numerical solution are presented for various duct modes and comparisons are made with extended analytical solutions for hard boundary condition. Deductions are made for effects of aerosol parameters on cut-off frequencies. In addition, the results for impedance boundary condition are verified with the results from a commercial code in the case of purely air. Then, the particle parameters are turned on and the results are shared for aerosol medium with impedance boundary.

In chapter 8, results are summarized and evaluated together, while conclusions are drawn and recommendations for future work are listed.

CHAPTER 2

LITERATURE SURVEY

2.1 History and Evolution of Suspension Acoustics

The history of the suspension acoustics may go back to Lord Rayleigh [48] who treated the interaction between the incident sound waves and small stationary obstacles of spherical shapes in non-viscous medium. He calculated the scattering effect of small particles and showed that the effect depends on the number of scattering particles and the ratio of scattering.

Sewell [1]extended Lord Rayleigh's solutions to a case where the viscosity of air was included. Hence, this partly made his solutions to be used to find the attenuation due to fog. He assumed that the particles are fixed in space. However; it is not the case for aerosols in the high frequency range. If the particles are small in size and their inertias are negligible, then they have the tendency to oscillate with the fluid without any lag.

Epstein [3] extended Sewell's formulations for spherical obstacles with inclusion of their oscillatory motion. The theory was then more accurate and be able to calculate the sound absorption coefficients for the cases where the particle size was small or the frequencies were high.

Knudsen et al. [6] measured the decay of acoustic perturbations in a reverberation room with water droplets and mineral oil droplets of known average radius and concentration. They measured sound absorption coefficient with respect to frequency for each situation and reported that as the frequency increased, the

attenuation increased as well. Those results were in approximate agreement with the previously developed theories of Sewell's and Epstein's.

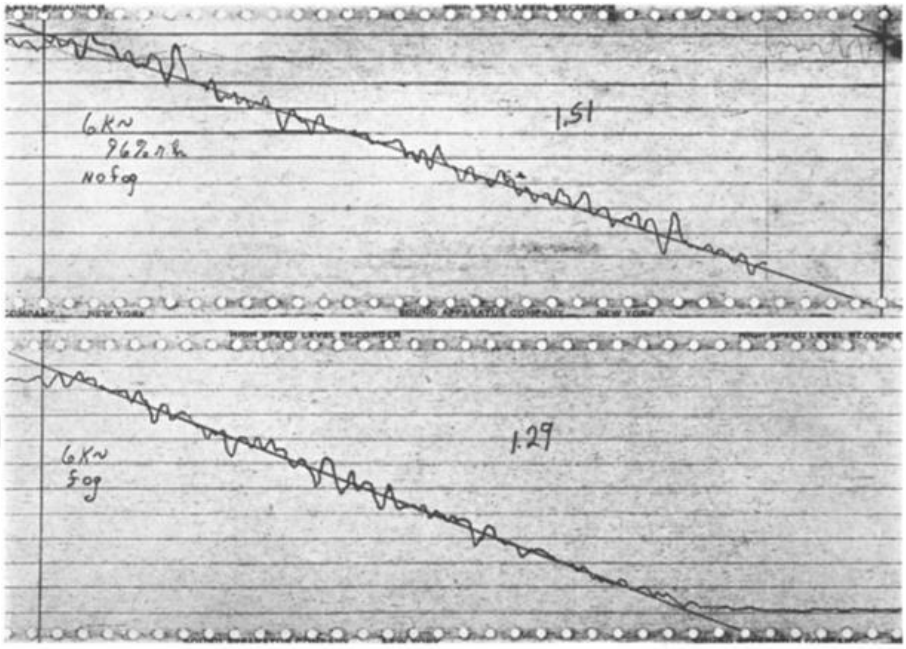


Figure 2.1. Measurement results of Knudsen et al.: Decay curves in a reverberation chamber for a frequency of 6,000 Hz, with no fog in the room (upper curve), and with a fairly dense artificial fog in the room (lower curve). [6]

Epstein and Carhart [7] included the effect of heat conduction between the particles and the medium into the previous prediction theory of Epstein's [3]. This made their theory suitable for finding the attenuation in fog. In their paper, they compared the total attenuation factor due to viscous and conduction effects with the experimental results of Knudsen et al. [6]. Although the frequency dependence of the two was consistent, the results did not match with each other exactly. Insufficiently controlled measurements were attributed as one possible reason to this.

Urick [4] developed a methodology to find the adiabatic compressibility of fine particles by measuring the sound velocity of a suspension of the particles in water. He used an acoustic interferometer working in ultrasonic range. He assumed that

the density and compressibility of the suspension is equivalent to the sum of the volume ratio of the substances. He checked the validity of his theory with the experiments. Subsequently, he worked on the formulation of sound absorption of suspension by relating it to the viscous drag between particles and fluid [5]. He used the well-known expression of Stokes' [2] which gives the drag force exerting on a sphere due to relative motion and viscosity. His predicted results on kaolin and sand particles showed poor coherency with the measurements done with pulse reflection technique. He concluded that effect of shape irregularities may have considerable effect and this could be corrected by considering an equivalent shape parameters.

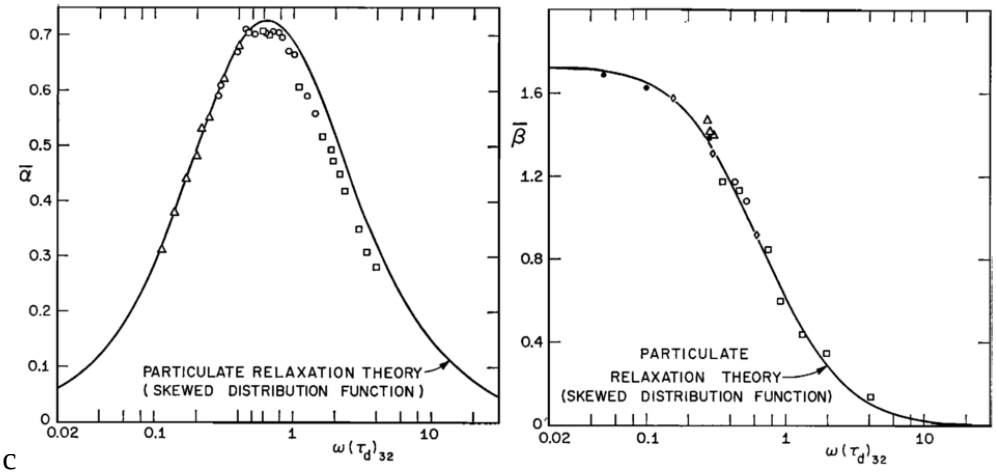
Watters et al. [8] presented their limited experimental research on the attenuation of sound due to water spray systems in special purpose test cell. In their report, the attenuation with respect to frequency bands were shown for several injection flow parameters.

Zink and Delsasso [9] conducted rather reliable measurements in a tube of aluminum oxide particles of known numbers and radii to obtain the attenuation and dispersion at different frequencies. They compared their data with the theoretical results of Epstein's [7] and showed that the total attenuation due to viscous and heat conduction effects agreed well with their measurements.

Chow [10] investigated the effects of surface tension and deformation of the droplets on the attenuation and concluded that surface tension is only influential when the particles are bubbles in a liquid. He also reported that even for large displacements of particle oscillation Epstein's theory [7] was valid. Together with Chu [12], they used Epstein's theory to calculate the dispersion related to momentum and heat exchange.

Temkin and Dobbins [13], [15] developed their own coupled-phase theory based on particulate relaxation process and continuum approach rather than preceding theories based on mostly scattering phenomena for calculating the attenuation and dispersion in an aerosol. Previously; they have presented the measurement results

of attenuation obtained with an impedance tube [11]. Their motivation was to validate the preceding theories to find the attenuation in order to calculate the effectiveness of using suspended particles to stabilize the propellant combustion in rocket motors. They made use optical measurements for finding the particles mean diameters. In general, the results showed good agreement with the prediction theories. However; the size range of the particles was not sufficient enough to see the maximum attenuation per frequency. In their second article [15], they presented the coupled phase theory in detail and put emphasize on the relation between particulate relaxation and maximum attenuation per wavelength. With their new theory, they could also calculated the change in phase speed (dispersion). They checked the accuracy of their results on attenuation with the previous theories[7], [10] as well as the measurement results of Zink and Delsasso's [9]. They showed good agreement. However; they needed more comprehensive test results, which covered further frequencies to show the maximum attenuation per wavelength and which included dispersion values as well. Shortly afterwards, they showed the attenuation and dispersion results of an aerosol composed of oleic acid and nitrogen measured with their own setup [13]. The results are very satisfying, showing very good agreement with their theoretical predictions (Figure.2.2).



c

Figure.2.2 Attenuation(left) and dispersion (right) results of coupled phase theory and measurements of Temkin and Dobbins's. [13]

Marble and Wooten [18] extended the theories of Temkin and Dobbins'[15] to include effects of evaporation and condensation on attenuation and dispersion. They divided particle phase into its corresponding fluid and gas phases and used Clausius-Clapeyron relationship while considering the diffusion controlled mass exchange. According to their results, mass exchange during evaporation and condensation considerably effected total attenuation.

Similar to Marble and Wooten's study[18], evaporation and condensation effects were also formulated by Cole and Dobbins [16]. They particularly investigated the case of sound propagation through atmospheric fog. According to their calculations, the attenuation due to mass exchange is effective in the sub-audible frequency range. Later, they measured the attenuation in a special cloud chamber and shared the results as well as the comparative conclusions with their theory(Figure 2.3) [19]. Accordingly, the results showed that attenuation due to the mass exchange in the low frequency range was many times greater than the others. However; the agreement between the theory and measurements was not very good.

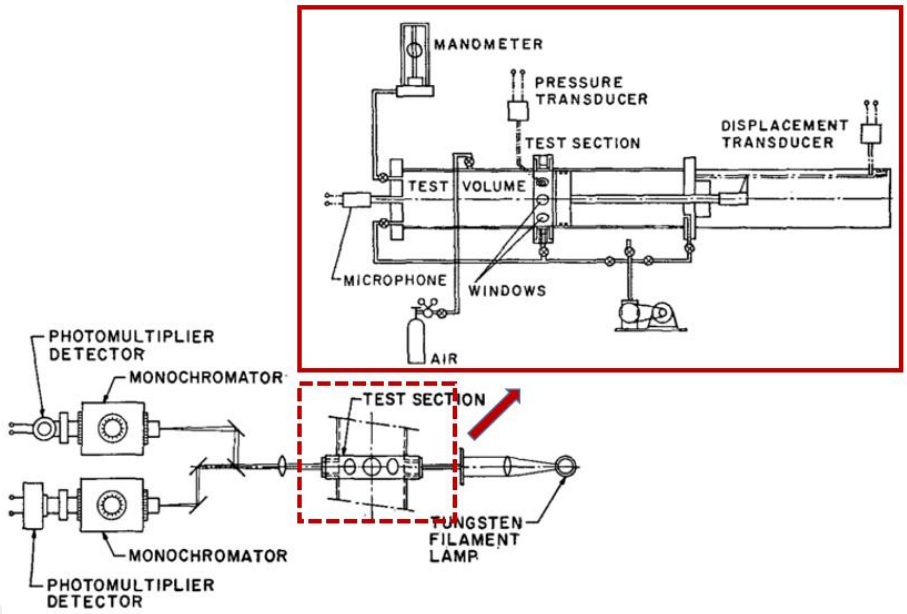


Figure 2.3 Schematic diagram of the cloud chamber and the optical system used by Cole and Dobbins. [19]

Harris [14] performed experimental studies on absorption of sound in air as a function of humidity and temperature. He shared the tabular results covering the temperature range from -10 °C to 30°C and frequency range 125 Hz to 12,500 Hz. Those results were then used by many others in the field of acoustics like room acoustics and atmospheric sciences as well as suspension acoustics.

Mecredy and Hamilton [21] also worked on the same subject to find the attenuation and dispersion in two-phase, one-component media. Their methodology was the same as coupled phase theory by Temkins's [15] since they also considered the problem as a continuum medium and derived the conservation equations correspondingly. They did not simplify the equations as others did. Thus, the quadratic equations were solved by Laguerre iteration technique to calculate attenuation and dispersion values.

Allegra and Hawley [20] applied Epstein and Carhart's [7] complete theory to predict attenuation of sound in emulsions. They put emphasis on the thermal transport process between the phases because researchers working especially on

emulsions neglected this effect. According to their results and comparison with the experimental outputs, the attenuation due to thermal effects seemed to be the major factor.

Marble and Candel [22] investigated the suitability of employing water fog to attenuate noise in a duct through Marble's theory [18]. They calculated the effective frequency values and the corresponding attenuation values of each exchange mechanism for specific radius values of droplets. In addition, they also provided some hints and partial solutions to the case when the duct modes would be of higher order. Their conclusions reported that it would be better to have water fog near the walls of the duct.

Davidson and Scott [23] investigated the cases where the finite amplitude wave propagation is in the form of stable and semi-stable waveforms. They conclusively reported that for the two main attenuation mechanisms; namely, momentum and heat, became significant for different part of waveforms.

Davidson [25] also studied the theoretical and experimental works of Cole and Dobbin's [19] and tried to find a way to correct their theory so as to reduce the mismatch between the theory and measurements. He handled the fundamental equations, checked the neglected terms and found out some mistakes. Consequently, he showed that corrected theory was then in good agreement with the test data.

Jaeschke et al.[24] worked on the damping performance of the water spraying in nozzle expansion area of the transonic jet engine. They predicted the attenuation by using the complete coupled phase theory which included all of the three dissipation mechanisms, namely mass, momentum and heat transfer. They correlated the droplet parameter by fitting the measurement results with the predicted values and concluded that the most contribution was due to mass exchange for the specified application conditions.

Lyman and Chen [28] solved the problem by considering a non-uniform gas-vapor-droplet mixture to see the effect of density and temperature gradients on the

attenuation and dispersion along the direction of the change. They solved the system equations explicitly by Runge-Kutta method. Their results showed that the gradients changed the attenuation and dispersion of the system and should be accounted when they had significant value.

Lyman [26] also investigated the case of measured large attenuation values in nozzle tests. Such an outcome could not be explained by existing theories. He thought that the effect of acoustic streaming might be the answer. According to the theoretical results he obtained, this effect could only become significant when sound levels exceeded 160 dB and the frequencies were above 16 kHz for droplets of 1μm radius.

Alforque et al. [27] analyzed the sound propagation through a bubbly liquid from the standpoint of nuclear reactor safety. Within this context, they made up a special experiment setup to measure the sound speed and attenuation. They presented the comparative results of theirs together with the theoretical predictions.

Wei et al. [30] looked through the case of sound attenuation in which sub-micron sized water droplets exist; for example with a Laval nozzle. They especially investigated the results of the previous literature which claimed hyperbolic increase in attenuation in theory for sub-micron sized particles. By inserting corrected terms for fog kinetics, they came to a conclusion that these particles could not attenuate to a certain degree.

Cheng et al. [29] studied the wave propagation through a bubbly liquid and developed their theoretical model which was based on conservation and Rayleigh equations together. They checked the validity of their model with the test data and it was well suited. The most engaging property of the model was to be able to predict attenuation and dispersion due to exchange of energy together with scattering.

Vetter and Culick [31] came up with the idea to find the mass loading and the size of the particles by measuring the resonance frequencies of duct chambers in which

suspended fluid flowed. They examined their methodology on the pulverized coal fluidized by air upon considerations to the applications in coal power plants. The results were promising in a sense that with the advances in signal processing and statistical methods the methodology would be better in future.

Evans [36] reviewed in his PhD thesis almost all of the literature regarding suspension acoustics till his time and categorized into three as scattering theory, coupled phase theory and porous media theory. He focused his efforts to extend coupled phase theory so as to provide an alternative to analyze the sound propagation in emulsions. He also compared these three methods with each other both qualitatively and quantitatively.

Tebbutt and Challis [33] investigated the widely used theories of wave propagation based on scattering in ultrasonic engineering which were namely; the Urick's model [5], Urick and Ament's model, Allegra and Hawley's model [20] and Harker and Temple's model [32]. They listed all of the physical parameters as inputs for each model, and then presented the comparative results of each for several suspension cases. Accordingly, proposed Allegra and Hawley's model came out to be the most versatile one.

Moss [49] designed and established test setups for measuring acoustical properties of aerosols both in audio and ultrasonic frequency ranges. In his thesis report, he summarized quite briefly the existing measurement methods. Also, he tried to predict the particle parameters from the acoustic test results and compared with the real values. Deduction of such parameters was reported to be challenging if the particle size distribution is not constant. The suggestion to overcome this situation was to sample the test data at well-chosen frequencies.

Slaton et al. [50] analyzed the effect of mechanical properties of a wall of circular tube on the attenuation of sound in air–water vapor mixture. According to their theoretical results, attenuation decreases due to reduction of diffusion capability of vapor. Hickey et al. [37] theoretically investigated the same case with wet walls by considering the diffusion of mass due to thermal effects, called

as Soret effect. The solution was achieved through coupled equations; however, the results showed that this effect is negligible.

Evans and Attenborough [38] compared the two theories; namely coupled phase model and core-shell (scattering) model, in the case of sound propagation in concentrated emulsions. They validated each theory with the measured data (oil-in-water emulsions). As a conclusion, they emphasized on the simplicity of the first model and its accuracy provided that the acoustic length of the radius is sufficiently small.

Gubaidullin [51] studied the case when the wave was like plane, spherical and cylindrical disturbances and the medium was a gas-vapor-drop mixture. He tracked the evolution of the waveform in time by solving system of equations numerically. In another study, he took into account of a second particle phase (sand particles) and calculated the attenuation and dispersion parameters of a mixture of gas with vapor, droplets and solid particles [45]. He showed that an additional peak appeared in the scaled attenuation results.

When the concentration level become finite, the classical coupled phase theory diverges from the experimental results. Baudoin et al. [52] considered this by modifying the theory in order to include hydrodynamic interactions. They compared the predicted results of theirs with the classical theory and the experiments done. Although the modified theory did not match completely with the test results, it seemed to be far more accurate.

Kandula [41], [42] treated this subject by including the nonlinear effects of relaxation processes and transpiration effects on droplet evaporation for the cases of high Reynolds numbers. In his papers, he shared some attenuation and dispersion results obtained from his theory and showed that there is a considerable difference between linear and nonlinear assumptions especially at higher frequencies. He also compared his results with the recent measurements of Norum [40] on jet exhaust noise reduction by water injection and reported their consistency.

2.2 Literature Survey on Application Areas

Understanding the acoustic wave propagation in an aerosol is very important in many engineering fields. Direct methodology is used in some of these fields to predict the parameters such as attenuation, dispersion, etc. Others make use of the reversed methodology to predict the characteristic system parameters about the particles; namely, size, number, concentration level, according to the measured acoustic parameters. Details of the corresponding literature have been shared below.

2.2.1 Acoustic Agglomeration

Particulate pollution is seriously harmful to human health and environment and is a significant contributor to atmospheric pollution. The main contributors to this problem are the vehicles and plants that use fossil fuels [53]. For suppression of the particles, the conventional techniques like particle filters, wet separators, electrostatic precipitators and cyclones are widely applied in the industry. However; these techniques' common disadvantage is that none of them is good at capturing the submicron particles[54]. For this reason, engineers employ acoustic agglomeration methods to enhance the filtering efficiency of these techniques [55].

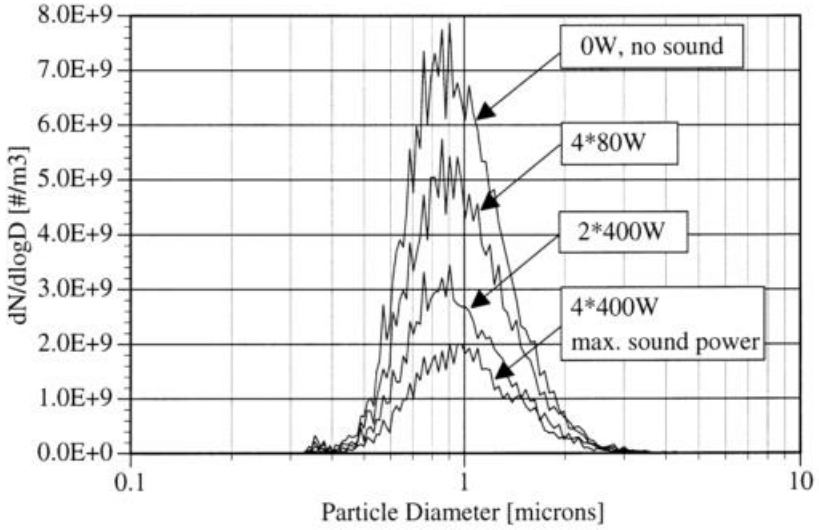


Figure 2.4 High-frequency (10 kHz) acoustic agglomeration of a trimodal aerosol.[53]

With the shortest definition, acoustic agglomeration is the process in which sound waves are deployed in suspensions to merge particles with each other so as to make larger particles. There are several mechanisms that are supposed to be effective in acoustic agglomeration[56]. The most pronounced mechanism is the so called orthokinetic effect. According to this effect, particles with different sizes happen to oscillate with different relaxation times and amplitudes and this results in an increase of probability of collisions [57].

In literatures on pollution [53], [55], [58]–[61], measurement results show that even if the distribution is not huge, particles are not exactly of same size. Thus, the relative motion of particles differs from each other, making orthokinetic effect to become a major factor for acoustic agglomeration. Most of the experimental studies have been made to find the influence of frequency, SPL, initial concentration level and duration of exposure on the agglomeration process (Figure 2.4) [53][58], [60]–[64]. The frequency of the sound seems to be the main parameter to be decided on. Most of the related studies show that it should be at

the frequency corresponding to the particles (mean diameter) relaxation time of momentum transfer (Figure 2.5) [53], [57], [60], [61], [63], [64].

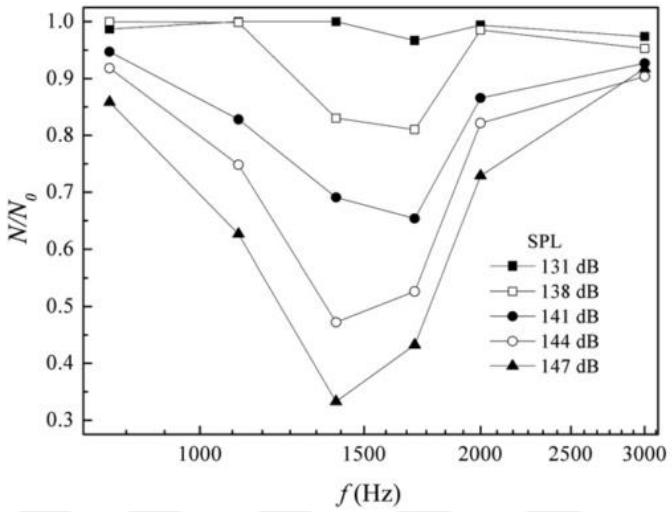


Figure 2.5 Influence of sound frequency on agglomeration.[60]

In addition, some researchers have investigated the effect of humidity on the acoustic agglomeration and have pointed out that it dramatically increases the effectiveness of the method [59], [65], [66]. Apart from these, other studies related to acoustic agglomeration are also available in the mentioned literature [67]–[75].

2.2.2 Jet Noise Suppression

Sound pressure levels can be extremely high in jet applications. Especially during space shuttle launches, such high level pressures can damage the shuttle structure, payload, and ground support equipment [40]. In order to avoid this, water injection is applied near the nozzle exit during lift-offs (Figure 2.6).



Figure 2.6 Water jet injection to nozzle exit for noise suppression.[44]

Effects of water injection parameters such as mass flow rate, injection location and injection angle is being tested for a long time by many researchers working for different associations [44], [76]–[80]. There are even specially designed test facilities for this purpose. Although not very detailed in the parameter specifics, it is generally mentioned that the reduced noise is directly proportional to the amount of sprayed water and can be maximum of 10 dB to 12 dB which is quite a big accomplishment for sound levels in the order of 170 dB.

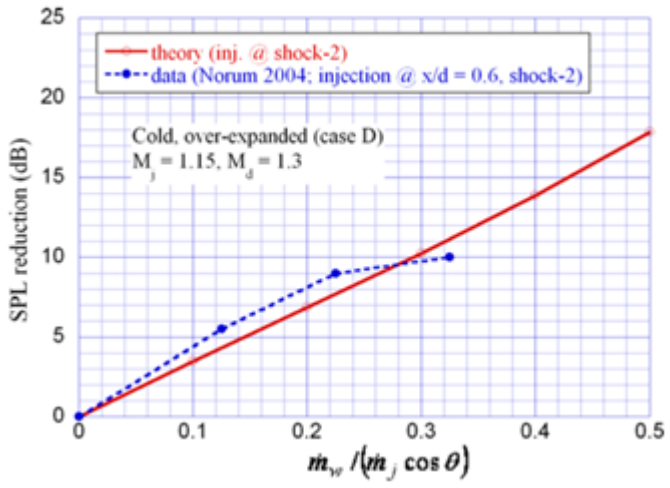


Figure 2.7 Predicted (Kandula's) and measured (Norum's) SPL reduction values for different mass flow rates.[81]

In addition to these experimental studies, Kandula [81], [82] has developed a one-dimensional prediction model for jet noise reduction by water injection. He has made many assumptions and used effective jet and droplet parameters in his model, based on particle relaxation theory of Temkin and Dobbins' [15]. His prediction results show good agreement with the experimental results of Norum (Figure 2.7) [40].

2.2.3 Suspension Characterizations

It is important to be able to determine the size or concentration of particles in the suspension-like media in real time. For this purpose acoustic measurements and calculations are preferred because they are nondestructive, practical and inexpensive. As an example; to increase the combustion efficiency, the size distribution of pulverized coal needs to be controlled. The effectiveness of the physical, chemical and bio- chemical processes can be increased by checking the settling of particles (sedimentation) in line or by visualization of the size distribution of particles in any domain as in the case of ultrasonic monitoring as in underwater and biomedical applications (Figure 2.8).

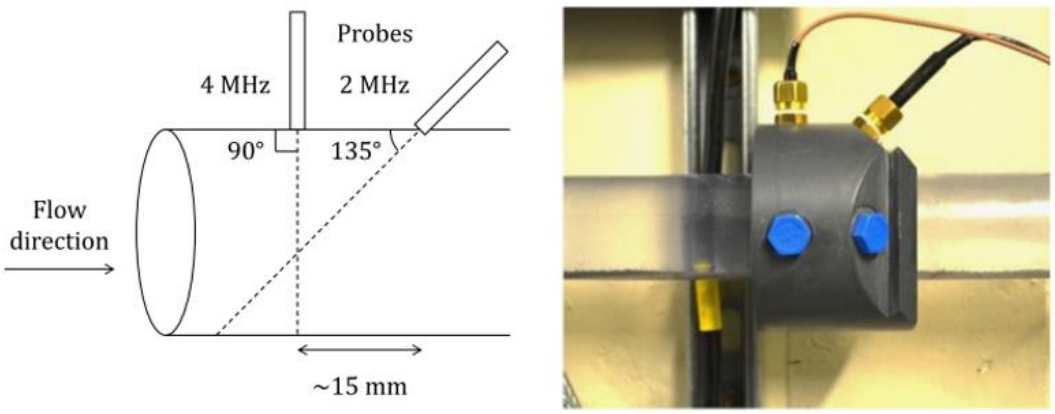


Figure 2.8 Measurement of particle concentration in horizontal, multiphase pipe flow using ultrasonic signals.[83]

Use of acoustic parameters to find suspension properties first started with the Urick's pioneering research on predicting compressibility of emulsions through measured phase velocity [4]. The methodology is based on the inversed theoretical model to construe the measured back scattered amplitude, acoustic speed or attenuation values in terms of particle size (distribution) and concentration. The critical point in reaching the most accurate results is the use of the theoretical model that encompasses the physical parameters in practice [84].

There are many experimental studies which focus on finding size and concentration parameters in literature. Some of them employ acoustical resonance measurements [31], [85], while others use attenuation and phase speed to calculate the size and concentration [39], [43], [84], [86]–[93]. Back scattered amplitudes are also widely considered as well as the prior parameters [83], [94]–[98].

2.3 Summary and Discussions

In this chapter, literature review on suspension acoustics has been given with the emphasis on the evolution of theories especially developed for aerosols. As summarized above, most of the studies have been performed analytically and experimentally only until recently while very few of them are related to numerical approaches. The reason for the lack of numerical studies in literature may be related to a) the fact that 1-D analytical approaches yield satisfactory results in some fields like atmospheric sciences, b) the problem itself may be very complex (e.g. jet noise) so that experimental studies are preferred or c) engineers have not yet implemented technical advances in terms of both numerical approaches and hardware technologies in the solutions. Although existing theoretical and experimental approaches yield very important outputs, to meet the new demands of industries and analyze the engineering problems in more detail, numerical solutions should be adapted. By this means, sound propagation in aerosols with complex geometries in 3-D and variable system parameters can be investigated.

In addition, the effect of mean flow (convection effect) on the sound propagation in aerosols have not yet been investigated in literature either theoretically or experimentally. In many studies, this effect has been either assumed to be the same as in single gas media or neglected.

Consequently, there is a need for a numerical methodology to solve acoustic wave propagation in aerosols which can account for mean flow effects, finite volume concentration effects, as well as having ability to solve 3-D problems. For this purpose, a numerical methodology in both 1-D and 3-D space based on finite difference method in frequency domain is aimed to be developed in this thesis. Moreover, the existing analytical approach of coupled phase approach in 1-D will be extended for mean flow and to 3-D axisymmetric cases.

CHAPTER 3

COUPLED PHASE THEORY

3.1 Introduction to Coupled-Phase Model

Suspensions are actually around us whether we are aware or not and their presence in many engineering applications is evident. First examples that come to mind; clouds in atmosphere, bubbles and particles in sea water, mixtures used in chemistry and food industry, emissions of various combustion processes, etc. While there are different expectations and situations for each example, it is very important for engineering to be able to calculate and interpret the vibrational motion of working media; in other words, acoustics, in these environments.

Coupled phase model was developed by Temkin and Dobbins[15] as an alternative to other prediction models to find the acoustical attenuation and dispersion parameters in suspensions and in such areas where corresponding assumptions were valid, coupled phase model yielded very successful results (Figure.2.2) when compared with experimental data[13]. As it is a very practical method besides its superiority for aerosol acoustics, it has been chosen as the reference theory in the studies made within the scope of this thesis.

Coupled phase theory is a continuum theory and is quite practical to numerical solution techniques for such acoustic problems. Conditions and assumptions associated with this theory can be outlined as[99]:

- Each phase occupies separate volumes so that continuum equations can be written for each phase.

• Physical dimensions of particles should be small with respect to the wavelengths of interest, thus scattering effects due to particles are neglected for the selected range of frequencies.

• The total number of the particles is assumed to be sufficiently high in a control volume to assume continuum approach.

• There should be enough number of particles so that average quantities for physical parameters can be used.

• The aerosol should be sufficiently dilute so that particle collisions can be ignored.

• The interaction between phases can be defined through predictable momentum and energy transfer functions.

• The distance between particles is assumed to be long enough so that there is no interaction between particles.

• Particles are assumed to be spherical in shape.

The most appropriate approach is the continuum theorem, as it is already in other engineering problems. Fortunately; these conditions and assumptions are valid in most of the engineering problems of aerosols.

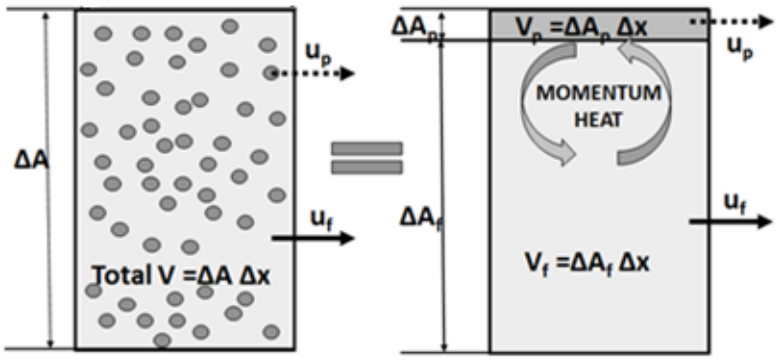


Figure 3.1 Schematic view of the problem and two phase representation of the control volume.

In Figure 3.1 the schematic representation of the coupled phase modelling is shown for 1-D problem which includes the momentum and heat interaction between the phases. In the next step, details of the derivation of the individual continuum equations for each phase will be shown. Before that, momentum and heat transfer of spherical particles under specified conditions will be investigated. In addition, basic suspension concentration parameters will be summarized.

3.2 Preliminaries of the Theory

3.2.1 Concentration Parameters

In order to find the dynamic response of the system to the forces and temperatures, it is subjected to, it is necessary to describe in the numerical equivalence of the concentration parameters related to the suspension medium. As mentioned in the previous section, this theory is based on continuum assumptions. Thus; a control volume (or a numerical discrete element) should have large number of particles but should be still sufficiently dilute; while the distribution of particles in the control volume is the same. Consequently, system parameters in the control volume can be described with single, averaged representative values which are calculated or measured.

3.2.1.1 Particle Size Distribution

In reality, the particles in the suspensions are not of the same size. This type of suspensions are termed as poly-dispersed. The information of this variation in size can be defined in terms of distribution functions. If the radius of any particle has an arbitrary value a and the number of particles of that diameter is $N_a(a)$, then, the total number of particles N_o in the control volume is;

$$N_o = \int_0^\infty N_a \, da \tag{3.1}$$

where da is the discrete definition for the radius of the particles. Then the arithmetic mean radius of the particles $\bar{a}$ can be calculated as;

$$\bar{a} = {\sum a \, N_a(a)}/{N_o} \tag{3.2}$$

3.2.1.2 Volume Concentration

As shown in Figure 3.1, the control volume of a suspension is made up of both the volumes of each particle and the volume of host fluid. By using the mean radius $\bar{a}$, one can calculate the volume of a single particle (by assuming the shape is spherical) $\bar{v}_p = {4\pi\bar{a}^3}/{3}$. If the total volume of the particles is defined as $\Delta V_p = N_o \bar{v}_p \Delta V$ and the total volume of the control volume as ΔV, then the particle volume concentration $\emptyset_v$ within the control volume is;

$$\emptyset_v = {\Delta V_p}/{\Delta V} = N_o \bar{v}_p \tag{3.3}$$

If the particles and the fluid are assumed to occupy separate volumes, then fluid volume concentration is simply $(1 - \emptyset_v)$. Dilute suspensions have very low $\emptyset_v$ values which make the volume concentration of the fluid to be assumed as approximately 1. This assumption is usually correct in the case of dilute aerosols.

3.2.1.3 Mass Concentration

Another parameter to quantify the portion of the particles in a suspension can be through mass. This parameter can be more significant when the particle volume concentration values are very low and almost zero, but the density ratio of particles to fluid is very high. In the same manner, the particle mass concentration $\emptyset_m$ in the control volume is;

$$\emptyset_m = {\Delta m_p}/{\Delta m} \tag{3.4}$$

where m_p is the total mass of the particles and m is the total mass of the whole control volume. For example, in the case of water droplets in air, the particle volume concentration of $\emptyset_v = 0.001$ yields $\emptyset_m = 1$.

3.2.1.4 Equivalent Suspension Density

One can also specify and use a single value for suspension density by volume averaging the total mass which is the linear sum of the mass of the particles and the fluid. In terms of parameters of volume concentration, the corresponding equivalent density of the fluid can be expressed as;

$$\rho_{eq} = \rho_f(1 - \emptyset_v) + \rho_p\emptyset_v \tag{3.5}$$

3.2.2 Force Acting on a Spherical Particle

The total force on the particle phase is the linear sum of the forces acting on each particle according to the theory. Thus, the force response of a spherical particle in oscillating fluid under acoustical conditions must be found beforehand. When a plane acoustic wave hits a particle in a fluid, it is forced to make a translational

motion. Many studies in literature have been undertaken to find this force in the field of fluid dynamics and several cases have been investigated in order to find the most appropriate formulation either analytically or empirically (Figure 3.2).

It was Newton who was first to deal with the drag force or resisting force on a spherical object moving through a fluid. His observations on cannonballs led him to relate the resistance force acting on the ball with the acceleration of displaced gas. This is true when Reynolds number (Re) has rather higher values (Re > 1000). However; this is not applicable to aerosols' acoustic motions because Reynolds number is very low (generally Re << 1).

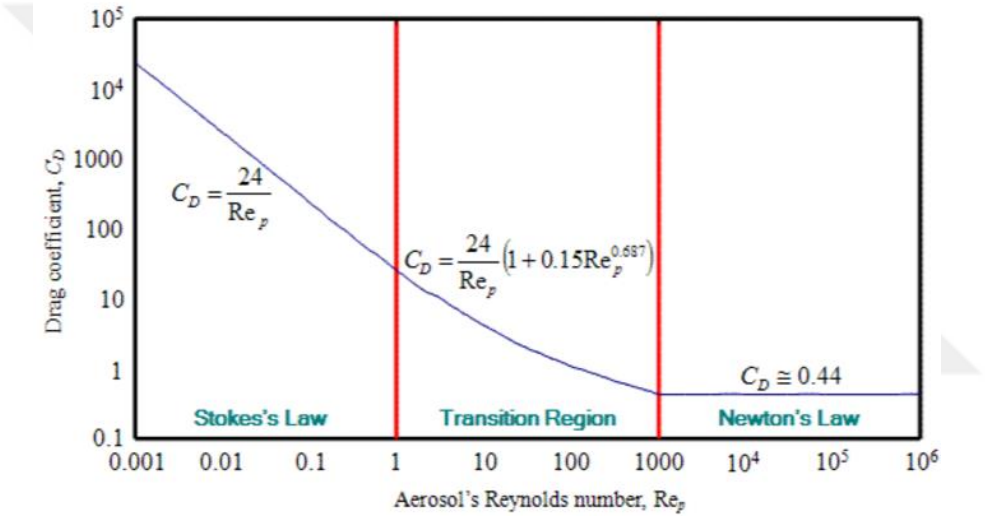


Figure 3.2 Drag coefficient with respect to Reynolds number[100]

In most of the cases for aerosols, particles adjust to steady response very quickly because they are very small in size. In addition, if the magnitude of fluid motion is not big as in the case of acoustic motion, then the gas (air) also can be considered as incompressible. Accordingly, it is suitable to adapt Stokes' equations to aerosol acoustics:

$$\nabla \cdot u = 0 \tag{3.6}$$

$$\rho \frac{\partial u}{\partial t} - \mu \nabla^2 u + \nabla \mathrm{p} = 0 \tag{3.7}$$

where u, ρ, μ and p are the velocity, density, dynamic viscosity and pressure of the flow, respectively. In Equation (3.7), the first term with time derivative represents the unsteady motion in the system. In Stokes' solution, this term has been neglected by considering a steady flow condition, thus ignoring the inertial effects which are valid for low Reynolds numbers. Likewise, here it will be assumed to have a steady oscillation of the particle and the inertial effects will be considered very low and neglected.

The schematic representation of the problem is illustrated in Figure 3.3. For simplicity, the spherical particle is assumed to be fixed in uniaxial flow. By solving for the velocity profile around the particle, one can find the pressure distribution and the net drag force on the particle. Even though the equations look simple, the analytical solution to the corresponding case is not very easy to derive. The full derivation of Stokes' law can be found in literature [99], [101].

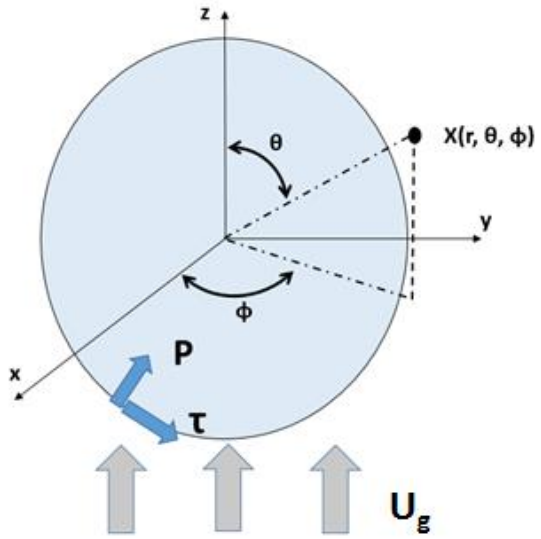


Figure 3.3 Schematic representation of a flow problem over a spherical particle

The net force on a spherical particle according to Stokes is the linear sum of the normal and tangential force components in flow direction on the surface of the particle:

$$F_n = \oint_S -Pcos\theta \, dS = 2\pi\mu_g a u_g \tag{3.8}$$

$$F_t = \oint_S \tau \, sin\theta \, dS = 4\pi\mu_g a u_g \tag{3.9}$$

where P, τ, S, μ_g, u_g are the normal pressure, shear, surface area of the sphere, dynamic viscosity and velocity of the gas, respectively. If the particle is allowed to oscillate, then relative velocity should be taken to find the net force as:

$$F_p = F_n + F_t = -6\pi\mu_g a(u_p - u_g) \tag{3.10}$$

where u_p is the velocity of the particle. This shows that the drag force is proportional to the velocity, the viscosity of the medium and the size of the particle. If the momentum equation for particle is to be written as:

$$\frac{du_p}{dt} = \frac{-6\pi\mu a}{m_p}\left(u_p - u_g\right) = -\frac{\left(u_p - u_g\right)}{\tau_d} \tag{3.11}$$

where m_p is the mass of the single particle. τ_d is called dynamic relaxation time and it is an important indicator showing the period of adjustment of the particles motion to the gas motion [99]. The significance of this parameter will be emphasized in the following chapters.

3.2.3 Heat Transfer to a Spherical Particle

Thermal state of the medium can change due to compression and expansion when acoustic wave propagates. This results in temperature oscillations in the field with the same frequency of the pressure wave. When the medium is pure; in other words single phased, and assumed to be unbounded, then the energy loss due to heat transfer is neglected in most of the cases. However; variations in temperature field of the medium will lead to a heat transfer to and from the particles if it is an aerosol.

Similar to the case of finding drag force for momentum equation in the previous section, the total heat transfer rate is required to be evaluated by first obtaining it on a single particle. Upon assuming the heat transfer coefficient is equal to k_g/a [13] if Reynolds number is small, one may predict the heat transfer rate by means of;

$$\dot{Q}_p = k_g \oint_S \vec{n} \cdot \nabla T \, dS \tag{3.12}$$

where the terms $\dot{Q}_p$, k_g, $\vec{n}$, ∇T, S are the heat transfer rate to the particle, thermal conductivity of gas, unit normal vector, temperature gradient and the surface area of sphere, respectively. The particles may be considered as rigid and it is assumed that there is no temperature variation inside the particles or assignment of an average temperature value is sufficient. In addition, if particles are so small and dilute, then their existence does not affect the temperature field of the host phase. These assumptions are justified when the medium is an aerosol and the particles are in micron size.

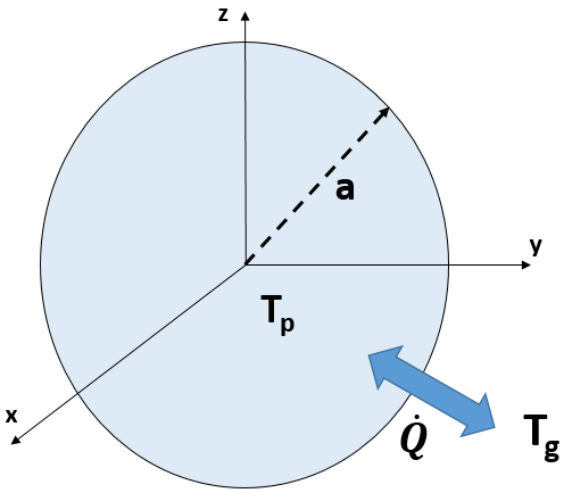


Figure 3.4 Schematic representation of a heat transfer problem onto a spherical particle

In Figure 3.4, heat transfer to a spherical rigid particle of radius a is represented. Together with the assumptions made above, the temperature gradient on the surface of the particle can be taken simply as the temperature difference between the phases.

$$\dot{Q}_p = -4\pi a k_g (T_p - T_g) \tag{3.13}$$

where T_p and T_g are the temperature of the particle and the gas, respectively. According the equation above, the heat transfer rate is dependent on thermal conductivity of the gas, size of the particle and the temperature difference. This equation can be modified to include the convective effects; however, in the case of aerosol acoustics this is not necessary.

If the energy (heat) equation for the particle is written by the heat transfer rate obtained here;

$$\frac{dT_p}{dt} = \frac{-4\pi a k_g}{m_p c_{pp}}\left(T_p - T_g\right) = -\frac{\left(T_p - T_g\right)}{\tau_T} \tag{3.14}$$

where c_{pp} is the specific heat capacity of the particle at constant pressure. τ_T is called thermal relaxation time and it is an important indicator showing the period of the particles ability to adjust its temperature to the temperature change on the boundary [99].

3.3 Conservation Equations

To arrive at the complete system of equations, the conservation equations for both phases should be derived by considering the assumptions specified previously in Section 3.1.

3.3.1 Conservation of Mass

Derivation of conservation of mass for particle and gas phase is undertaken separately. An infinitesimal volume dV of an aerosol is considered as shown in Figure 2.1 and there is a unidirectional motion in x axis with a velocity $U(x,t)$. The total volume occupied by the particles will be $\emptyset_v dV$ which is also equal to $A_p dx$ where A_p is cross sectional area of the volume occupied by the particle

phase. The corresponding mass of the particle phase will be $\rho_p \emptyset_v dV$ where ρ_p is constant. Change in the mass of the particle phase will be through boundaries of A_p and will be equal to $u_p A_p \rho_p$. To satisfy the continuity for the particle phase, the rate of change should be equal to the mass transfer in and out:

$$\frac{\partial}{\partial t}(\rho_p \emptyset_v) + \frac{\partial}{\partial x}(\rho_p \emptyset_v u_p) = 0 \tag{3.15}$$

Since the particle density is not expected to change, it can be removed. Accordingly, only the volume concentration level is expected to change. The corresponding equation becomes;

$$\frac{\partial \emptyset_v}{\partial t} + u_p \frac{\partial \emptyset_v}{\partial x} + \emptyset_v \frac{\partial u_p}{\partial x} = 0 \tag{3.16}$$

If there is no mean flow in the system, then the second term in equation above will be of negligible value and can be dropped out. Another way to express this equation is by means of substantial derivative representation. The continuity equation with substantial derivative is also given below:

$$\frac{D\emptyset_v}{Dt} + \emptyset_v \frac{\partial u_p}{\partial x} = 0 \tag{3.17}$$

The continuity equation for the gas phase can be derived similarly. The result is given directly here;

$$\frac{\partial}{\partial t}\rho_g(1-\emptyset_v) + u_g \frac{\partial}{\partial x}\rho_g(1-\emptyset_v) + \rho_g(1-\emptyset_v)\frac{\partial u_g}{\partial x} = 0 \tag{3.18}$$

In all of terms on the left hand side (LHS) of the equation, there exists the term $(1-\emptyset_v)$. Since we are dealing with dilute aerosols ($\emptyset_v < 0.001$), this term is very close to the value of 1, thus it can be dropped. Otherwise, it is also possible to keep that term but still it is not necessary to differentiate on it. The simplified version will take the form given by:

$$(1-\emptyset_v)\left(\frac{D\rho_g}{Dt}+\rho_g\frac{\partial u_g}{\partial x}\right)=0 \tag{3.19}$$

3.3.2 Conservation of Linear Momentum

The second conservation principle is the momentum equation which is also known as Newton's second law. It states that the rate of change of momentum is equal to the surface and body forces. Starting with the particle phase first, the momentum is equal to $\rho_p\emptyset_v dV u_p$. Let's start with Reynold's transport theorem:

$$\frac{\partial}{\partial t}\left(\rho_p\emptyset_v u_p\right)+\frac{\partial}{\partial \mathrm{x}}\left(\rho_p\emptyset_v u_p u_p\right)+f=0 \tag{3.20}$$

where f is an arbitrary load term. After some arrangements, this equation can be modified as;

$$\rho_p\emptyset_v\left(\frac{\partial u_p}{\partial t}+u_p\frac{\partial u_p}{\partial \mathrm{x}}\right)+u_p\left(\frac{\partial \rho_p\emptyset_v}{\partial t}+u_p\frac{\partial \rho_p\emptyset_v}{\partial \mathrm{x}}\right)+f=0 \tag{3.21}$$

The second term on LHS of the equation is simply the conservation of mass for the particle phase and should be zero. Then, body loads or surface forces can be implemented as loading terms as;

$$\rho_p \emptyset_v \left(\frac{\partial u_p}{\partial t} + u_p \frac{\partial u_p}{\partial \mathrm{x}} \right) + \Delta p_p + f_p - \Delta \tau_p - \rho_p \emptyset_v B_p = 0 \tag{3.22}$$

where p_p, f_p, τ_p and B_p are hydrostatic pressure, external surface load, deviatoric stress and body load per unit mass respectively. If the particles are rigid, then hydrostatic pressure and deviatoric stress terms will disappear. If the harmonic response of the particles is of the prime interest, body load term can also be neglected. Hence, the simplified momentum equation for the particle phase is expressed by;

$$\rho_p \emptyset_v \left(\frac{\partial u_p}{\partial t} + u_p \frac{\partial u_p}{\partial \mathrm{x}} \right) = - f_p \tag{3.23}$$

In the same manner the momentum equation for the gas phase can be derived as;

$$\rho_g (1 - \emptyset_v) \left(\frac{\partial u_g}{\partial t} + u_g \frac{\partial u_g}{\partial \mathrm{x}} \right) + (1 - \emptyset_v) \Delta p_g = f_p \tag{3.24}$$

As distinct from the particle equation, the pressure term is kept here and the sign of the external force changes. The deviatoric stress term is also neglected for gas by considering the medium to be air or any gas with the viscosity close to that of air. This is because the attenuation and dispersion effect due to thermal and viscous losses in the molecular stage is reported to be very low in the frequency range of interest [102] and they are not the main concern of this study.

3.3.3 Conservation of Energy

Having defined the conservation equations of mass and momentum, the next equation to consider is the energy equation. In classical acoustics, usually there is no need to check the energy property of the system since the motion is assumed to be isentropic and lossless meaning it is reversible. In this case, even if the process as a whole is again isentropic, heat transfer may take place between the phases and this is not exactly reversible. So, the energy balance of the system needs to be derived focusing on the heat exchange phenomena. According to the first law of thermodynamics, the rate of change of internal energy of a system is equal to the heat transfer rate and work done to the system. The corresponding equation for the gas phase is;

$$\frac{DE_g}{Dt} = \dot{Q}_g + \dot{W}_g \tag{3.25}$$

where E_g is the internal energy of the gas phase, $\dot{Q}_g$ is the heat transfer rate to the gas phase and $\dot{W}_g$ is the rate of work done on the gas phase. The rate of change of internal energy at constant volume is also equal to;

$$\frac{DE_g}{Dt} = (1 - \emptyset_v)\, \rho_g c_{vg} \frac{DT_g}{Dt} \tag{3.26}$$

where c_{vg} and T_g are the specific heat constant at constant volume and temperature (average) of the gas, respectively. $\dot{Q}_g$ is the negative signed of $\dot{Q}_p$ which has already been derived for the particle phase in Section 3.2.3. $\dot{W}_g$ is due the compression and expansion of the gas which can be expressed per infinitesimal volume as;

$$\dot{W}_g = -P_{og} \frac{\partial u_g}{\partial x} \tag{3.27}$$

where P_{og} is the static pressure of the gas. Merging the last two equations into the first equation yields:

$$(1 - \emptyset_v)\, \rho_g c_{vg} \left(\frac{\partial T_g}{\partial t} + u_g \frac{\partial T_g}{\partial \mathrm{x}} \right) + P_{og} \frac{\partial u_g}{\partial x} = \dot{Q}_g \tag{3.28}$$

In the same manner, the energy equation for particle phase can be derived and expressed by;

$$\emptyset_v \rho_p c_{pp} \left(\frac{\partial T_p}{\partial t} + u_p \frac{\partial T_p}{\partial \mathrm{x}} \right) = \dot{Q}_p \tag{3.29}$$

where c_{pp} and T_p are the specific heat at constant pressure and temperature of the particle phase, respectively. As it can be recognized, there is no pressure term related to work done on the particles since they are assumed to be rigid.

3.3.4 Equation of State

To complete the system of equations and have an exact solution, it is required to have equations of state for each phase. One of the phase in an aerosol is the gas for which we can use explicit analytical relations. On the other hand, there is no need for a state equation for the particle phase due to their rigid behavior. Starting with an arbitrary state equation that relates pressure, density and entropy parameters;

$$p_g = p_g(\rho_g, S_g) \tag{3.30}$$

For an infinitesimal variation in pressure, it can be re-written as;

$$dp_g = \left(\frac{dp_g}{d\rho_g}\right)_S d\rho_g + \left(\frac{dp_g}{dS_g}\right)_\rho dS_g \tag{3.31}$$

where S_g is the entropy of the gas. Since the process is assumed to be an isentropic, the second term on the right hand side (RHS) is zero. Then, the equation reduces to;

$$dp_g = \left(\frac{dp_g}{d\rho_g}\right)_S d\rho_g \tag{3.32}$$

where $c^2 = \left(dp_g/d\rho_g\right)_S$ is square of the speed of sound. When the system of equations do not contain temperature as independent variable, then the above equation will be adequate. But, when there exist temperature variables in the system, then we need to use another equation. According to ideal gas theory, the relation between pressure, density and temperature is described as;

$$p_g = R\rho_g T_g \tag{3.33}$$

where R is the thermodynamic gas constant. Again for an infinitesimal change, it can be linearized as;

$$dp_g = R\left(\rho_g dT_g + T_g d\rho_g\right) \tag{3.34}$$

This can be adapted to the system as a supplementary equation when we need to solve for temperature variables.

3.4 System of Equations

Now that all the preliminaries and fundamental equations are given, the equations can be rearranged to complete the system of equations. The problem is categorized into two main cases in the theoretical reference [99]. In order to compare and check the numerical results which are presented in the following chapters, these two cases are shown here together with their analytical solutions.

3.4.1 Sound Propagation with Only Momentum Exchange

In the first case, the sound propagation in an aerosol is assumed to happen with isothermal conditions in which temperature changes will be neglected. By considering this scenario, only momentum exchange between the particles and the gas is allowed to happen. Accordingly, the energy equation is unnecessary and the equation of state is only needed to relate pressure with density. For simplicity, mean flow is assumed to be zero, implying there is no convective effects. As stated before, the particles are assumed as rigid, spherical particles and the acoustical length or Helmholtz Number is sufficiently small $(k.a < 1)$. The corresponding equations are given below:

$$(1 - \emptyset_v)\left(\frac{\partial \rho_g}{\partial t} + \rho_{go}\frac{\partial u_g}{\partial x}\right) = 0 \tag{3.35}$$

$$\rho_{go}\frac{\partial u_g}{\partial t}+\frac{\partial p_g}{\partial x}=\frac{1}{(1-\emptyset_v)}6\pi\mu_g a N_o\left(u_p-u_g\right) \tag{3.36}$$

$$p_g-{c_o}^2\rho_g=0 \tag{3.37}$$

$$\frac{\partial \emptyset_v}{\partial t}+\emptyset_v\frac{\partial u_p}{\partial x}=0 \tag{3.38}$$

$$\rho_p\emptyset_v\frac{\partial u_p}{\partial t}=-6\pi\mu_g a N_o\left(u_p-u_g\right) \tag{3.39}$$

where N_o is the total number of particles in the control volume. The first three equations belong to the gas phase while the other two belong to the particle phase. If the dependencies on time and space is considered to be harmonic, then simplification on the derivative terms as $\partial/\partial t=-i\omega$ and $\partial/\partial x=i\hat{k}$ can be made. Here, ω is the circular frequency and $\hat{k}$ is the wave number. The hat on the wave number means that it is complex-valued. As the main interest is to find out how the acoustic wave propagates, determination of the complex wave number is focused. The term $(1-\emptyset_v)$ can be considered as equal to 1 because the aerosol is assumed to be dilute. The continuity equation for the particle concentration is not necessary and by means of the state equation we can express the density perturbation of the gas phase in terms of pressure. Through these simplifying assumptions, the number of equations reduces to three and they can be re-written in matrix form as;

$$\begin{bmatrix} \rho_{go}\hat{k} & 0 & -\omega/{c_o}^2 \\ -i\omega + \sigma_m/\tau_d & -\sigma_m/\tau_d & i\,\hat{k}/\rho_{go} \\ -1/\tau_d & -i\omega + 1/\tau_d & 0 \end{bmatrix} \begin{pmatrix} \hat{u}_g \\ \hat{u}_p \\ \hat{p}_g \end{pmatrix} = 0 \tag{3.40}$$

where σ_m is called the mass loading and is equal to the ratio of the mass of the particles to the mass of the fluid(air) in a unit volume. A non-trivial solution requires that determinant of 3x3 matrix is equal to zero. This solution yields the simplest form for the complex wave number as given below [99];

$$\hat{k}^2 = \frac{\omega^2}{{c_o}^2}\left(1 + \frac{\sigma_m}{1 - i\omega\tau_d}\right) \tag{3.41}$$

Since that $\hat{k}$ is a complex number, its physical meaning is that the acoustic wave will be attenuated as it propagates. If it is separated into its real and imaginary parts and insert into the propagation formula, it becomes;

$$P(x,t) = P_i e^{-\alpha x + i(k_r x - \omega t)} \tag{3.42}$$

where P_i is the initial amplitude of the wave, k_r is the real part and α is the imaginary part of $\hat{k}$. The amount of attenuation is expressed with α. Due to this energy loss, there will also be a dispersion in the phase speed which is equal to $c(\omega) = \omega/k_r$. Now if the solution α [99] is revisited, one obtains;

$$\alpha_{low} \approx \frac{\omega}{2c_o}\sigma_m \frac{\omega\tau_d}{1 + \omega^2{\tau_d}^2} \tag{3.43}$$

where α_{low} means that it is valid if the mass loading is low ($\sigma_m \ll 1$). If this is not the case, the more generalized version is given below with a dependency in the phase speed (dispersion):

$$\alpha \approx \sigma_m \frac{\omega\, c(\omega)}{2{c_o}^2} \frac{\omega\tau_d}{1+\omega^2{\tau_d}^2} \tag{3.44}$$

If the attenuation is needed per wavelength (frequency) rather than per unit distance, then another constant called attenuation per wavelength; $\bar{\alpha} = \alpha\ c_o/\omega$ may be used instead;

$$\bar{\alpha} \approx \sigma_m \frac{c(\omega)}{2c_o} \frac{\omega\tau_d}{1+\omega^2{\tau_d}^2} \tag{3.45}$$

This is the general solution for dilute aerosols. On the other hand; for dilute aerosols with low mass loading ratio, the solution is as given below [99];

$$\bar{\alpha}_{\,low} \approx \frac{\sigma_m}{2} \frac{\omega\tau_d}{1+\omega^2{\tau_d}^2} \tag{3.46}$$

To make it easier to understand the solution, the attenuation results are shown in Figure 3.5 for water droplets in air at 0 ^{o}C temperature per unit mass loading. The radii of the droplets are taken as 10 x 10^{-6} m.

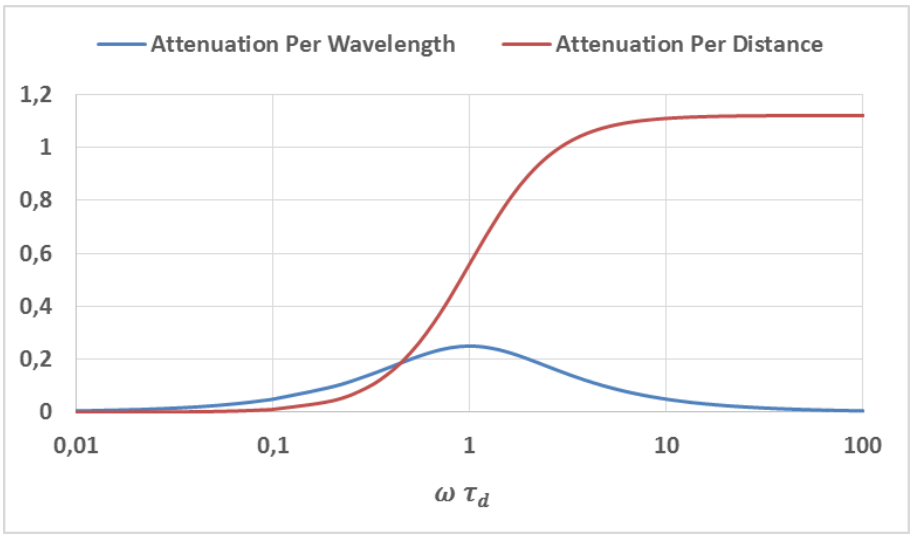


Figure 3.5 Attenuation results scaled to mass loading in air with water droplets.

Results show that both attenuation characteristics per wavelength and per distance parameters converge to zero at lower frequencies. At a certain frequency which is equal to the dynamic relaxation time (Eq 3.11), the attenuation per wavelength has a maximum value. This happens because the relative velocity at this specific frequency reaches its maximum in return causing more loss of energy due to viscosity. Towards the higher frequencies attenuation per wavelength decreases while the attenuation per distance converges to the maximum value.

The real part of the wavenumber which is the phase speed can be obtained through the equation below [99];

$$ {c_o}^2 \Big/ {c(\omega)^2} = 1 + \sigma_m \frac{1}{1 + \omega^2 {\tau_D}^2} \tag{3.47} $$

When the frequency is close to zero, the dispersion ratio converges to a value of $(1 + \sigma_m)$. On the other hand; it converges to unity meaning it is equal to the speed of sound of the gas phase towards the higher frequencies.

3.4.2 Sound Propagation with Momentum and Heat Exchange

For the second case, the isothermal condition in the first case is put away and temperature variables are included in the problem so as to solve the heat transfer between these phases. Thus, energy equations are included in the system and the state equation is modified to include temperature variable. The problem in this state can be investigated to find the attenuation and dispersion results due to both momentum and heat transfer between phases. The other assumptions and conditions specified for first case are also valid for this case. The corresponding governing equations are expressed as:

$$(1-\emptyset_v)\left(\frac{\partial \rho_g}{\partial t}+\rho_{go}\frac{\partial u_g}{\partial x}\right)=0 \tag{3.48}$$

$$\rho_{go}\frac{\partial u_g}{\partial t}+\frac{\partial p_g}{\partial x}=\frac{1}{(1-\emptyset_v)}6\pi\mu_g a N_o\left(u_p-u_g\right) \tag{3.49}$$

$$p_g-RT_{go}\rho_g-R\rho_{go}T_g=0 \tag{3.50}$$

$$(1-\emptyset_v)\,\rho_g c_{vg}\frac{\partial T_g}{\partial t}+P_{og}\frac{\partial u_g}{\partial x}=4\pi k_g a N_o\left(T_p-T_g\right) \tag{3.51}$$

$$\frac{\partial \emptyset_v}{\partial t}+\emptyset_v\frac{\partial u_p}{\partial x}=0 \tag{3.52}$$

$$\rho_p\emptyset_v\frac{\partial u_p}{\partial t}=-6\pi\mu_g a N_o\left(u_p-u_g\right) \tag{3.53}$$

$$\emptyset_v \rho_p c_{pp} \frac{\partial T_p}{\partial t} = -4\pi k_g a N_o \left(T_p - T_g\right) \tag{3.54}$$

The first four equations belong to the gas phase while the other three belong to the particle phase. Again, derivative terms can be changed into as $\partial/\partial t = -i\omega$ and $\partial/\partial x = i\hat{k}$ for harmonic phenomena. Likewise, the term $(1 - \emptyset_v)$ can be considered as equal to 1 because the aerosol is assumed to be dilute. The continuity equation for the particle concentration is not necessary. We can write u_p and T_p in terms of u_g and T_g respectively by the momentum and energy equations of the particle phase as:

$$u_p = \frac{u_g}{(1 - i\omega\tau_d)} = B_M u_g \tag{3.55}$$

$$T_p = \frac{T_g}{(1 - i\omega\tau_T)} = B_T T_g \tag{3.56}$$

Then, these equations are used in the momentum and energy equations of the gas phase to eliminate the particle variables. After these arrangements, the number of equations to be solved is decreased to four. The matrix representation is:

$$\begin{bmatrix} -i\omega & i\rho_{go}\hat{k} & 0 & 0 \\ 0 & -i\omega + \sigma_m/\tau_d\,(1 - B_M) & i\hat{k}/\rho_{go} & 0 \\ -\bar{R}T_{go} & 0 & 1 & -\bar{R}\rho_{go} \\ 0 & i\hat{k}P_{og}/\rho_{go}c_{vg} & 0 & -i\omega + \sigma_m c_{pp}/\tau_T c_{vg}\,(1 - B_T) \end{bmatrix} \begin{pmatrix} \hat{\rho}_g \\ \hat{u}_g \\ \hat{p}_g \\ \hat{T}_g \end{pmatrix} = 0 \tag{3.57}$$

A non-trivial solution can be obtained if the determinant of 4x4 matrix is made equal to zero. The result for attenuation per distance for low mass loading ($\sigma_m \ll 1$) can be obtained as given in theoretical reference as [15];

$$\alpha_{low} \approx \frac{\omega}{2c_o}\sigma_m \left\{ \frac{\omega\tau_d}{1+\omega^2{\tau_d}^2} + (\gamma_g - 1)\frac{c_{pp}}{c_{pg}}\frac{\omega\tau_t}{1+\omega^2{\tau_T}^2} \right\} \tag{3.58}$$

The first term in the parenthesis corresponds to the viscous losses which are already obtained in the previous section while the second term corresponds to the thermal losses due to heat transfer between the phases. The attenuation constant per wavelength is simply written as;

$$\bar{\alpha}_{low} \approx \frac{1}{2}\sigma_m \left\{ \frac{\omega\tau_d}{1+\omega^2{\tau_d}^2} + (\gamma_g - 1)\frac{c_{pp}}{c_{pg}}\frac{\omega\tau_t}{1+\omega^2{\tau_T}^2} \right\} \tag{3.59}$$

For comparison attenuation results due to viscous and thermal effects are displayed in Figure 3.6. The x-axis of the plot is adjusted to $\omega\tau_d$, so a maximum value due to viscous friction when it is equal to 1. The ratio between the dynamic relaxation time and thermal relaxation time is almost constant for air and it is close to four (it is equal to 4.18 here). Thus, $\omega\tau_T = 1$ corresponds to $\omega\tau_d = 0.24$. The attenuation curve corresponding to the heat conduction reaches its maximum at this frequency and it seems that the peak is twice as big as the other. As a conclusion, one can say that in the aerosol of air and water droplets, attenuation due to heat conduction may be more significant than the heat conduction due to viscous friction towards the lower frequencies. However, one should not forget that this analytical solution is based on the assumption that the aerosol is dilute and the mass loading is very low. In the following chapters, the

problem will be investigated when the mass loading is almost equal to one and its effect cannot be neglected.

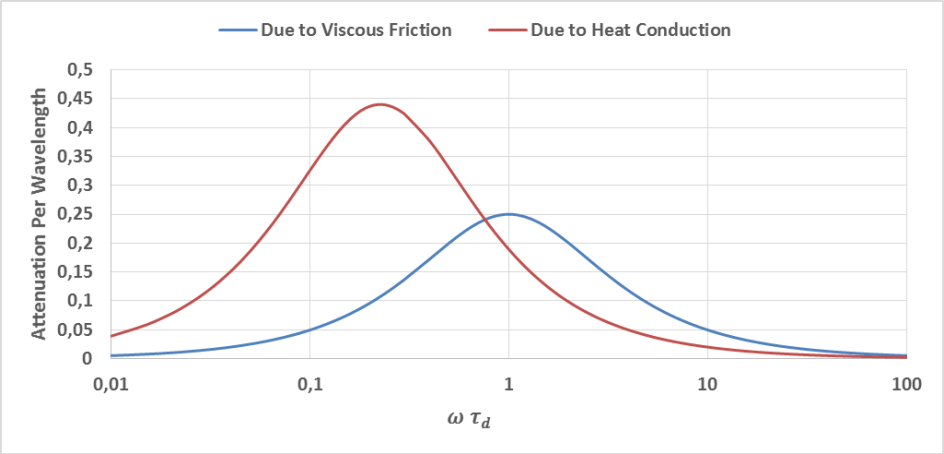


Figure 3.6 Attenuation results per wavelength due to viscous and thermal losses scaled to mass loading in air with water droplets.

The attenuation results per distance are also shown in Figure 3.7 for comparison. Again, the abscissa of the plot is adjusted to $\omega\tau_d$. If the results are compared, attenuation per distance for frequencies above $\omega\tau_d = 1$, is dominated by viscous friction. It is almost two times more effective than heat conduction effects. It can be concluded that for noise suppression problems in a wide range of frequencies, one may focus on momentum exchange while not forgetting that the heat exchange may be significant in a narrow band at the lower frequencies.

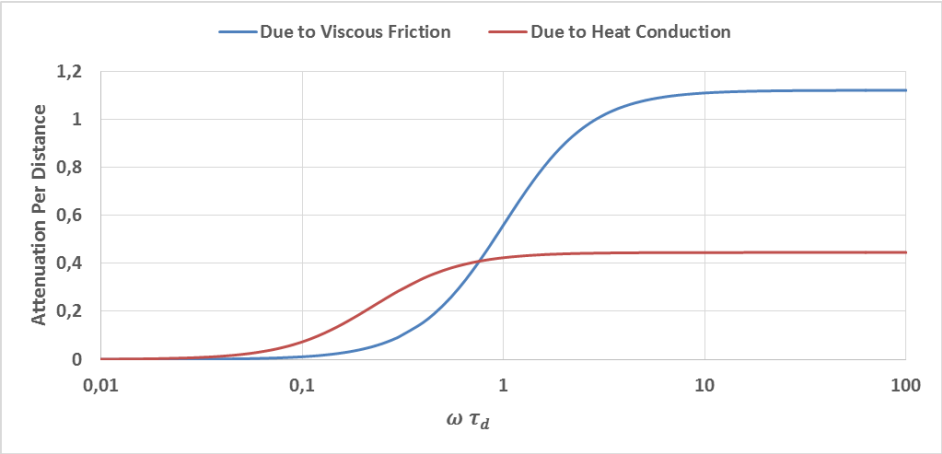


Figure 3.7 Attenuation results per meter due to viscous and thermal losses scaled to mass loading in air with water droplets.

The second parameter; namely the phase speed, can be obtained in the same manner by solving the determinant of the matrix again for complex wave number and then by checking its imaginary component. The simplified equation is expressed as [15];

$$ {c_o}^2 \Big/ {c(\omega)}^2 = 1 + \sigma_m \left\{ (\gamma_g - 1) \frac{c_{pp}}{c_{pg}} \frac{1}{1 + \omega^2 {\tau_T}^2} + \frac{1}{1 + \omega^2 {\tau_D}^2} \right\} \qquad (3.60) $$

The first term in parenthesis corresponds to the heat conduction while the second corresponds to the viscous drag.

The analytical results of dispersion ratio normalized to unit mass loading are plotted for viscous and thermal effects separately in Figure 3.8. It is observed that towards the higher frequency end, both converges to a value of unity. This means that the phase speed attains the value as if there are no droplets in air. Towards the lower frequency end, both lines converge to a specific value while the dispersion due to heat conduction seems to be more significant. To mention again, these results are valid if the mass loading is very low.

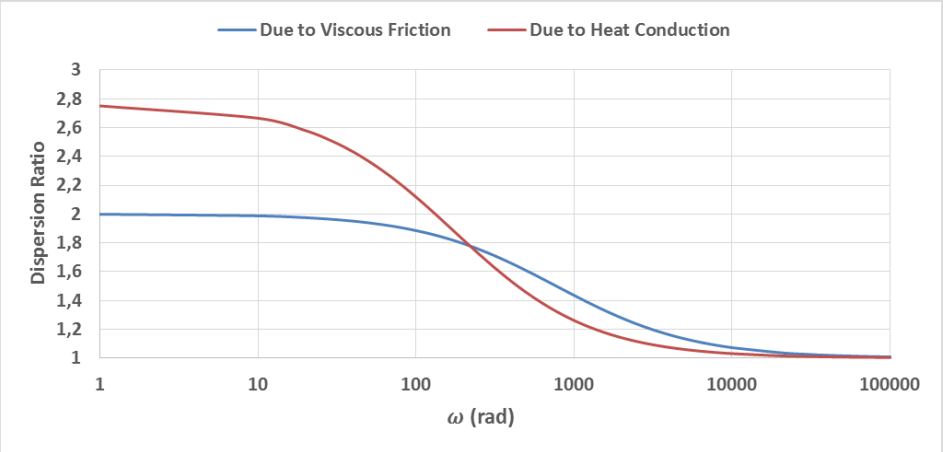


Figure 3.8 Dispersion ratio for viscous and thermal effects scaled to unit mass loading in air with water droplets.

3.5 Summary and Comments

In this chapter, the preliminaries of the coupled phase theory have been given. It is based on continuum theory. Fundamental equations needed to complete the system matrix have been derived for an aerosol and the corresponding assumptions have been specified in parallel. It is of utmost importance to address the theory at this depth in order to make the problem solvable by numerical techniques in the next step. Also, having understood the lacking parts and the constraints of the reference theory, it is possible to determine where the doctoral work can contribute to the theory.

System of equations have been derived for two cases, namely, with and without heat conduction effects between the phases. The analytical solution for each case is based on the assumption that an aerosol is dilute and the mass loading parameter is very low. The wave propagation is considered to be one dimensional plane wave. The mean flow effect is not included in the solution, either. As shown in Chapter 2, the experimental results that comply with these constraints and the theoretical results overlap at a very high level (Figure.2.2). On the other

hand, a numerical method is needed to be developed to obtain the solutions which the existing theoretical approaches fail to yield. These can briefly be listed as given below;

- The effect of finite volume concentrations,
- The effect of mean flow (convection effects),
- The effect of higher order duct modes,

on the attenuation and dispersion results.

CHAPTER 4

ONE DIMENSIONAL SOLUTIONS

The solutions to the acoustic wave propagation problems are usually obtained through analytical methods which have been developed under limiting conditions and assumptions. As mentioned in the previous chapter, the theoretical coupled phase solution has also its own limitations some of which can be overcome by dealing the problem by means of numerical methods. In this chapter, a numerical methodology based on finite difference method in frequency domain for solving the acoustic wave propagation problem in an aerosol is described. The main aim is to obtain the attenuation and dispersion results without making assumptions as many as the analytical reference does. In addition, the analytical solution will be extended to include the mean flow effect and the corresponding results will be compared with the numerical ones.

4.1 Numerical Approach

4.1.1 Model Development

Acoustic wave propagation problems may be classified depending on how complex they are. For example, if the problem does not include non-uniformity in the background (flow gradients in spatial coordinates, multi-phase etc.), solutions are obtained easily through linearized acoustic wave equation where only one acoustic variable is sufficient to describe the others. Otherwise; governing equations cannot be reduced into one equation and thus matrix equations needs to be solved for more than one system variable. There are several numerical

methods; namely, finite volume, finite element or finite difference, used to solve such problems in literature. Each of them has its own advantages and drawbacks. In this thesis, finite difference method has been chosen to be an appropriate method due to its efficiency and simplicity.

Wave propagation will be considered to be one dimensional (plane wave) as it is in the analytical method. In order to build a numerical model that allows plane wave propagation, a physical environment with boundaries is needed. The most appropriate example corresponding to this is the propagation of the acoustic wave in a channel with a circular cross section with perfectly reflective walls. A representative figure showing acoustic pressure variation fixed in time is given Figure 4.1 below. To allow only plane wave propagation, the diameter of the duct should not be higher than the first cut-off frequency for the first higher order mode in three dimensional models. This condition is satisfied anyway since the discretization of the problem will only be in axial direction hereby.

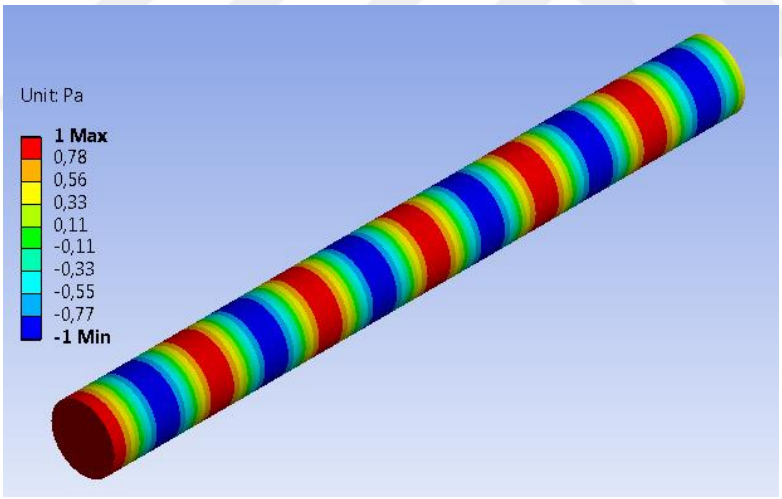


Figure 4.1 Representation of plane wave propagation in a circular-sectioned duct with full reflective walls.

The problem geometry considered in the present study is a circular duct filled with air and water droplets as depicted in Figure 4.2. In micro scale there might be countless number of droplets per unit volume which makes it impossible to track

individual particles toward a solution. However, successful results were obtained when the entire system was considered consisting of a single continuous particle phase with average parameters[101].

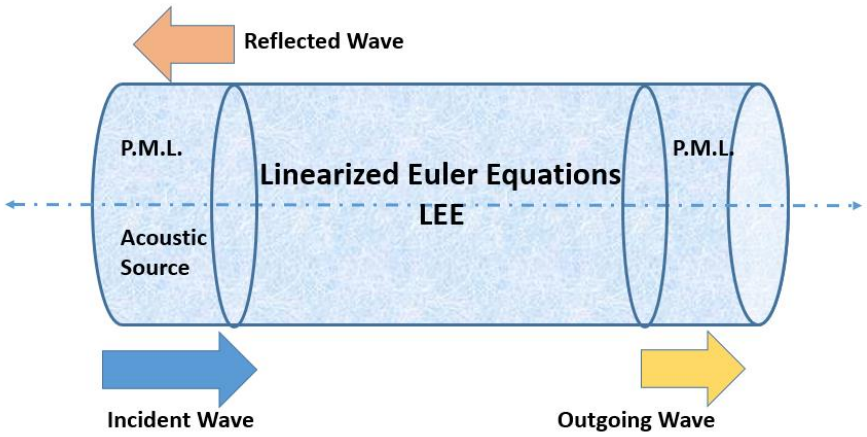


Figure 4.2 Illustration of the numerical problem with PML boundary definitions.

Each phase satisfies fundamental conservation laws and has its own state equation. The linearized Euler equations (LEE) are to be derived in frequency domain for describing propagation of sound waves. As for any other boundary value problems (since the problem domain is needed to be truncated) the definition of the conditions on the boundaries is one of the most challenging stage. In literature, there are several acoustic boundary conditions that permit the outgoing waves to leave the domain without being reflected (or with minimal reflection). The most popular two are;

- Radiation Boundary Condition: The Robin condition is used to apply an absorbing boundary. It is assumed that the boundary surface has the same impedance as the medium. This definition is restricted to have good accuracy only if the local wave (that impinges on the boundary) is planar. The mathematical formulation is as given below:

$$\frac{\partial p}{\partial \vec{n}} + j\omega \frac{1}{c_o} p = 0 \tag{4.1}$$

where $\vec{n}$ is the normal vector, c_o is the speed of sound and ω is the circular frequency.

- Perfectly Matched Layers (PML): This definition was first proposed by Hu [103], [104], and then extended to axisymmetric problems for solving turbo machinery noise radiation problem [105]–[107]. The theory behind this method is to have layers of elements that can absorb all outgoing waves while preserving the incoming (propagating) waves. Also this condition can be used to define the acoustic wave input on the boundary by decomposing the wave field into reflected and incoming waves [106].

According to their capabilities, PML condition has been chosen to be the most suitable boundary condition for acoustic problems to be covered in this study. More details of this method and its implementation will be given in the following sections.

4.1.2 Governing Equations

The 1-D, time-dependent, linearized Euler equations (LEE) are transformed into the frequency domain by assuming the perturbations of the primitive-dependent variables are of the form;

$$q'(x,t) = \Re\{\hat{q}(x)e^{i\omega t}\} \tag{4.2}$$

where;

$$q'(x,t) = \left[\rho_g', u_g', p_g', T_g', \emptyset_v{}', u_p', T_p'\right]^T \tag{4.3}$$

$$\hat{q}(x) = \left[\hat{\rho}_g, \hat{u}_g, \hat{p}_g, \hat{T}_g, \widehat{\emptyset}_v, \hat{u}_g, \hat{T}_g\right]^T \tag{4.4}$$

where ρ_g' is the density perturbation, u_g' is the axial velocity perturbation, p_g' is the pressure perturbation and T_g' is the temperature perturbation for the gas phase (air) while $\emptyset_v{}'$ is the volume concentration perturbation, u_p' is the axial velocity perturbation and T_p' is the temperature perturbation for the particle phase (water droplets). A hat on a variable means it is complex-valued and ω is the circular frequency.

The linearized system of equations for the two phase model with mean flow is given in from Eq. (4.5) to Eq. (4.11). As the time dependence of the system variables is specified as in Eq. (4.2), the time derivative terms are replaced with $i\omega$ for harmonic variation in time. One can see additional terms on the left hand side of the equations starting with σ_x which are damping terms related to perfectly matched layer (PML) equations solved in narrow regions at both ends of the duct. How these equations are applied is explained in the next section. The losses due to viscous effects (friction) and heat conduction on the tube surfaces are ignored.

$$i\omega\hat{\rho}_g + u_o\frac{\partial\hat{\rho}_g}{\partial x} + \rho_{go}\frac{\partial\hat{u}_g}{\partial x} + \sigma_x\hat{\rho}_g + \frac{\sigma_x M}{1-M^2}\frac{1}{c_o}\left(u_o\hat{\rho}_g + \rho_{go}\hat{u}_g\right) = 0 \tag{4.5}$$

$$\begin{aligned} i\omega\hat{u}_g + u_o\frac{\partial\hat{u}_g}{\partial x} + \frac{1}{\rho_{go}}\frac{\partial\hat{p}_g}{\partial x} - \frac{1}{\rho_{fo}}F_D\left(\hat{u}_p - \hat{u}_g\right) + \sigma_x\hat{u}_g \\ + \frac{\sigma_x M}{1-M^2}\frac{1}{c_o}\left(u_o\hat{u}_g + \frac{1}{\rho_{go}}\hat{p}_g\right) = 0 \end{aligned} \tag{4.6}$$

$$\hat{p}_g - \bar{R}T_{go}\hat{\rho}_g - \bar{R}\rho_{go}\hat{T}_g = 0 \tag{4.7}$$

$$i\omega\hat{T}_g + u_o\frac{\partial\hat{T}_g}{\partial x} + \frac{P_o}{\rho_{go}c_{vg}}\frac{\partial\hat{u}_g}{\partial x} - \frac{1}{\rho_{go}c_{vg}}Q_c\left(\hat{T}_p - \hat{T}_g\right) + \sigma_x\hat{T}_g + \frac{\sigma_x M}{1-M^2}\frac{1}{c_o}\left(u_o\hat{T}_g + \frac{P_o}{\rho_{go}c_{vg}}\hat{u}_g\right) = 0 \tag{4.8}$$

$$i\omega\widehat{\emptyset}_v + u_o\frac{\widehat{\emptyset}_v}{\partial x} + \emptyset_{vo}\frac{\partial\hat{u}_p}{\partial x} + \sigma_x\widehat{\emptyset}_v + \frac{\sigma_x M}{1-M^2}\frac{1}{c_o}\left(u_o\widehat{\emptyset}_v + \emptyset_{vo}\hat{u}_p\right) = 0 \tag{4.9}$$

$$i\omega\hat{u}_p + u_o\frac{\partial\hat{u}_p}{\partial x} + \frac{1}{\rho_{po}\emptyset_{vo}}F_D\left(\hat{u}_p - \hat{u}_g\right) + \sigma_x\hat{u}_p + \frac{\sigma_x M}{1-M^2}\frac{1}{c_o}u_o\hat{u}_p = 0 \tag{4.10}$$

$$i\omega\hat{T}_p + u_o\frac{\partial\hat{T}_p}{\partial x} + \frac{1}{\rho_{po}c_{pp}\emptyset_{vo}}Q_c\left(\hat{T}_p - \hat{T}_g\right) + \sigma_x\hat{T}_p + \frac{\sigma_x M}{1-M^2}\frac{1}{c_o}u_o\hat{T}_p = 0 \tag{4.11}$$

The first four equations correspond to the fluid phase while the others to the particle phase. $\emptyset_{vo}$, ρ_{go}, ρ_{po} , $\bar{R}$, T_{go}, P_o, c_{vg}, c_{pp} are the average volume concentration of particles, the density of the gas, the density of the particles, the specific gas constant of the gas, the temperature of the gas, the static pressure value of the gas, specific heat capacity at constant volume of the gas and specific heat capacity of particles at constant pressure, respectively. The linearized relation between temperature, density and pressure is defined by Eq. (4.7) assuming the air is an ideal gas. Due to the fact that the compressibility of the water droplets is very low compared to air, the particle pressure perturbations are neglected which results in no need for the state equation for the particle phase. In other words, the water droplets are considered as rigid particles as they are in reference [99].

The coupling between the two phases is thought to be through momentum transfer F_D and heat transfer Q_c acting on the particles. To proceed with the solution of the problem, these transfer mechanisms must be specified beforehand. However, if the rigid particles are assumed to have spherical shape and the Reynolds number (Re) based on relative velocity is considered to be low (Re << 1), the coupling functions can be defined through the drag force given for Stokes flow and heat conduction equations as;

$$F_D = 6\pi\mu_g a_p N \tag{4.12}$$

$$Q_c = 4\pi k_g a_p N \tag{4.13}$$

where μ_g and k_g are the dynamic viscosity and heat conductivity of the gas, respectively, while a_p is the mean radius and N is the total number (per unit volume) of the particles. By checking the Eq. (4.12) and Eq. (4.13), the total effect on a control volume is considered as the linear summation of the effects on the each particle, which can be regarded as true when the suspension is dilute.

4.1.3 Boundary Conditions and Acoustic Source Definitions

Anechoic boundary conditions are needed to let the acoustic perturbations leave the numerical domain without reflections. This is achieved by PML definitions in small regions at each end. PML equations are based on Hu's formulation [104]. Except the state equation for the fluid phase, a spatially damping factor σ_x is included in each equation. The form of the damping factor is given by

$$\sigma_x = (1 - M^2) c_o \sigma_{max} \left| \frac{x - x_i}{L_{ref}} \right|^2 \tag{4.14}$$

where, x_i is the location of the interface, c_o is the isentropic speed of sound, L_{ref} is the reference length of the PML region and σ_{max} is taken as $\sigma_{max}\,\Delta x / L_{ref} = 2$ [106], [107]. Damping factor σ_x should have a value of zero at the interface and increase towards the outer edge exponentially in order to be an efficient radiation boundary.

Total perturbations (for the gas) are to be separated into incident and reflected components to define the acoustic sources in one of the PML regions as;

$$\hat{q}\,(x) = \begin{bmatrix} \hat{\rho}_g \\ \hat{u}_g \\ \hat{p}_g \\ \hat{T}_g \end{bmatrix} = \begin{bmatrix} \hat{\rho}_{g,in} \\ \hat{u}_{g,in} \\ \hat{p}_{g,in} \\ \hat{T}_{g,in} \end{bmatrix} + \begin{bmatrix} \hat{\rho}_{g,ref} \\ \hat{u}_{g,ref} \\ \hat{p}_{g,ref} \\ \hat{T}_{g,ref} \end{bmatrix} \tag{4.15}$$

where subscripts g, in and g, ref corresponds to the incident and reflected components of the acoustic variables for the gas. One can simply set the reflected part to be equal to zero and define the source terms as coming from the incident components on the right hand side of Eq. (4.5) to Eq. (4.8). The resulting equations for the gas phase are as given below;

$$\begin{aligned} i\omega\hat{\rho}_g + u_o \frac{\partial \hat{\rho}_g}{\partial x} + \rho_{go} \frac{\partial \hat{u}_g}{\partial x} + \sigma_x \hat{\rho}_g + \frac{\sigma_x M}{1 - M^2} \frac{1}{c_o} \left(u_o \hat{\rho}_g + \rho_{go} \hat{u}_g \right) \\ = \left[i\omega\hat{\rho}_{g,in} + u_o \frac{\partial \hat{\rho}_{g,in}}{\partial x} + \rho_{go} \frac{\partial \hat{u}_{g,in}}{\partial x} + \sigma_x \hat{\rho}_{g,in} \right. \\ \left. + \frac{\sigma_x M}{1 - M^2} \frac{1}{c_o} \left(u_o \hat{\rho}_{g,in} + \rho_{go} \hat{u}_{g,in} \right) \right] \end{aligned} \tag{4.16}$$

$$i\omega\hat{u}_g + u_o\frac{\partial\hat{u}_g}{\partial x} + \frac{1}{\rho_{go}}\frac{\partial\hat{p}_g}{\partial x} + \sigma_x\hat{u}_g + \frac{\sigma_x M}{1-M^2}\frac{1}{c_o}\left(u_o\hat{u}_g + \frac{1}{\rho_{go}}\hat{p}_g\right)$$
$$= \left[i\omega\hat{u}_{g,in} + u_o\frac{\partial\hat{u}_{g,in}}{\partial x} + \frac{1}{\rho_{go}}\frac{\partial\hat{p}_{g,in}}{\partial x} + \sigma_x\hat{u}_{g,in} + \frac{\sigma_x M}{1-M^2}\frac{1}{c_o}\left(u_o\hat{u}_{g,in} + \frac{1}{\rho_{go}}\hat{p}_{g,in}\right)\right] \quad (4.17)$$

$$\hat{p}_g - \bar{R}T_{go}\hat{\rho}_g - \bar{R}\rho_{go}\hat{T}_g = \left[\hat{p}_{g,in} - \bar{R}T_{go}\hat{\rho}_{g,in} - \bar{R}\rho_{go}\hat{T}_{g,in}\right] \quad (4.18)$$

$$i\omega\hat{T}_g + u_o\frac{\partial\hat{T}_g}{\partial x} + \frac{P_o}{\rho_{go}c_{vg}}\frac{\partial\hat{u}_g}{\partial x} + \sigma_x\hat{T}_g + \frac{\sigma_x M}{1-M^2}\frac{1}{c_o}\left(u_o\hat{T}_g + \frac{P_o}{\rho_{go}c_{vg}}\hat{u}_g\right)$$
$$= \left[i\omega\hat{T}_{g,in} + u_o\frac{\partial\hat{T}_{g,in}}{\partial x} + \frac{P_o}{\rho_{go}c_{vg}}\frac{\partial\hat{u}_{g,in}}{\partial x} + \sigma_x\hat{T}_{g,in} + \frac{\sigma_x M}{1-M^2}\frac{1}{c_o}\left(u_o\hat{T}_{g,in} + \frac{P_o}{\rho_{go}c_{vg}}\hat{u}_{g,in}\right)\right] \quad (4.19)$$

One may recognize that coupling terms have been dropped out. This is because there is no need for a coupled solution in the PML region. However, what is needed to know beforehand is the information about incident waves. Together with the definition of the wave number as $k = \omega/c_o$ and$\partial/\partial x = -ik$, the perturbations can be obtained from the corresponding governing equations.

$$\hat{p}_{g,in} = Ae^{-ik\,x}e^{i\omega t} \quad (4.20)$$

$$\hat{u}_{g,in} = \frac{k}{\rho_{go}(\omega - u_o k)}\hat{p}_{g,in} \quad (4.21)$$

$$\hat{\rho}_{g,in} = \frac{\rho_{go} k}{(\omega - u_o k)} \hat{u}_{g,in} \tag{4.22}$$

$$\hat{T}_{g,in} = \frac{k\, P_o}{\rho_{go} C_{vg} (\omega - u_o k)} \hat{u}_{g,in} \tag{4.23}$$

where A is an arbitrary amplitude value of the incident pressure perturbations.

4.1.4 Numerical Schemes

The numerical solution of the problem ultimately requires that a linear matrix system be formed and solved directly or iteratively in order to compute the acoustic variables simultaneously at each grid. If the matrix size is sufficiently small with respect to the RAM capacity of the solution computer, direct methods are preferred since they are faster and more robust. One critical issue is choosing the most appropriate numerical scheme for spatial discretization of the problem shown in Figure 4.2.

Different types of numerical schemes appeared in literature for solving the present type of governing equations. Most suitable schemes for preserving the dispersion relation of the governing equations are based on high-order discretization. Among them one important scheme is the so-called dispersion relation preserving (DRP) scheme of Tam and Webb [108] which is based on minimizing the dispersion error of the numerical scheme over a given range of wavenumbers. This idea was later extended to other variants of both finite difference [109] and finite volume schemes [110]. Collocation based schemes, such as linear B-spline Galerkin scheme [111], have also found use in literature. For example, Özyörük [112] reported that B-spline Galerkin method has compatible or even better dispersion properties. However, in this thesis, due to loss of formal accuracy at and near the domain boundaries of non-uniform cross-sectional geometries, standard 4th-order finite difference scheme with sufficient number of grid points per wavelength (NPPW) was preferred rather than linear B-spline Galerkin scheme. Quite high-

resolution meshes (number of control volumes) with uniform spacing are used to make sure dispersion errors are minimal (NPPW ~ 40). The illustration of the numerical discretization is shown in Figure 4.3.

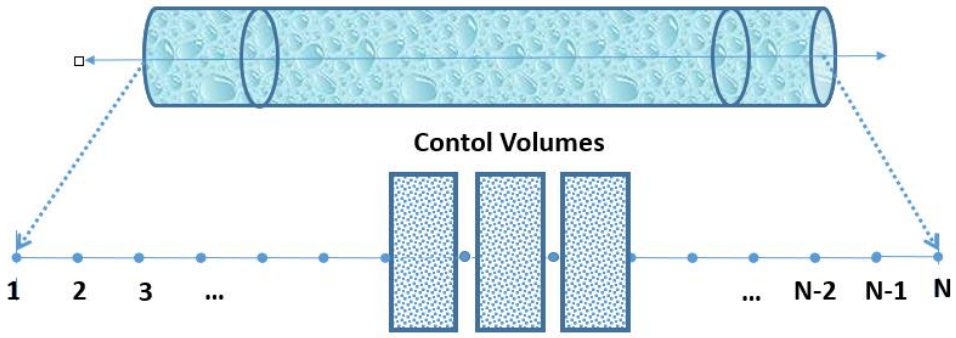


Figure 4.3 The illustration of the numerical discretization for 1-D solution.

The coefficients used for 1-D spatial discretization are given in Table 4.1. As mentioned before, the scheme has 4th order accuracy for inner nodes, while the order is decreased by one for those at the boundaries.

Table 4.1 Finite difference coefficients used for 1-D spatial discretization

	X-3	*X-2*	*X-1*	*X*	*X+1*	*X+2*	*X+3*
Node 1	-	-	-	-11/6	3	-3/2	1/3
Node 2	-	-	-2/6	-3/6	1	-1/6	-
Node 3 : N-2	-	1/12	-2/3	0	2/3	-1/12	-
Node N-1	-	1/6	-1	3/6	2/6	-	-
Node N	-1/3	3/2	-3	11/6	-	-	-

4.1.5 Verification of the Code

The numerical code has been developed in MATLAB software. Before using the code for aerosol solution, the developed algorithms are tested against sound

propagation through an infinite circular duct without any particles, in other words, the medium is considered as a single phase air. The results have been obtained for two different cases which are a) without mean flow and b) with mean flow conditions and they have been checked with the analytical results.

4.1.5.1 Solver Verification: Wave propagation in an infinite circular duct without particles

The first validation case is for plane wave propagation in an infinite duct without water droplets. In the developed code the volume concentration of the water droplets is just fixed to a very low number ($\emptyset_{vo} = 10^{-15}$) as if the medium purely consists of air. The exact case includes no end boundaries, but in numerical solution the domain is finite and PML equations are applied to damp the outgoing waves at duct ends. The acoustic source with a frequency of 500 Hz is included in the PML equations on the left side, so that waves propagate to the right. They get absorbed through the right PML. The lengths of PMLs are taken twice as the wavelength. The damping factors σ_x are varied from zero at the interface between the interior region and PML to about 40,000 by the left and right end. Logarithmic plot of σ_x is shown in Figure 4.4. NPPW is kept fixed to 40 as pointed out before.

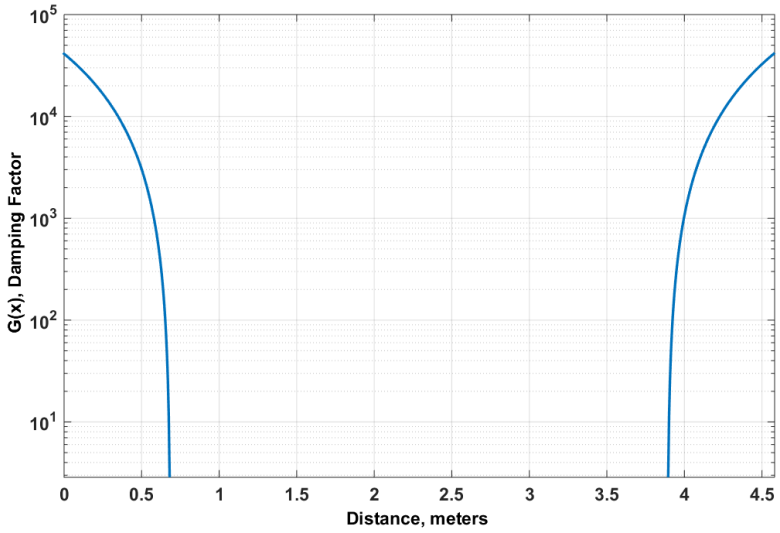


Figure 4.4 Variation of the damping factor σ_x w.r.t axial distance at f = 500 Hz.

Without Mean Flow

Computational and exact, closed-form results are compared in Figure 4.5. Except the PML at the right boundary where the pressure perturbation dies out, the computational results match perfectly with the exact solution in the inner region as well as the left PML where the acoustic source is defined. Note that the difference appearing at the right end is due to absorption of the computed waves by the PML equations to prevent reflections.

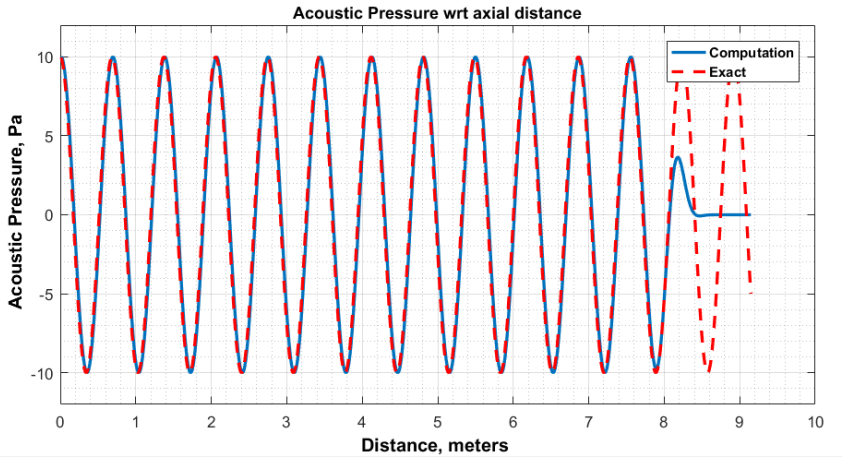


Figure 4.5 Comparison of the computed pressure perturbations with exact solution at f = 500 Hz.

In Figure 4.6, the computed numerical dispersion ratio ${c_o}^2/c(\omega)^2$ is plotted as a function of frequency starting from 10 Hz to 8,000 Hz. No noticeable dispersion (change) is observed in the considered frequency range. This is an expected result because the mesh resolution has been taken sufficiently high.

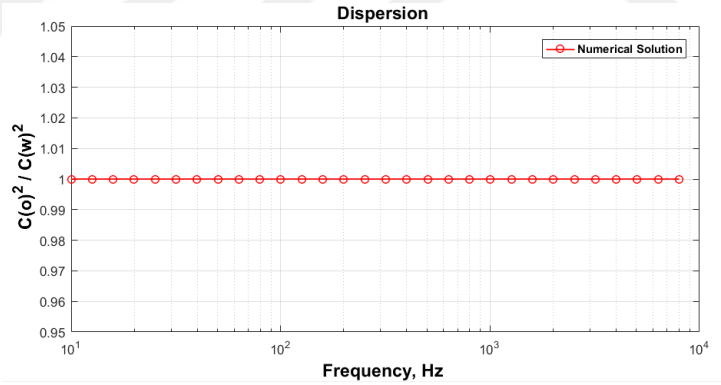


Figure 4.6 The computed dispersion ${c_o}^2/c(\omega)^2$ results versus frequency.

Consequently, the verification of the 1-D code has been completed by single phase medium without mean flow condition.

With Mean Flow

Computational and exact results are compared in Figure 4.7 and Figure 4.8, for mean flow conditions $u_o = 100$ m/s, $u_o = -100$ m/s respectively. Except the right end location (PML exit boundary), computed results match perfectly with the analytical results.

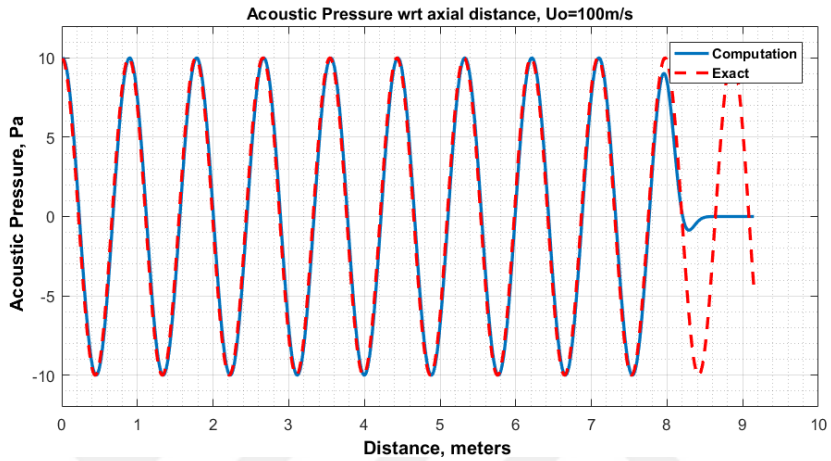


Figure 4.7 Comparison of the computed pressure perturbations at u_o=100 m/s with exact solution at f = 500 Hz.

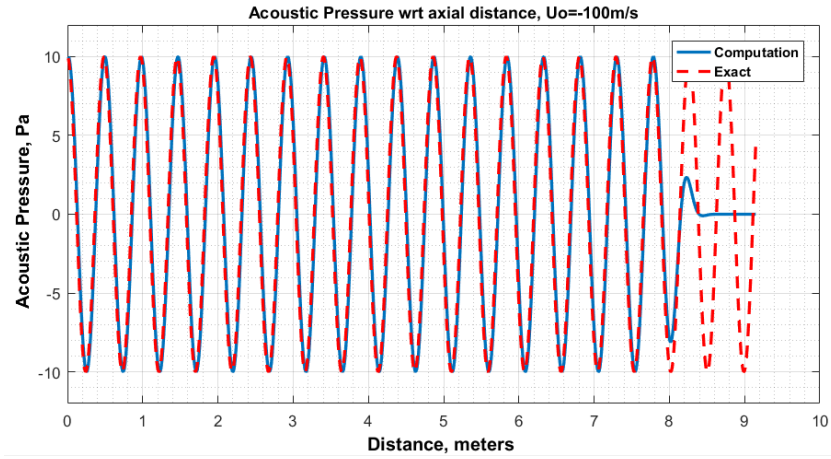


Figure 4.8 Comparison of the computed pressure perturbations at u_o=-100 m/s with exact solution at f = 500 Hz.

In Figure 4.9 and Figure 4.10, the computed numerical dispersion ratios $c_o{}^2/c(\omega)^2$ are plotted for flow conditions $u_o = 100$ m/s, $u_o = -100$ m/s, respectively. According to the theory [102], the dispersion changes with the mean flow velocity in accordance with the relation $^{c_o}/_{c(\omega)} = {}^{1}/_{(1+u_o/c_o)}$. The computed results show perfect coherence with the theoretical results. Consequently, the validation cases show that the developed code is highly accurate and the boundary conditions work well for the case of sound propagation without particles.

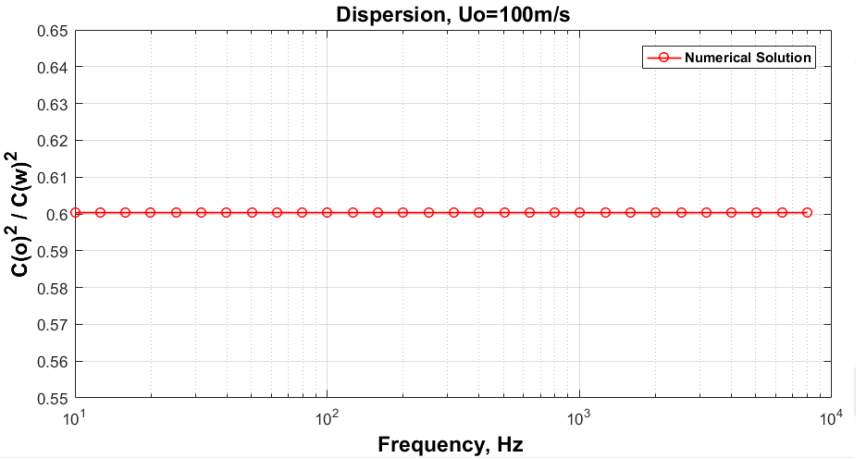


Figure 4.9 The computed dispersion $c_o{}^2/c(\omega)^2$ results with respect to frequency, u_o=100 m/s.

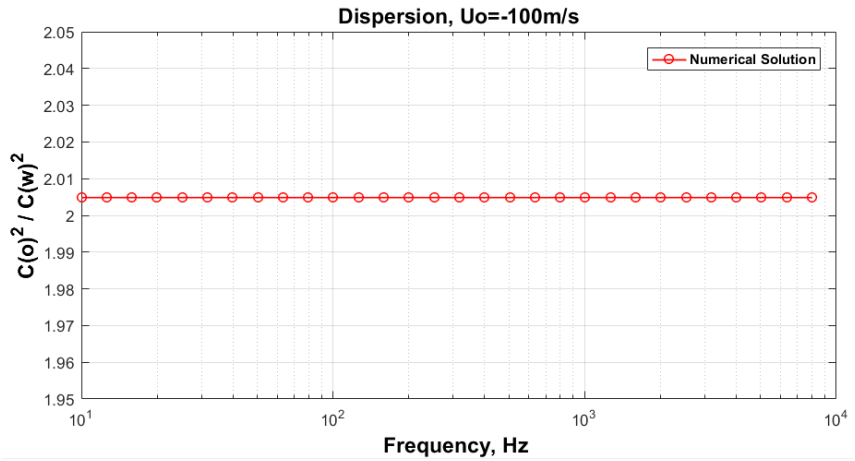


Figure 4.10 The computed dispersion $c_o{}^2/c(\omega)^2$ results with respect to frequency, u_o=-100 m/s.

4.2 Extensions to the Theoretical Solution for Mean Flow

Although there is a mean flow condition in most of the related applications of aerosol acoustics, existing analytical models do not include this effect. The numerical code based on finite difference method has the capability to account for convection (mean flow) effects on wave propagation in an aerosol. In order to compare the numerical results, theoretical approach of Temkin's [99] coupled phase model for stationary medium has been extended so as to include mean flow effects.

4.2.1 Sound Propagation with Momentum Exchange under Mean Flow

The first case involves evaluation of the attenuation and dispersion parameters for a medium composed of air and water droplets without thermal effects. Since the energy transfer between the phases is only allowed through momentum exchange, the energy equations are indeed not required. The equation of state is used to write $\hat{\rho}_g$in terms of $\hat{p}_g$. The derivative terms have been written as $\partial/\partial t = -i\omega$ and $\partial/\partial x = i\hat{k}$. After these simplifications, the corresponding system of equations take the form given below;

$$-i\frac{\omega}{{c_o}^2}\hat{p}_g + i\frac{\hat{k}\,u_o}{{c_o}^2}\hat{p}_g + i\hat{k}\,\rho_{go}\hat{u}_g = 0 \tag{4.24}$$

$$\left(-i\omega + i\hat{k}\,u_o + \frac{\sigma_m}{\tau_d}\right)\hat{u}_g - \frac{\sigma_m}{\tau_d}\hat{u}_p + i\hat{k}\,\hat{p}_g = 0 \tag{4.25}$$

$$-\frac{1}{\tau_d}\hat{u}_g + \left(-i\omega + i\hat{k}\,u_o + \frac{1}{\tau_d}\right)\hat{u}_g = 0 \tag{4.26}$$

Upon re-arranging the equations to get a single matrix equation, it ended up with;

$$\begin{bmatrix} \rho_{go}\hat{k} & 0 & -\omega + u_o\hat{k}/{c_o}^2 \\ -i\omega + iu_o\hat{k} + \sigma_m/\tau_d & -\sigma_m/\tau_d & i\,\hat{k}/\rho_{go} \\ -1/\tau_d & -i\omega + iu_o\hat{k} + 1/\tau_d & 0 \end{bmatrix} \begin{pmatrix} \hat{u}_g \\ \hat{u}_p \\ \hat{p}_g \end{pmatrix} = 0 \tag{4.27}$$

It is not easy to get $\hat{k}$ in terms of other parameters directly. In order to achieve this, a complete analytical solution has been implemented by using the Symbolic Math Toolbox™ of MATLAB® software[113]. By setting the determinant of the matrix equal to zero, complex values of $\hat{k}$ has been calculated for specified frequencies and fixed system parameters. The real part of $\hat{k}$ is equal to $c(\omega)/\omega$ which is called the phase speed and the imaginary part is α (attenuation per distance). The corresponding results will be shared in the following chapter.

4.2.2 Sound Propagation with Momentum and Thermal Exchange under Mean Flow

In the second case, sound propagation with thermal effects and mean flow condition will be investigated. Similar to the first case, the derivative terms have been taken as $\partial/\partial t = -i\omega$ and $\partial/\partial x = i\hat{k}$. The momentum exchange is also included in the solution together with the heat exchange between phases. u_p and T_p can be written in terms of u_g and T_g by using Eq. (3.53) and Eq. (3.54), respectively, thus eliminating the equations of momentum and energy for particles. The corresponding system matrix can be arranged as given below;

$$\begin{bmatrix} -\omega + \hat{k}u_o & \rho_{go}\hat{k} & 0 & 0 \\ 0 & -i\omega + i\hat{k}u_o + B & \hat{k}/\rho_{go} & 0 \\ -\bar{R}T_{fo} & 0 & 1 & -\bar{R}\rho_{go} \\ 0 & \hat{k}P_o/\rho_{go}C_{vg} & 0 & -\omega + \hat{k}u_o + D \end{bmatrix} \begin{pmatrix} \hat{\rho}_g \\ \hat{u}_g \\ \hat{p}_g \\ \hat{T}_g \end{pmatrix} = 0 \tag{4.28}$$

where;

$$B = \frac{\sigma_m}{\tau_d}\left(1 - \frac{1}{\left(1 - i\left(\omega + \hat{k}u_o\right)\tau_d\right)}\right) \tag{4.29}$$

$$D = \frac{c_{pp}}{c_{vg}}\frac{\sigma_m}{\tau_d}\left(1 - \frac{1}{\left(1 - \left(\omega + \hat{k}u_o\right)\tau_t\right)}\right) \tag{4.30}$$

To obtain a non-trivial solution for $\hat{k}$ determinant of 4x4 matrix must be zero. In order to achieve this, a complete analytical solution has again been implemented by using the Symbolic Math Toolbox™ of MATLAB® software. The corresponding results will be shared in the next chapter.

CHAPTER 5

ONE DIMENSIONAL RESULTS AND COMPARISONS

In this chapter, acoustic results obtained by the numerical code are shared and compared with the analytical results of coupled-phase theory which have already been verified with the experimental results. The results are then extended to several different cases for system inputs in order to see the corresponding outputs. In addition, the acoustic results of mean flow conditions are presented together with the comparison of numerical code and extended analytical solutions.

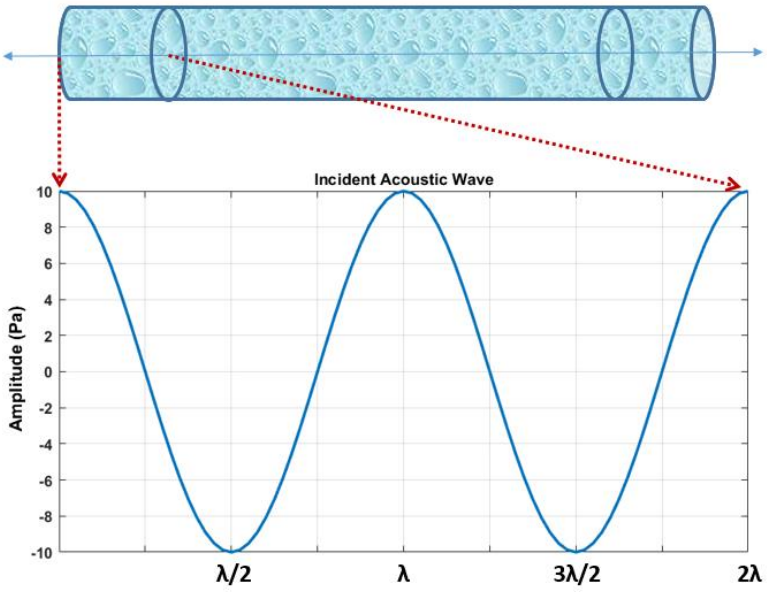


Figure 5.1 Representation of the 1-D problem and the definition of the incident acoustic wave.

As shown in Figure 5.1, the incident acoustic wave have been defined on the left side of the numerical domain. The value of NPPW is taken as 40 and it is fixed for

any frequency. The total number of NPPW in the solution domain is 400 which is equal to a value of 10 complete wavelengths. So, the total number of the solution grids is kept constant by adjusting the length of the elements. This will keep the numerical solution both stable and accurate as we are interested in the acoustic outputs per unit scales. As mention before, PML equations are used for non-reflecting outlet and inlet condition as well as incident wave definition. In all of the numerical solutions here, PML regions are adjusted to cover two times the wavelength of the solution frequency. Thus, incident wave has also the same wavelength which is sufficiently long for a correct numerical solution. The damping factors σ_x are varied from zero at the interface between the interior region and PML to about 40,000 by the left and right end. Logarithmic plot of the σ_x is shown in Figure 5.2.

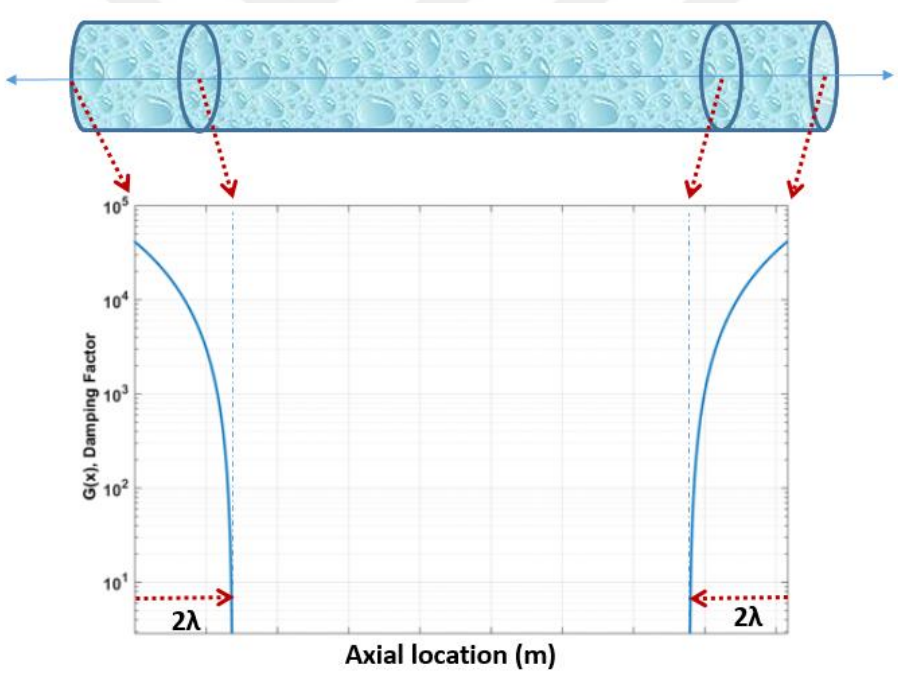


Figure 5.2 Variation of the damping factor σ_x for calculations

5.1 Sound Propagation with Only Momentum Exchange

The first set of result will be shared for the case where heat transfer between the two phases is neglected.

5.1.1 Comparisons with Analytical Results

Both numerical and analytical solutions have been calculated with the system parameters given in Table 5.1. The corresponding physical properties for the materials have been shared in Appendix-A.

Table 5.1 System parameters used in the numerical solution.

Parameters	**Gas Phase**	**Particle Phase**	**Particle Size (Average)**	**Volume Concentration**
Value	Air @ 20^{o}C	Water Droplets @ 20^{o}C	5 x 10^{-6} m	0.1%,0.01%, 0.001%

In Figure 5.3 the computed scaled attenuation parameter $\hat{\alpha} = \alpha\, c_o/\omega$ is plotted for three different volume concentrations, $\emptyset_{vo} = 0.001\,\%$, $\emptyset_{vo} = 0.01\%$ and $\emptyset_{vo} = 0.1\,\%$. It is clear from the presented results that when the volume concentration is as low as % 0.001, the numerical and analytical results match perfectly. As the volume concentration goes up to % 0.1, the numerical results for the scaled attenuation get lower in value than the analytical reference one for dilute suspensions with very low mass ratio. This is an expected outcome because the generalized version of Eq. (3.46) includes an additional term $c(\omega)\,/c_o$ as a multiplier where $c(\omega)$ is the dispersed wave speed. Thus, when the phase speed changes, the attenuation also changes accordingly.[114]

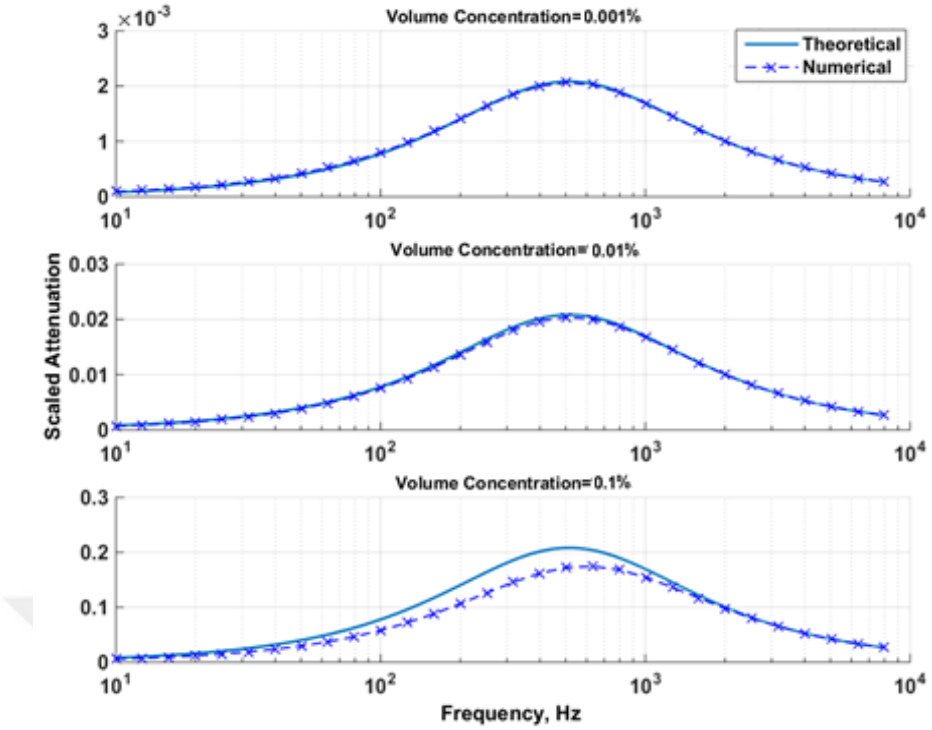


Figure 5.3 Comparison of the computed scaled attenuation $\hat{\alpha} = \alpha\ c_o/\omega$ with theoretical (analytical) solution which is valid for low mass loading σ_m solid line is the theoretical (analytical) and dashed line is the numerical.

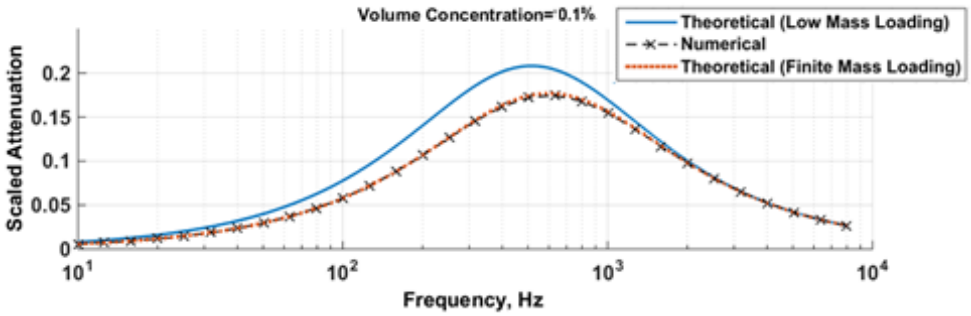


Figure 5.4 Comparison of the computed scaled attenuation $\hat{\alpha} = \alpha\ c_o/\omega$ with theoretical (analytical) solution which is valid for finite mass loading σ_m, solid line is the theoretical (analytical) and dashed with line is the numerical.

The comparison of the scaled attenuations for $\emptyset_{vo} = 0.1\,\%$ is shown in Figure 5.4. It is evident that the numerical results agree perfectly with the reference solutions that include the effect of finite mass loading. From the same graph, one can also recognize that when the mass loading becomes finite, the value of the frequency that corresponds to the maximum scaled attenuation changes. It has a tendency to shift up as the acoustic waves are more dispersed.

In Figure 5.5 the variation of the calculated numerical dispersion ratio ${c_o}^2/c(\omega)^2$ for volume concentrations is shown together with the analytical results.

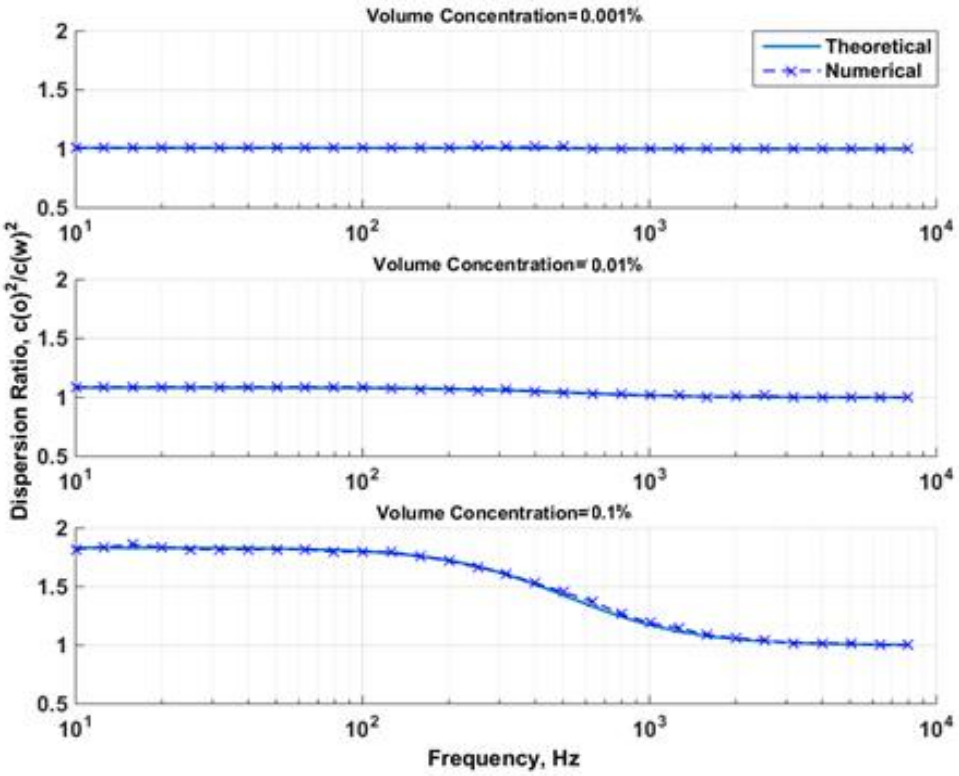


Figure 5.5 Comparison of the computed dispersion ${c_o}^2/c(\omega)^2$with theoretical (analytical) solution which is valid for low mass loading σ_m, solid line is the theoretical (analytical) and dashed with line is the numerical.

These results indicate that the numerical dispersion variation matches almost perfectly with the analytical reference for both low and higher volume

concentrations. The acoustic wave seems to be more dispersed towards the low frequency limit while the phase speed is equal to the isentropic speed of sound of purely air beyond the frequency which corresponds to the dynamic relaxation time given in Eq. (3.11).

5.1.2 Additional Numerical Results

In addition to the results given in the preceding section, additional results obtained for parametric cases are shared in order to show the relation between the outputs and input variables. Similar to the previous case, system parameters used in the calculations are the same as given in Table 5.1.

Acoustic pressure amplitudes along the duct fixed in time is shown in Figure 5.6 for three different volume concentration levels of 0.001%, 0.01% and 0.1%. The frequency of the incident wave is equal to 1,000Hz. In analogous with the previously given results, it can be also seen here that the amplitudes decay more rapidly as the concentration level increases. Especially for the concentration level is equal to 0.1%, it is quite clear that the dispersion occurs as the wavelengths become narrower.

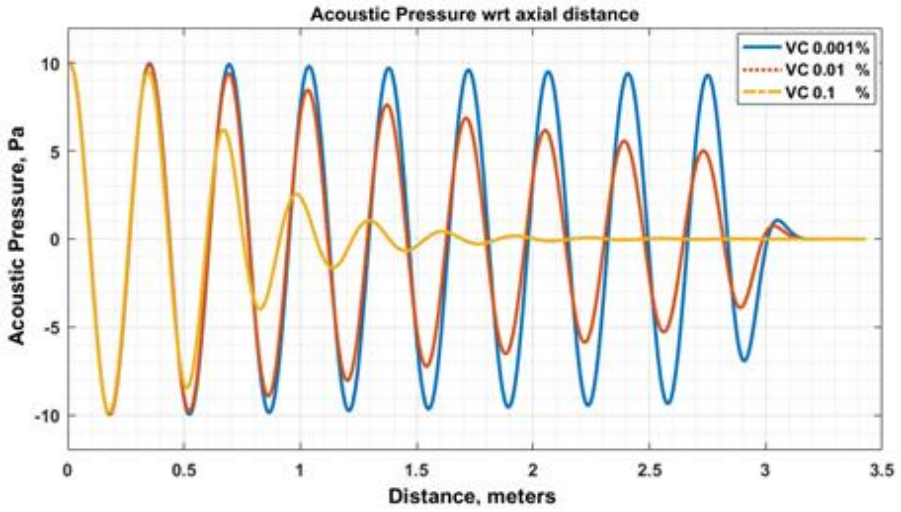


Figure 5.6 Acoustic pressure amplitudes for particle volume concentration levels of 0.001%, 0.01% and 0.1%.

Another representation of the acoustic pressure is shown in Figure 5.7, by operating the pressure amplitudes in dB scale. It is interesting to see that for the corresponding system parameters at 1,000 Hz, the attenuation is nearly 20 dB per meter when the concentration is 0.1%.

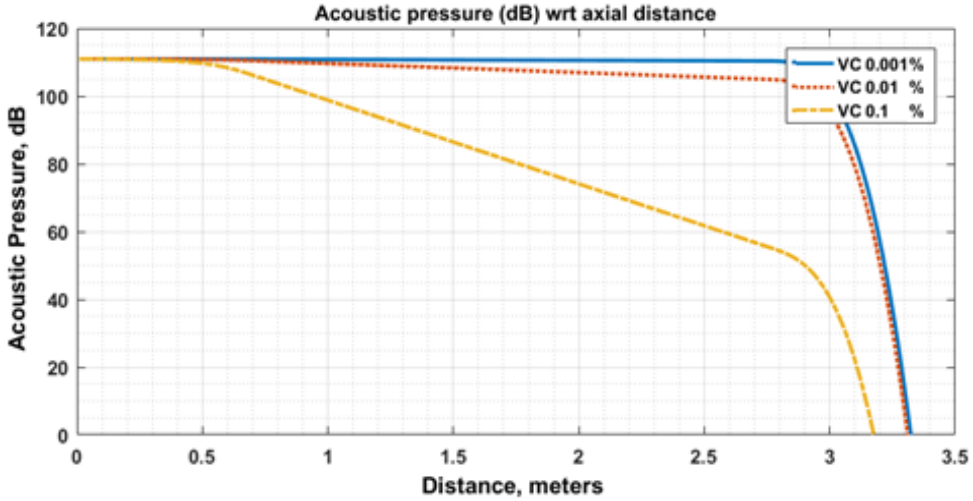


Figure 5.7 Acoustic pressure levels in dB scale for particle volume concentration levels of 0.001%, 0.01% and 0.1%.

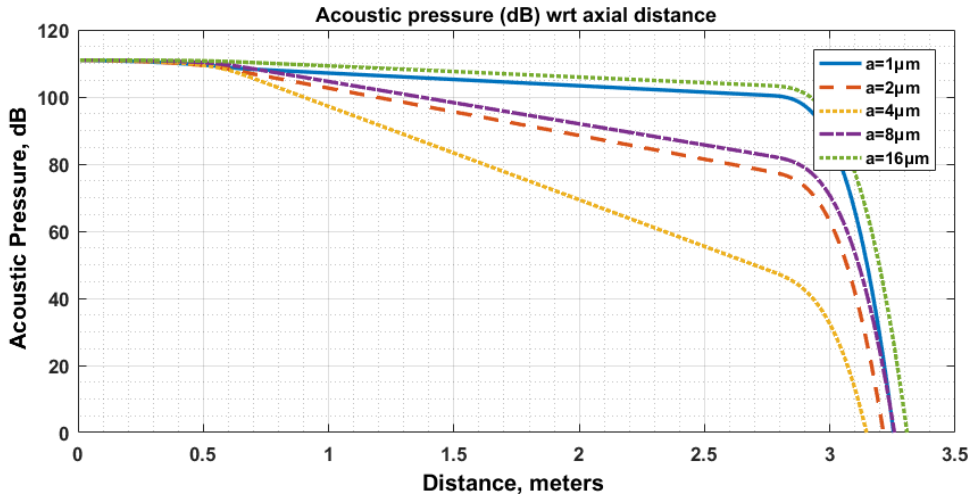


Figure 5.8 Acoustic pressure levels in dB scale for particle size of 1μm, 2μm, 4μm, 8μm and 16μm, at frequency of 1,000 Hz.

The effect average particle size at fixed frequency of 1,000 Hz on the attenuation is shown in Figure 5.8. The acoustic pressure results have been obtained for five different particle radius values of 1μm, 2μm, 4μm, 8μm and 16μm. The relation is not fully linear. The decrease in dB level has its maximum value when the particle radius is equal to 4μm. As the size decreases or increases, the scaled attenuation gets lower. To understand the dependency of the attenuation on the particle size clearly, numerical code has been used to obtain attenuation per meter for the frequency range of 16 Hz and 16,000 Hz and the corresponding plot has been given below in Figure 5.9. When the particle is larger, the attenuation parameter reaches its maximum at lower frequency value and for the frequencies higher than that frequency, the attenuation is constant. On the other hand, when the particle is smaller, then the maximum value of the attenuation parameter is much higher, but it reaches its maximum at higher frequencies. Consequently, the optimum size of the particle in order to have maximum attenuation is dependent on the frequency.

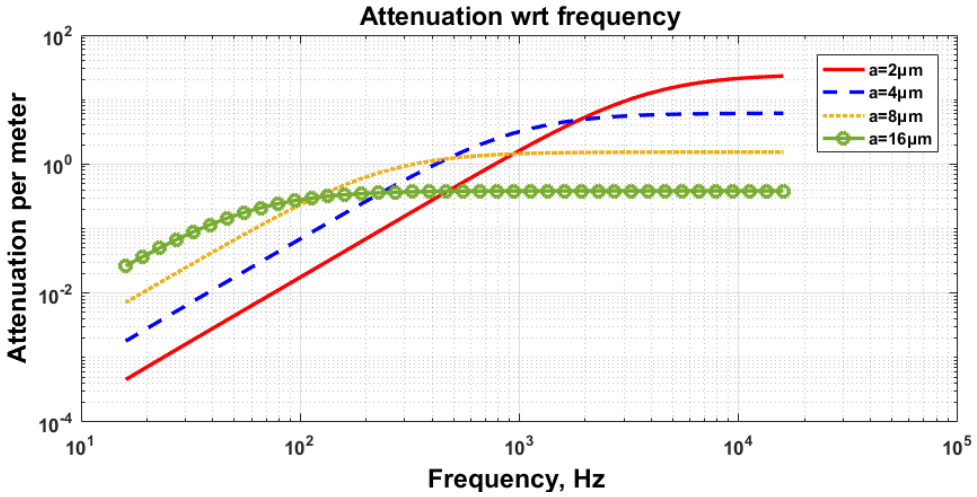


Figure 5.9 Attenuation per meter versus frequency for particle size of 2μm, 4μm, 8μm and 16μm

In terms of wavelength, the attenuation can also be interpreted as done before. The scaled attenuation parameter $\hat{\alpha} = \alpha\, c_o/\omega$ is plotted against frequency for four different particle size (Figure 5.10). It can be seen that there is a maximum value and a corresponding frequency in terms of attenuation as the theory tells [99].

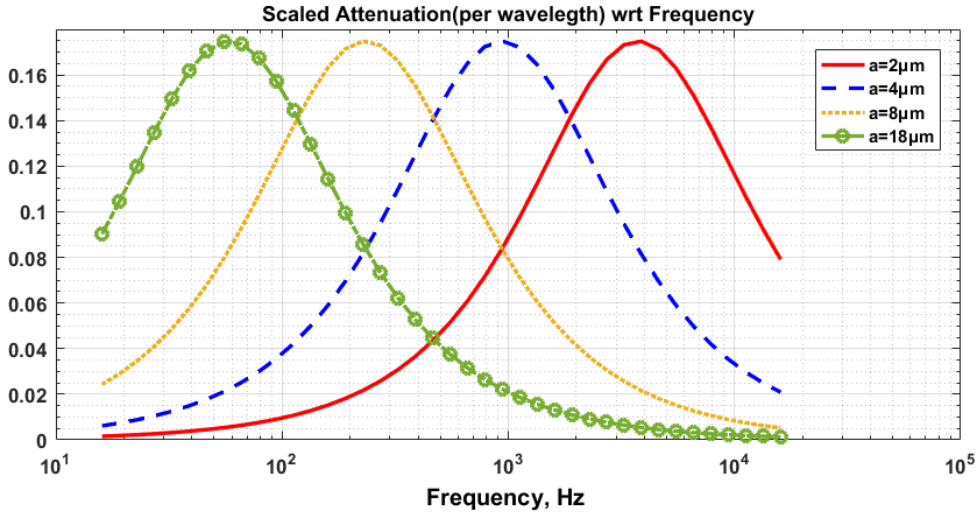


Figure 5.10 Scaled attenuation $\hat{\alpha} = \alpha\, c_o/\omega$ versus frequency for particle size of 2μm, 4μm, 8μm and 16μm.

5.2 Sound Propagation with Only Heat Exchange

Similar to the only momentum exchange case, numerical and analytical solutions have been calculated with the system parameters given in Table 5.1. Sound propagation under the effects of heat transfer between air and water droplets is studied. In order to compare the results more conveniently with the reference ones, the dynamic viscosity is taken as almost zero so that the momentum transfer vanishes

The scaled attenuation computed numerically is plotted in Figure 5.11 against the theoretical solution of Temkins' [99] which is valid for dilute aerosols with very low mass loading. It is clear that, when the volume concentration is $\emptyset_{vo} = 0.001$ %, the numerical results and the analytical results match perfectly in the whole frequency range. As in the isothermal case, when the volume concentration increases and mass loading becomes finite, the results start differing. This is because Eq. (3.59) is only valid for negligible mass loadings. Although the reference does not have the analytical scaled attenuation solution corresponding to the thermal effects with finite mass loading, it was stated that the finite mass loading has around eight times more effect on the attenuation due heat transfer than the attenuation due to momentum transfer [15]. According to the verified results given in section one in this chapter, when the volume concentration is 0.1 %, the ratio of scaled attenuation at the frequency that correspond to the relaxation time for finite and negligible mass loadings is 0.82 regarding the only momentum case. The same ratio is around 0.091 for the case of heat conduction. As a result, nine times more effect than the momentum case was calculated which is quite consistent with that of the reference.[114]

Another interesting observation from Figure 5.11 is that the effect of having finite mass loading changes the frequency that corresponds to the maximum scaled attenuation quite a lot, shifting it up to higher frequencies. This may be due to the considerable change in suspensions equivalent single phase thermodynamic properties as the volume concentration increases.

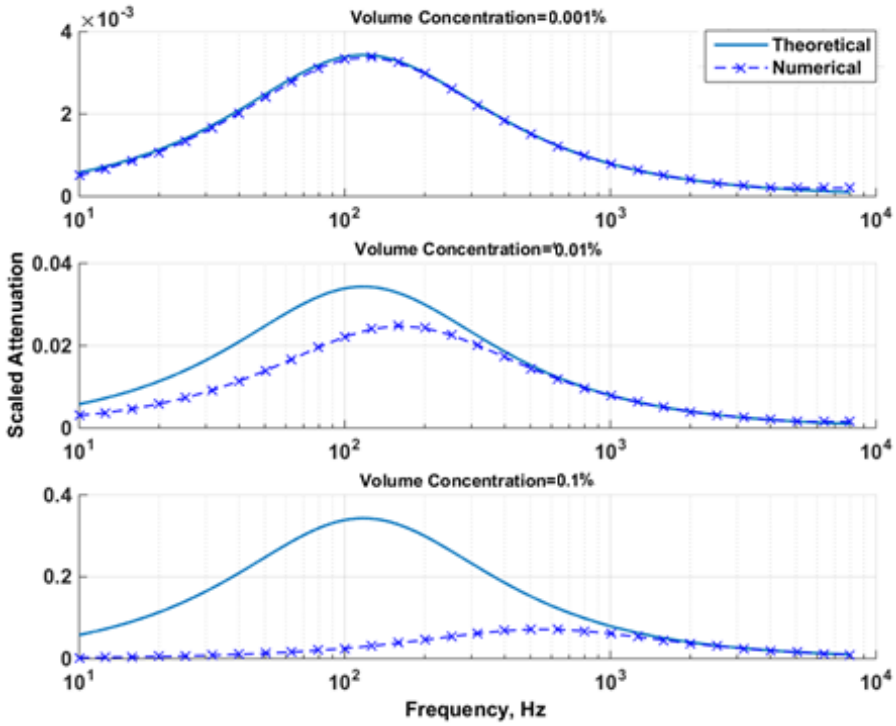


Figure 5.11 Comparison of the computed scaled attenuation $\hat{\alpha} = \alpha\, c_o/\omega$ with theoretical (analytical) solution which is valid for low mass loading σ_m, solid line is the theoretical and dashed with line is the numerical.

In Figure 5.12, the numerical dispersion ratio ${c_o}^2/c(\omega)^2$ is plotted for volume concentrations, the same as previous cases against the analytical solution which is valid for negligible mass loadings. When the volume concentration is 0.001 %, the dispersion is very small and both numerical and analytical approaches yield the same result. As the concentration level increases, unlike the only momentum exchange case, the numerical dispersion results differ from the analytical one. When the volume concentration is 0.1 %, Eq. 3.60 is no longer valid since it is based on small mass loading assumption. Apart from this comparison, it can be seen that the dispersion has its maximum value towards the lower frequency end and it is almost zero towards the higher end.

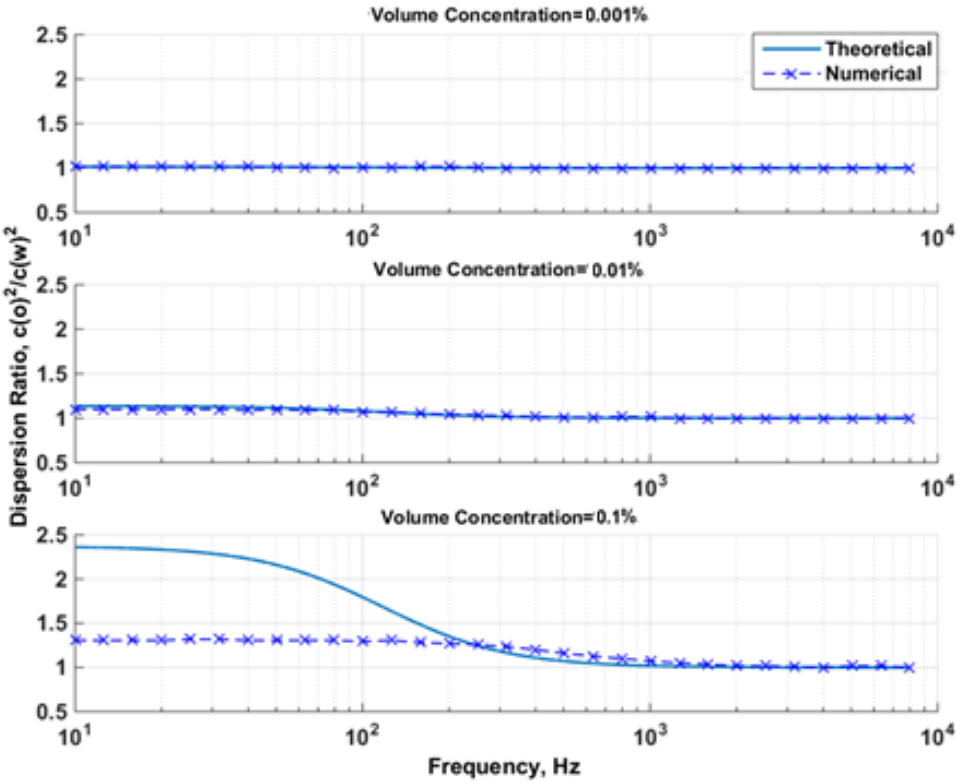


Figure 5.12 Comparison of the computed dispersion $\hat{\alpha} = \alpha\, c_o/\omega$ with theoretical (analytical) solution which is valid for low mass loading σ_m solid line is the theoretical and dashed with line is the numerical.

5.3 Sound Propagation with Only Momentum Exchange under Mean Flow

Both numerical and analytical solutions have been calculated with the system parameters given in Table 5.2.

Table 5.2 System parameters used in the numerical solution with mean flow.

Parameters	Gas Phase	Particle Phase	Particle Size (Average)	Volume Concentration	Flow Velocity (Mach)
Value	Air @ 20°C	Water Droplets @ 20°C	5 x 10^{-6} m	0.1%,0.01%, 0.001%	-0.1, 0, 0.1

In this case, the interaction between droplets and air is only through momentum exchange. In order to see the effect of finite volume concentration together with up and down stream flows, the results have been obtained for different parameter sets.

Both numerical and analytical results are presented for three different volume concentration levels. In Figure 5.13, one can see the attenuation per meter α (which shows the decay of pressure amplitude per unit length) results with respect to frequency. Both numerical and analytical approaches yield the same values. The effect of upstream flow on the attenuation constant is positive especially towards the high frequencies while the effect of downstream flow is negative.

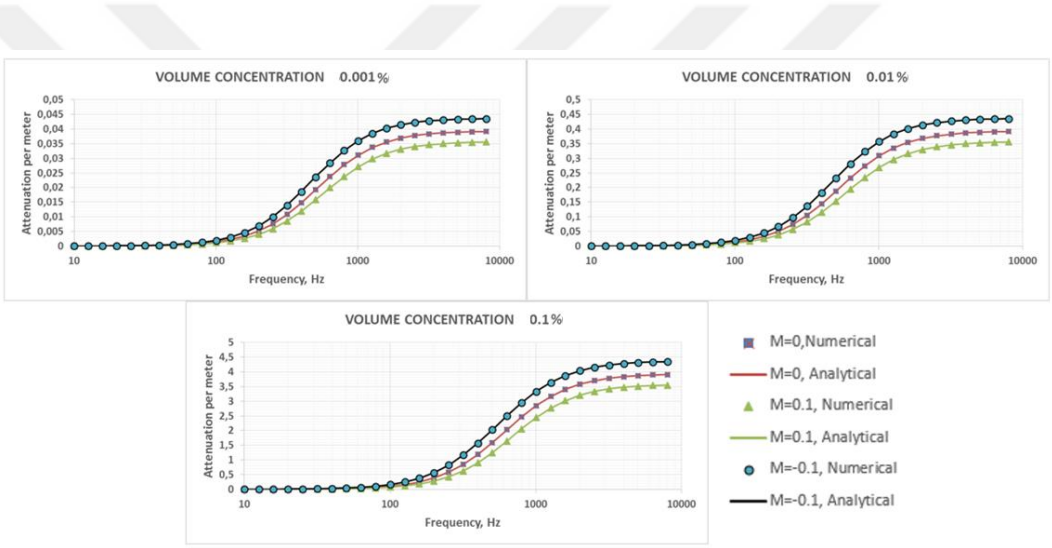


Figure 5.13 Numerical and analytical attenuation for three different volume concentration levels.

The scaled attenuation parameter "$\hat{\alpha} = \alpha\, c_o/\omega$" is shown in Figure 5.14. One can recognize that for an upstream flow there is an increase in the peak level and a shift in frequency of the peak to the left, while it is vice versa for a downstream flow.

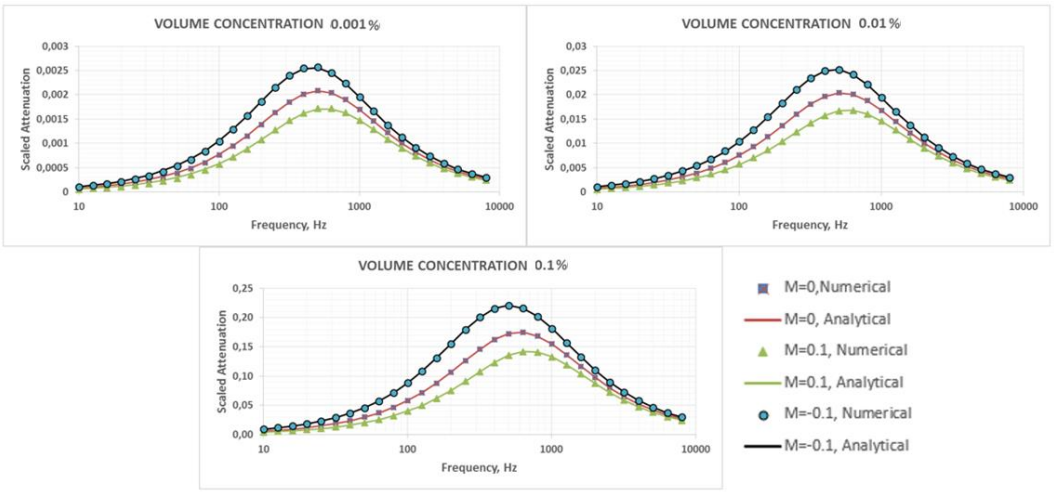


Figure 5.14 Numerical and analytical scaled attenuation $\hat{\alpha} = \alpha\, c_o/\omega$ for three different volume concentration levels.

To see the effect of concentration together with flow, the scaled attenuation (analytical) results are also shown in Figure 5.15. The abbreviation "VC" stands for volume concentration thereby. An increase in concentration level shifts the peak towards the higher frequencies ant this behavior is the same for each flow condition. The mean flow also shifts the peak but it direction of the shift is dependent on the direction of the flow. If the mean flow is downstream (in the direction of the sound wave propagation), the shift of the peak is amplified towards up. In contrary, the effect of upstream mean flow is shifting the peak frequency down, thus the total shifting is neutralized with the effect due to particles.

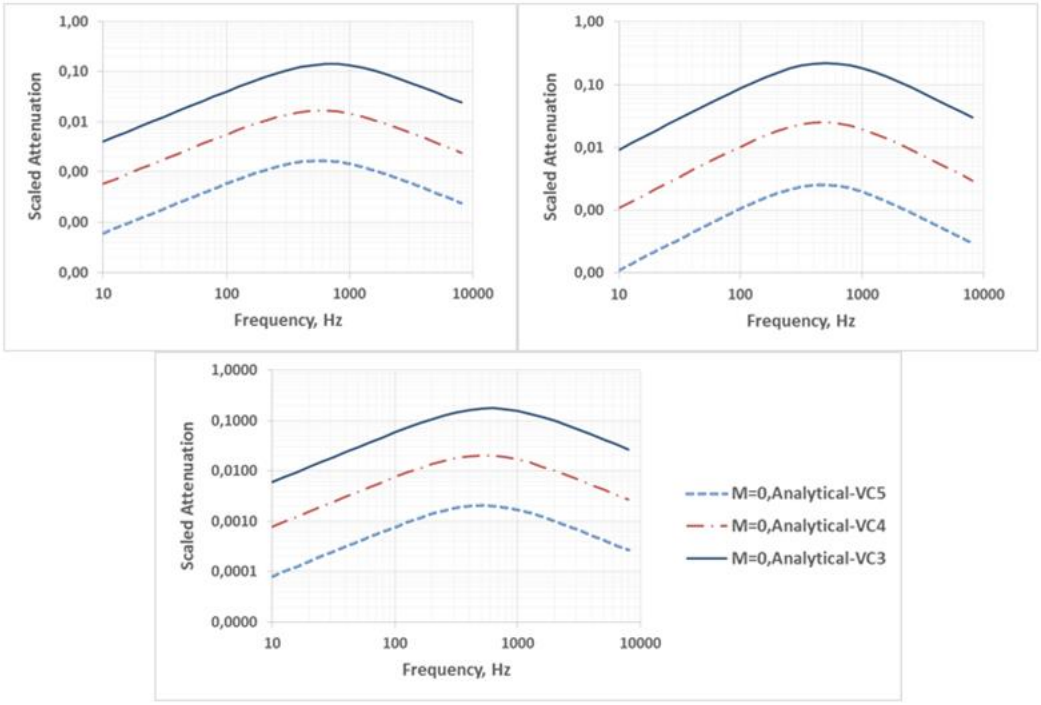


Figure 5.15 Analytically obtained scaled attenuations, parameter sets of M=0, M=0.1 and M=-0.1 for three different concentration level.

Dispersion "$c_o{}^2/c_{(\omega)}{}^2$" results are shown in Figure 5.16. It is obvious from the results that towards the higher frequencies (above the frequency value of the relaxation time) dispersion is only dependent on the mean flow and converges to the same value for each concentration level according to known relation[102]:

$$c_{(\omega)} = {c_o}/{(1 \pm M)} \tag{5.1}$$

However, towards the lower frequencies, dispersion is dependent on both aerosol and convection parameters and it increases significantly when concentration level goes up.

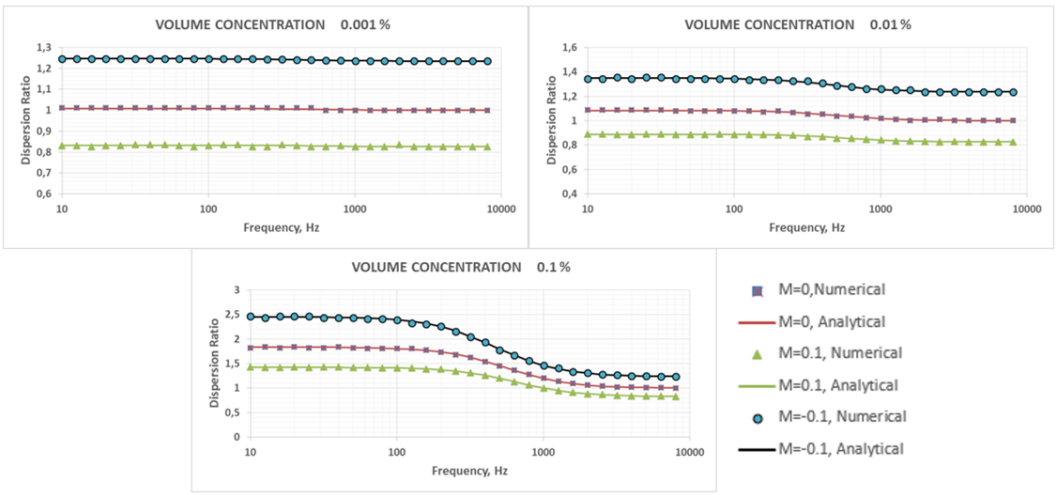


Figure 5.16 Numerical and analytical dispersion ratio ${c_o}^2/{c_{(\omega)}}^2$ for three different volume concentration levels.

As a conclusion, both numerical and analytical results are exactly the same. For low concentration levels, the effect of flow on dispersion is uniform throughout the frequency range; while the effect is amplified towards lower frequencies (than the relaxation frequency) for higher concentration levels. The frequency value which corresponds to the maximum of scaled attenuation "$\hat{\alpha} = \alpha\, c_o/\omega$" shifts towards left or right depending on the direction of the flow. As expected, attenuation values increase when the flow is upstream and they decrease when the flow is downstream.

5.4 Sound Propagation with Momentum and Heat Exchange under Mean Flow

In this case the interaction between droplets and air is through momentum and heat exchange together. Both numerical and analytical results are presented for three different volume concentration levels. In Figure 5.17, attenuation α results are shown with respect to frequency. Both numerical and analytical approaches yield the same values. Similar to the only momentum case, the effect of upstream

flow on the attenuation constant is positive especially towards the high frequencies while it is negative for downstream flow.

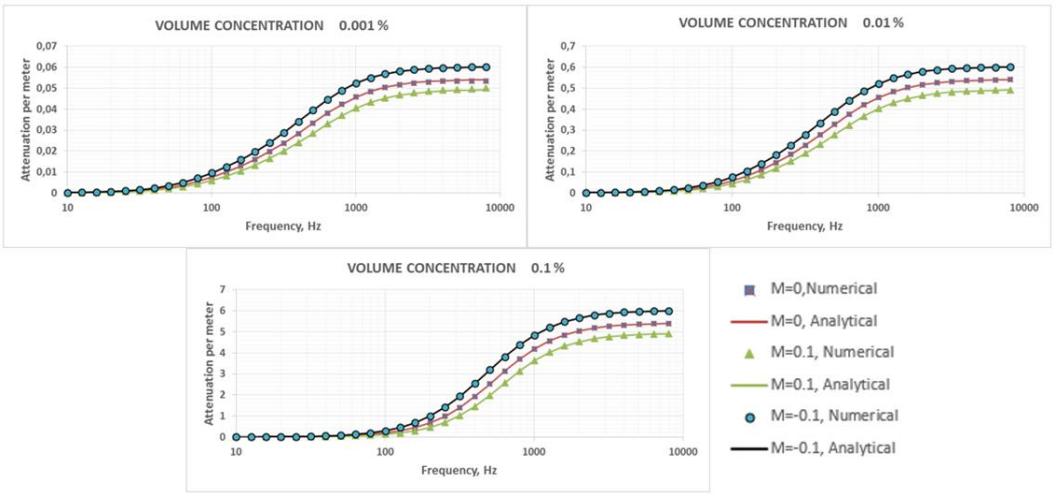


Figure 5.17 Numerical and analytical attenuation for three different volume concentration levels.

The shifting trend of the peak frequency for the scaled attenuation is similar to the previous case. However, the peak value does not increase proportionally with respect to concentration level. The numerical and analytical results match with each other (Figure 5.18).

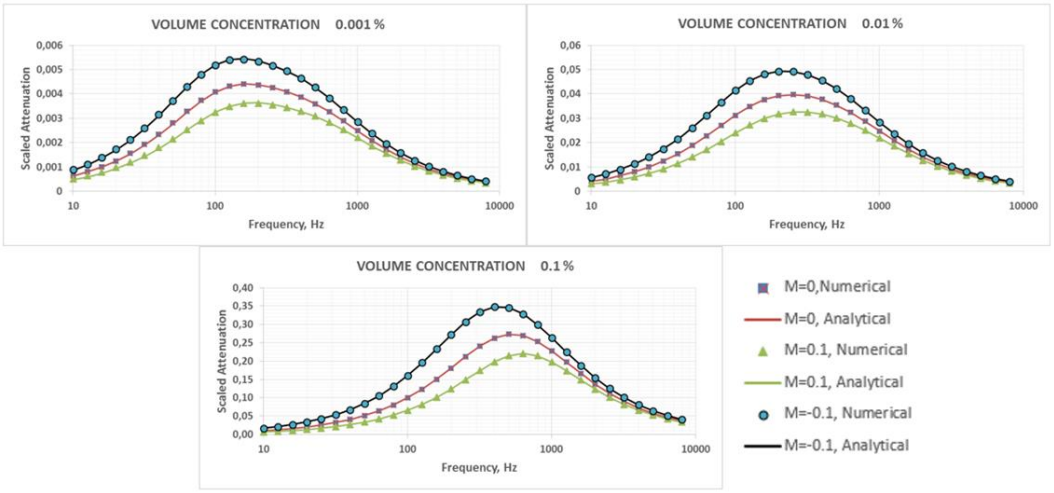


Figure 5.18 Numerical and analytical scaled attenuation $\hat{\alpha} = \alpha\, c_o/\omega$ for three different volume concentration levels.

In Figure 5.19, the scaled attenuation (analytical) results are also shown focusing on the dependency on the concentration level. What is interesting in here is that at lower concentration values (VC=0.001%) the frequency of the peak is closer to 100 Hz whereas at higher concentration values (VC=0.1%) it is rather closer to 1,000 Hz as in the case of only momentum exchange. This implies that as the concentration level increases, the attenuation due to momentum is becoming more dominant than the attenuation due to heat exchange. And, it is vice versa at lower concentration values.

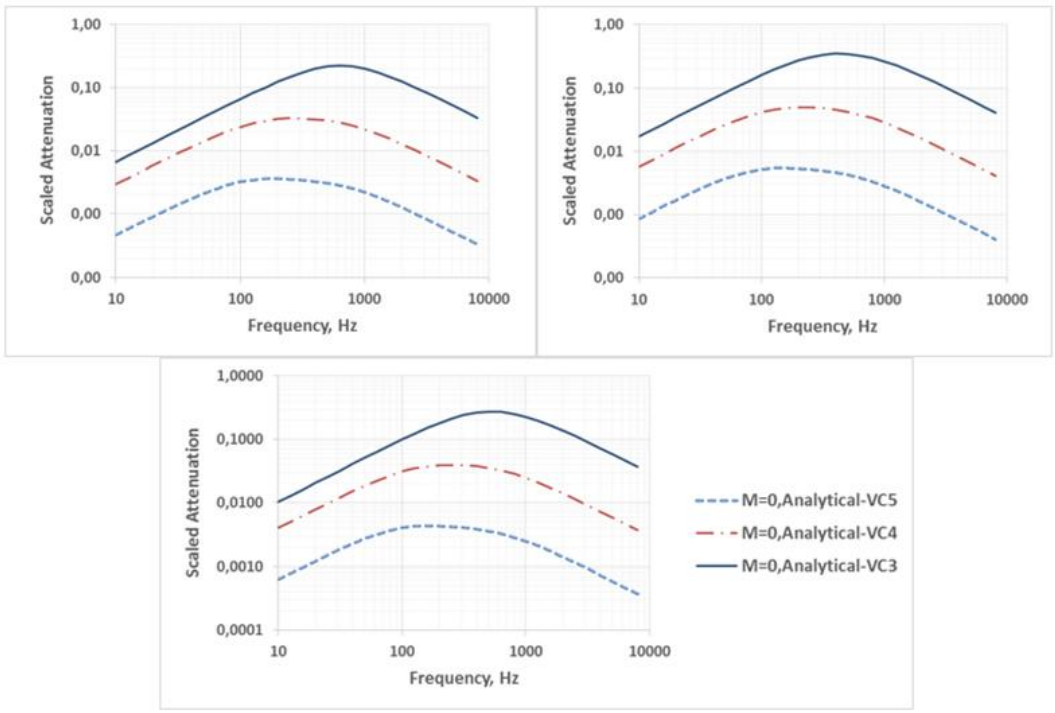


Figure 5.19 Analytically obtained scaled attenuations, parameter sets of M=0, M=0.1 and M=-0.1 for three different concentration level.

Dispersion "$c_o{}^2/c_{(\omega)}{}^2$" results are shown in Figure 5.20. Similar to the previous case, dispersion is only dependent on the mean flow towards the higher frequencies (above the frequency value of the relaxation time) and converges to the same value for each concentration level according to Eq. (5.1). Compared to the case where only momentum exchange occurs, dispersion is more effected by the concentration level towards lower frequency end.

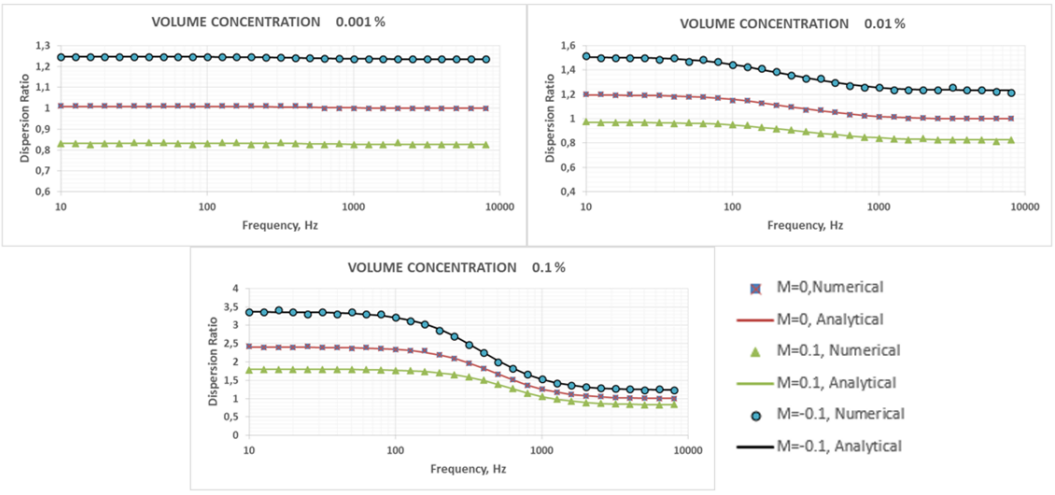


Figure 5.20 Numerical and analytical dispersion ${c_o}^2/{c_{(\omega)}}^2$ for three different volume concentration levels.

To sum up, both approaches yield the same result. The scaled attenuation results show that when the concentration level is low, the maximum scaled attenuation value is mostly due to heat exchange. As the concentration level goes up, momentum exchange seem to be more significant. Furthermore, the effect of mean flow is comparatively different on the scaled attenuation when the concentration level is high (momentum interaction is dominant) than the concentration level is low (heat exchange is significant).

Lastly, dispersion in the higher frequency limit seems to be dependent only on the mean flow, while it is affected by both aerosol and mean flow parameters in the lower frequency limit. This behavior has been observed in both only momentum and the latter cases.

5.5 Summary

The effects of primary system parameters, namely particle size, concentration level and mean flow, on attenuation and dispersion are summarized in Table 5.3 and Table 5.4, respectively.

Table 5.3 The effects of the system parameters on attenuation

	Effect on Attenuation
Particle Size	- With larger particles, maximum attenuation is at lower frequencies, - With smaller particles, maximum attenuation is at higher frequencies.
Volume Concentration Level	- Higher concentrations have higher attenuation, - Scaled attenuation value is not linearly proportional with concentration level, - As concentration level increases, it shifts the frequency of the peak scaled attenuation towards higher frequencies.
Mean Flow	- Attenuation increases if upstream or decreases if downstream at higher frequencies, - It does not have effect on attenuation at lower frequencies, - Shifts the frequency of the peak scaled attenuation to left if upstream, to right if downstream.

Table 5.4 The effects of the system parameters on dispersion

	Effect on Dispersion
Particle Size	- As they get smaller, the dispersed frequency range gets widened towards higher frequency end.
Volume Concentration Level	- Higher concentrations cause more dispersion.
Mean Flow	- The level of dispersion positively changes if upstream, negatively changes if downstream, - At higher frequency limit, dispersion is constant.

CHAPTER 6

THREE DIMENSIONAL (AXISYMMETRIC) SOLUTIONS

In this chapter, the numerical model which has been developed for 1-D acoustic wave propagation problem in an aerosol is extended to 3-D axisymmetric version. By this means, the model will have the capability of solving the problem with additional effects like;

- Higher order duct modes (radial and azimuthal),
- Wall boundary conditions (reflective or impedance type),
- Varying properties of medium in 2-D (X-R Plane).

Similar to the previous case, the main aim is to obtain the attenuation and dispersion results. Since there exists no analytical solution for the axisymmetric case in literature, the corresponding analytical solution has also been developed herein. Results of the numerical model will be compared with those of both 1-D (plane wave) solutions and the analytical results of 3-D axisymmetric case with hard wall condition in the next chapter.

6.1 Numerical Approach

6.1.1 Model Development

Sound propagation is considered to be three dimensional in this case. In order to understand the limitation of plane wave propagation, 3-D wave equation should be studied in a duct which is regarded to be of circular cross section in the scope

of this thesis. As the problem geometry exhibits symmetry around its axis as shown in Figure 6.1, it possible to adopt an axisymmetric approach to the solution.

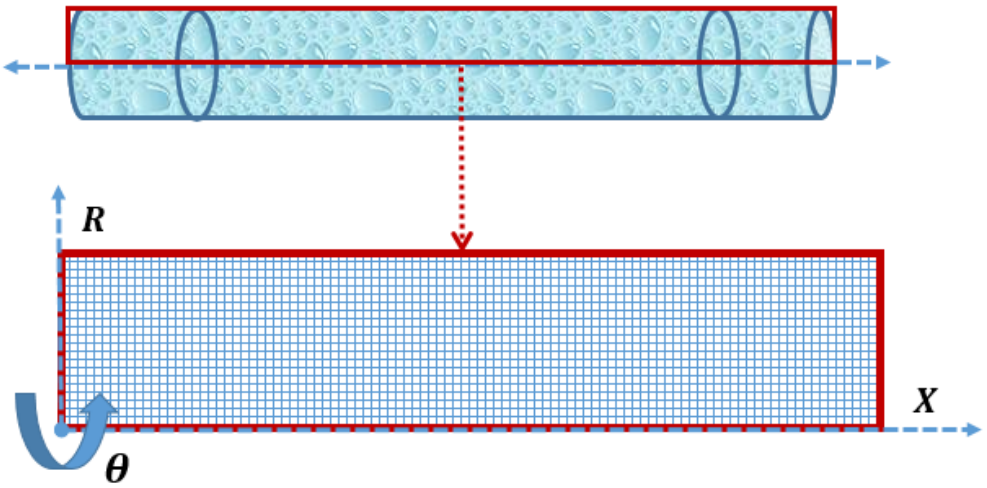


Figure 6.1 Representation of the axisymmetric problem

The corresponding wave equation in cylindrical coordinates is as given below;

$$\frac{\partial^2 \hat{p}}{\partial r^2} + \frac{1}{r}\frac{\partial \hat{p}}{\partial r} + \frac{1}{r^2}\frac{\partial^2 \hat{p}}{\partial \theta^2} + \frac{\partial^2 \hat{p}}{\partial x^2} - \frac{1}{{c_o}^2}\frac{\partial^2 \hat{p}}{\partial t^2} = 0 \tag{6.1}$$

where r is the radial distance and θ is the azimuthal angle. By means of using separation of variables and implementing the boundary conditions (assuming hard walls), one gets the solution as given below. The details of the derivation are given in Appendix-B.

$$\hat{p}_{(r,\theta,x,t)} = \sum_{m=0}^{\infty}\sum_{n=0}^{\infty} J_{m(k_{r,m,n}r)} e^{im\theta} e^{i\omega t} \times \left(A_{m,n} e^{-ik_{x,m,n}x} + B_{m,n} e^{+ik_{x,m,n}x}\right) \tag{6.2}$$

where J is Bessel functions of the first kind, A and B are arbitrary amplitudes, m is the nodal planes where the sound pressure is zero and n is coaxial nodal cylindrical surfaces and the wave number in axial direction $k_{x,m,n}$ is expressed as:

$$k_{x,m,n} = \sqrt{\left({k_0}^2 - {k_{r,m,n}}^2\right)} \tag{6.3}$$

When $m = 0$ and $n = 0$, then $k_{x,m,n} = k_0$ is the case where no higher order modes exist and only plane wave propagates. If $k_{r,m,n}$ is greater than zero, then $k_{x,m,n}$ may have either a real value meaning the sound wave will propagate along axis of the duct, or it has an imaginary value which means the sound wave cannot propagate. For a circular sectioned infinite duct with hard wall boundary condition, $k_{r,m,n}r$ values have been obtained for different integer values of m and n [102]. The corresponding shapes in duct sections are shown together with the $k_{r,m,n}r$ values in Figure 6.2. These shapes are also called as acoustic duct modes in literature.

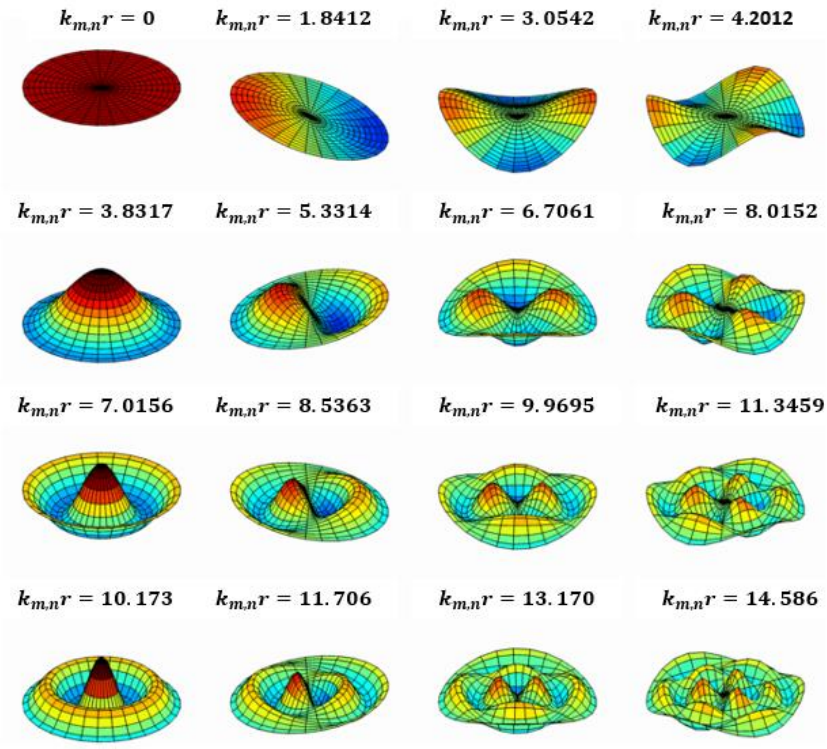


Figure 6.2 Acoustic duct modes and the corresponding wavenumbers of a circular duct

The Bessel functions with respect to $k_{r,m,n}r$ are also shown in Figure 6.3. As it can be seen, $k_{r,m,n}r$ values should be equal to the value where the derivative of the function is zero.

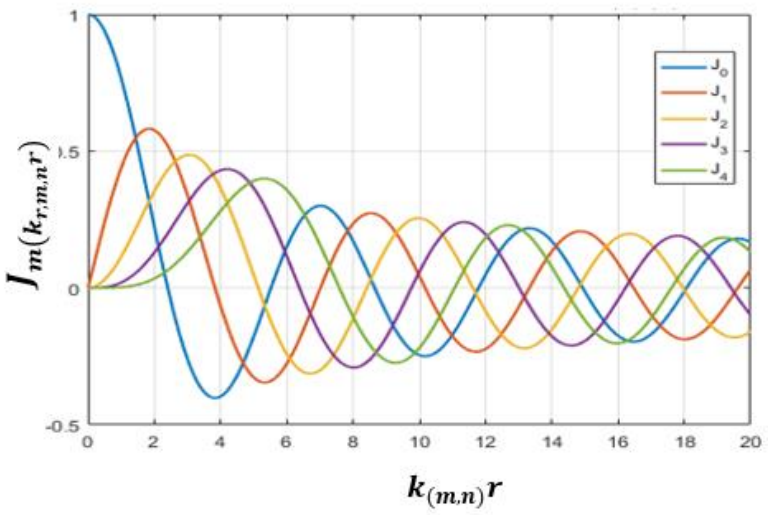


Figure 6.3 Bessel functions of the first kind for m=0, 1, 2, 3, 4.

Having reviewed the axisymmetric solution and the conditions of sound propagation for higher order duct modes within purely air medium, the analysis will proceed with the details on aerosols which is the main subject of the thesis.

6.1.2 Governing Equations

The primitive dependent variables of axisymmetric problem 3-D linearized Euler equations (LEE) for axisymmetric problem are of the form as given below;

$$q'(x,r,m,t) = \Re\{\hat{q}(x,r,w)e^{i\omega t}e^{im\theta}\} \tag{6.4}$$

where;

$$q'(x,r,m,t) = \left[\rho_g', u_g', v_g', w_g', p_g', \emptyset_v', u_p', v_p', w_p'\right]^T \tag{6.5}$$

$$\hat{q}(x,r,m) = \left[\hat{\rho}_g, \hat{u}_g, \hat{v}_g, \hat{w}_g, \hat{p}_g, \hat{\emptyset}_v, \hat{u}_p, \hat{v}_p, \hat{w}_p\right]^T \tag{6.6}$$

where v_g' is the radial velocity perturbation, w_g' is the azimuthal velocity perturbation for the gas phase (air) while u_p' is the radial velocity perturbation, w_p' is the azimuthal velocity perturbation for the particle phase (water droplets). A hat on a variable means it is complex-valued and ω is the circular frequency. The remaining variables have already been specified in Chapter 4.

The linearized system of equations for the two phase model is given below. The time derivative terms are replaced with $i\omega$ for harmonic variation in time. The energy transfer between the phases is considered to be through momentum. Also, the medium is considered to be stationary, in other words, the solution will be obtained for no mean flow condition.

$$i\omega\hat{\rho}_g + \rho_{go}\left\{\frac{\partial\hat{u}_g}{\partial x} + \frac{\partial\hat{v}_g}{\partial r} + \frac{\hat{v}}{r} + \frac{1}{r}\frac{\partial\hat{w}_g}{\partial\theta}\right\} = 0 \tag{6.7}$$

$$i\omega\hat{u}_g + \frac{1}{\rho_{go}}\frac{\partial\hat{p}_g}{\partial x} - \frac{1}{\rho_{go}}F_D\left(\hat{u}_p - \hat{u}_g\right) = 0 \tag{6.8}$$

$$i\omega\hat{v}_g + \frac{1}{\rho_{go}}\frac{\partial\hat{p}_g}{\partial r} - \frac{1}{\rho_{go}}F_D\left(\hat{v}_p - \hat{v}_g\right) = 0 \tag{6.9}$$

$$i\omega\hat{w}_g + \frac{1}{\rho_{go}r}\frac{\partial\hat{p}_g}{\partial\theta} - \frac{1}{\rho_{go}}F_D\left(\hat{w}_p - \hat{w}_g\right) = 0 \tag{6.10}$$

$$i\omega\hat{p}_g + \gamma p_{go}\left\{\frac{\partial\hat{u}_g}{\partial x} + \frac{\partial\hat{v}_g}{\partial r} + \frac{\hat{v}}{r} + \frac{1}{r}\frac{\partial\hat{w}_g}{\partial\theta}\right\} = 0 \tag{6.11}$$

$$i\omega\widehat{\emptyset}_v + \emptyset_{vo}\left\{\frac{\partial\hat{u}_p}{\partial x} + \frac{\partial\hat{v}_p}{\partial r} + \frac{\hat{v}}{r} + \frac{1}{r}\frac{\partial\hat{w}_p}{\partial\theta}\right\} = 0 \tag{6.12}$$

$$i\omega\hat{u}_p + \frac{1}{\emptyset_{vo}\rho_{po}}F_D\left(\hat{u}_p - \hat{u}_g\right) = 0 \tag{6.13}$$

$$i\omega\hat{v}_p + \frac{1}{\emptyset_{vo}\rho_{po}}F_D\left(\hat{v}_p - \hat{v}_g\right) = 0 \tag{6.14}$$

$$i\omega\hat{v}_p + \frac{1}{\emptyset_{vo}\rho_{po}}F_D\left(\hat{w}_p - \hat{w}_g\right) = 0 \tag{6.15}$$

Totally, there are nine equations for nine system variables. The first five equations correspond to the gas phase while the others are to the particle phase. The coupling between the two phases in three dimensions can similarly be achieved by means of summing all the drag forces acting on particles as:

$$F_D = 6\pi\mu_g aN \tag{6.16}$$

It is quite cumbersome to solve such a high number of system equations. As stated earlier, the main interest is to obtain the attenuation and dispersion parameters of the system, by solving the wave propagation problem in the numerical domain. Thus, there will be some assumptions and re-arrangements according to the given statements below:

- Adiabatic state equation is used to find density in terms of pressure perturbations. This implies there is no need to find the density perturbation of the gas phase,

- The perturbation of particle concentration does not change the solution (order of magnitude). There exists no need to solve for the particle concentration perturbation,

- The velocity perturbations of particle phase in three directions are linearly related through the momentum equations. This implies there is no need to find the particle velocity perturbations,

- The problem is axisymmetric, thus the dependency of variations in azimuthal direction will be related to $e^{-im\emptyset}$. Hence, the solution domain will be two dimensional (X-R Plane),

- Non-reflecting or anechoic BC's on each side of the domain are satisfied with PML definitions as in the 1-D case.

Accordingly, the system of equations takes the form given below;

$$i\omega\hat{u}_g - \frac{\sigma_m}{\tau_d}\left(\frac{1}{1+i\omega\tau_d}\right)\hat{u}_g + \frac{1}{\rho_{go}}\frac{\partial\hat{p}_g}{\partial x} + \frac{\sigma_R}{i\omega}\frac{1}{\rho_{go}}\frac{\partial\hat{p}_g}{\partial x} + \left[(\sigma_X+\sigma_R) + \frac{\sigma_X\sigma_R}{i\omega}\right]\hat{u}_g = 0 \tag{6.17}$$

$$i\omega\hat{v}_g - \frac{\sigma_m}{\tau_d}\left(\frac{1}{1+i\omega\tau_d}\right)\hat{v}_g + \frac{1}{\rho_{go}}\frac{\partial\hat{p}_g}{\partial r} + \frac{\sigma_R}{i\omega}\frac{1}{\rho_{go}}\frac{\partial\hat{p}_g}{\partial r} + \left[(\sigma_X+\sigma_R) + \frac{\sigma_X\sigma_R}{i\omega}\right]\hat{v}_g = 0 \tag{6.18}$$

$$i\omega\hat{w}_g - \frac{\sigma_m}{\tau_d}\left(\frac{1}{1+i\omega\tau_d}\right)\hat{w}_g - i\frac{m}{\rho_{go}r}\hat{p}_g - \frac{\sigma_R}{\omega}\frac{m}{\rho_{go}r}\hat{p}_g + \left[(\sigma_X+\sigma_R)+\frac{\sigma_X\sigma_R}{i\omega}\right]\hat{w}_g = 0 \quad (6.19)$$

$$i\omega\hat{p}_g + \gamma p_{go}\left\{\frac{\partial\hat{u}_g}{\partial x}+\frac{\partial\hat{v}_g}{\partial r}+\frac{\hat{v}_g}{r}-i\frac{m}{r}\hat{w}_g\right\} + \left[(\sigma_X+\sigma_R)+\frac{\sigma_X\sigma_R}{i\omega}\right]\hat{p}_g + \frac{\sigma_R}{i\omega}\gamma p_{go}\frac{\partial\hat{u}_g}{\partial x} + \frac{\sigma_x}{i\omega}\gamma p_{go}\left(\frac{\partial\hat{v}_g}{\partial r}+\frac{\hat{v}_g}{r}\right) - im\left[\frac{(\sigma_X+\sigma_R)}{i\omega}\frac{\gamma p_{go}}{r}+\frac{\sigma_X\sigma_R}{(i\omega)^2}\frac{\gamma p_{go}}{r}\right]\hat{w}_g = 0 \quad (6.20)$$

The additional terms on the left hand side of the equations starting with σ_x and σ_R; which are the damping terms in axial and radial directions, respectively, are related to PML equations and have non-zero values in narrow regions at each end of the solution domain.

Eventually, the system ends up with four equations corresponding to the four unknowns given below:

$$\hat{q}(x) = \left[\hat{u}_g, \hat{v}_g, \hat{w}_g, \hat{p}_g\right]^T \quad (6.21)$$

6.1.3 Boundary Conditions and Acoustic Source Definitions

Similar to the implementation done in the 1-D case, the non-reflecting or anechoic termination boundary conditions on each end have been satisfied by using PML equations. Now that the solution domain is two dimensional, there is a need to use a second damping parameter. Two spatial damping factors are used in each equation. The function of the damping factors are as given below:

$$\sigma_x = c_o \sigma_{max} \left| \frac{x - x_i}{L_{ref}} \right|^2 \tag{6.22}$$

$$\sigma_R = c_o \sigma_{max} \left| \frac{r - r_i}{L_{ref}} \right|^2 \tag{6.23}$$

Where, x_i and r_i is the location of the interfaces between PML region and LEE region in axial and radial directions, respectively. $\sigma_{max}\,\Delta x/L_{ref} = 2$ is implemented similar to the case of 1-D solution.

One should define boundary conditions on the walls and on the axis as well as the solution domain is two dimensional. However; there are two issues which can cause the numerical solution to fail. The first one is that $r = 0$ has a singular value in equations having terms $1/r$. This can be overcome by simply starting the numerical domain at a radius equal to infinitesimal value rather than zero. The second issue is that there is an exceptional duct mode with zero azimuthal mode J_0 (m=0) which has a different condition on the axis. While the radial derivative of pressure perturbation is equal to zero for the zero azimuthal mode, it is not (it may have negative or positive real values) so for the other azimuthal modes. This is handled by introducing a conditional definition for the zero azimuthal mode in the model or just extrapolating from the inner nodes. Other than that, there will be definition of hard boundary condition on the walls at $r = r_{wall}$. The corresponding conditions on the boundaries are shown in Table 6.1.

Table 6.1 Hard wall boundary conditions on the axis and on the wall.

Boundary	$\hat{p}$	$\hat{u}$	$\hat{v}$	$\hat{w}$
Wall	${}^{\partial p}/_{\partial r} = 0$	Extrapolated	$v = 0$	Extrapolated
Axis	Extrapolated	Extrapolated	$v = 0$	Extrapolated

Acoustic source input is defined on the left PML region. This is achieved by setting the reflected part to be equal to zero and defining the source terms as coming from the incident components on the right hand side of Eq. (6.17) to Eq. (6.20). The resulting equations are given below;

$$\begin{aligned} i\omega\hat{u}_g - \frac{\sigma_m}{\tau_d}\left(\frac{\omega}{1-i\omega\tau_d}\right)\hat{u}_g + \frac{1}{\rho_{go}}\frac{\partial\hat{p}_g}{\partial x} + \frac{\sigma_R}{i\omega}\frac{1}{\rho_{go}}\frac{\partial\hat{p}_g}{\partial x} \\ + \left[(\sigma_X+\sigma_R) + \frac{\sigma_X\sigma_R}{i\omega}\right]\hat{u}_g \\ = i\omega\hat{u}_{g,in} - \frac{\sigma_m}{\tau_d}\left(\frac{\omega}{1-i\omega\tau_d}\right)\hat{u}_{g,in} + \frac{1}{\rho_{go}}\frac{\partial\hat{p}_{g,in}}{\partial x} \\ + \frac{\sigma_R}{i\omega}\frac{1}{\rho_{go}}\frac{\partial\hat{p}_{g,in}}{\partial x} + \left[(\sigma_X+\sigma_R) + \frac{\sigma_X\sigma_R}{i\omega}\right]\hat{u}_{g,in} \end{aligned} \tag{6.24}$$

$$\begin{aligned} i\omega\hat{v}_g - \frac{\sigma_m}{\tau_d}\left(\frac{\omega}{1-i\omega\tau_d}\right)\hat{v}_g + \frac{1}{\rho_{go}}\frac{\partial\hat{p}_g}{\partial r} + \frac{\sigma_R}{i\omega}\frac{1}{\rho_{go}}\frac{\partial\hat{p}_g}{\partial r} \\ + \left[(\sigma_X+\sigma_R) + \frac{\sigma_X\sigma_R}{i\omega}\right]\hat{v}_g \\ = i\omega\hat{v}_{g,in} - \frac{\sigma_m}{\tau_d}\left(\frac{\omega}{1-i\omega\tau_d}\right)\hat{v}_{g,in} + \frac{1}{\rho_{go}}\frac{\partial\hat{p}_{g,in}}{\partial r} \\ + \frac{\sigma_R}{i\omega}\frac{1}{\rho_{go}}\frac{\partial\hat{p}_{g,in}}{\partial r} + \left[(\sigma_X+\sigma_R) + \frac{\sigma_X\sigma_R}{i\omega}\right]\hat{v}_{g,in} \end{aligned} \tag{6.25}$$

$$
\begin{aligned}
&i\omega\hat{w}_g - \frac{\sigma_m}{\tau_d}\left(\frac{\omega}{1-i\omega\tau_d}\right)\hat{w}_g - i\frac{m}{\rho_{go}r}\hat{p}_g - \frac{\sigma_R}{\omega}\frac{m}{\rho_{go}r}\hat{p}_g \\
&\qquad + \left[(\sigma_X+\sigma_R) + \frac{\sigma_X\sigma_R}{i\omega}\right]\hat{w}_g \\
&\qquad = i\omega\hat{w}_{g,in} - \frac{\sigma_m}{\tau_d}\left(\frac{\omega}{1-i\omega\tau_d}\right)\hat{w}_{g,in} - i\frac{m}{\rho_{go}r}\hat{p}_{g,in} \\
&\qquad - \frac{\sigma_R}{\omega}\frac{m}{\rho_{go}r}\hat{p}_{g,in} + \left[(\sigma_X+\sigma_R) + \frac{\sigma_X\sigma_R}{i\omega}\right]\hat{w}_{g,in}
\end{aligned} \tag{6.26}
$$

$$
\begin{aligned}
&i\omega\hat{p}_g + \gamma p_{go}\left\{\frac{\partial\hat{u}_g}{\partial x} + \frac{\partial\hat{v}_g}{\partial r} + \frac{\hat{v}_g}{r} - i\frac{m}{r}\hat{w}_g\right\} + \left[(\sigma_X+\sigma_R) + \frac{\sigma_X\sigma_R}{i\omega}\right]\hat{p}_g \\
&\qquad + \frac{\sigma_R}{i\omega}\gamma p_{go}\frac{\partial\hat{u}_g}{\partial x} + \frac{\sigma_x}{i\omega}\gamma p_{go}\left(\frac{\partial\hat{v}_g}{\partial r} + \frac{\hat{v}_g}{r}\right) \\
&\qquad - im\left[\frac{(\sigma_X+\sigma_R)}{i\omega}\frac{\gamma p_{go}}{r} + \frac{\sigma_X\sigma_R}{(i\omega)^2}\frac{\gamma p_{go}}{r}\right]\hat{w}_g = 0 \\
&\qquad = i\omega\hat{p}_{g,in} + \gamma p_{go}\left\{\frac{\partial\hat{u}_{g,in}}{\partial x} + \frac{\partial\hat{v}_{g,in}}{\partial r} + \frac{\hat{v}_{g,in}}{r} - i\frac{m}{r}\hat{w}_{g,in}\right\} \\
&\qquad + \left[(\sigma_X+\sigma_R) + \frac{\sigma_X\sigma_R}{i\omega}\right]\hat{p}_{g,in} + \frac{\sigma_R}{i\omega}\gamma p_{go}\frac{\partial\hat{u}_{g,in}}{\partial x} \\
&\qquad + \frac{\sigma_x}{i\omega}\gamma p_{go}\left(\frac{\partial\hat{v}_{g,in}}{\partial r} + \frac{\hat{v}_{g,in}}{r}\right) \\
&\qquad - im\left[\frac{(\sigma_X+\sigma_R)}{i\omega}\frac{\gamma p_{go}}{r} + \frac{\sigma_X\sigma_R}{(i\omega)^2}\frac{\gamma p_{go}}{r}\right]\hat{w}_{g,in}
\end{aligned} \tag{6.27}
$$

The subscripts ending with "in" mean that they are the incident components of the perturbations. Together with the definition of the axial wave number as $k_{x,m,n} = \sqrt{\left({k_0}^2 - {k_{r,m,n}}^2\right)}$ and spatial derivative in x direction as $\partial/\partial x = -ik_{x,m,n}$, the perturbations for incident components can be obtained from the corresponding equations given below:

$$\hat{p}_{g,in} = J_{m(k_{r,m,n}r)} A e^{im\theta} e^{-ik_{x,m,n}x} \tag{6.28}$$

$$\hat{u}_{g,in} = \frac{k_{x,m,n}}{\rho_{go}\omega}\hat{p}_{g,in} \tag{6.29}$$

$$\hat{v}_{g,in} = -\frac{{}^{\partial \hat{p}_{g,in}}/_{\partial r}}{i\rho_{go}\omega} \tag{6.30}$$

$$\hat{w}_{g,in} = -\frac{{}^{\partial \hat{p}_{g,in}}/_{\partial \theta}}{i\rho_{go}r\omega} \tag{6.31}$$

In the numerical model, one must choose the duct acoustic mode prior to the solution and select the corresponding Bessel function. If the corresponding axial wave number has a real value, then the acoustic wave will propagate along the duct. Otherwise, the waveform will diminish and there will be no acceptable solution. Another issue is that the equations of velocity perturbations given just above in radial and azimuthal directions have spatial derivatives in terms of pressure in radial and azimuthal directions, respectively. There are two options to find the numerical counterparts. The first option is to find the analytical solution of the first and second derivatives of Bessel functions, and the other one is to obtain the solution by means of numerical methods. In the developed code for the numerical model, the first option is selected because the code is written in MATLAB® and it has the capability to take derivatives using Symbolic Math Toolbox™ software [113].

6.1.4 Numerical Scheme

As 1-D numerical solution results have showed very successful status in terms of accuracy and speed, 4^{th} order standard finite difference scheme is also implemented for the purpose of spatial discretization in 2-D case. The grids have been defined with two indices, namely, axial and radial components (Figure 6.4). The maxima in axial and radial directions are named as M and N, respectively. Due to the fact that the problem domain herein is more complex, there are many distinguishable grids and each of them has different weighting coefficients related to their location in the domain. The weighting coefficients corresponding to axial and radial derivative terms for calculation nodes are shown in Table 6.2 and Table 6.3.

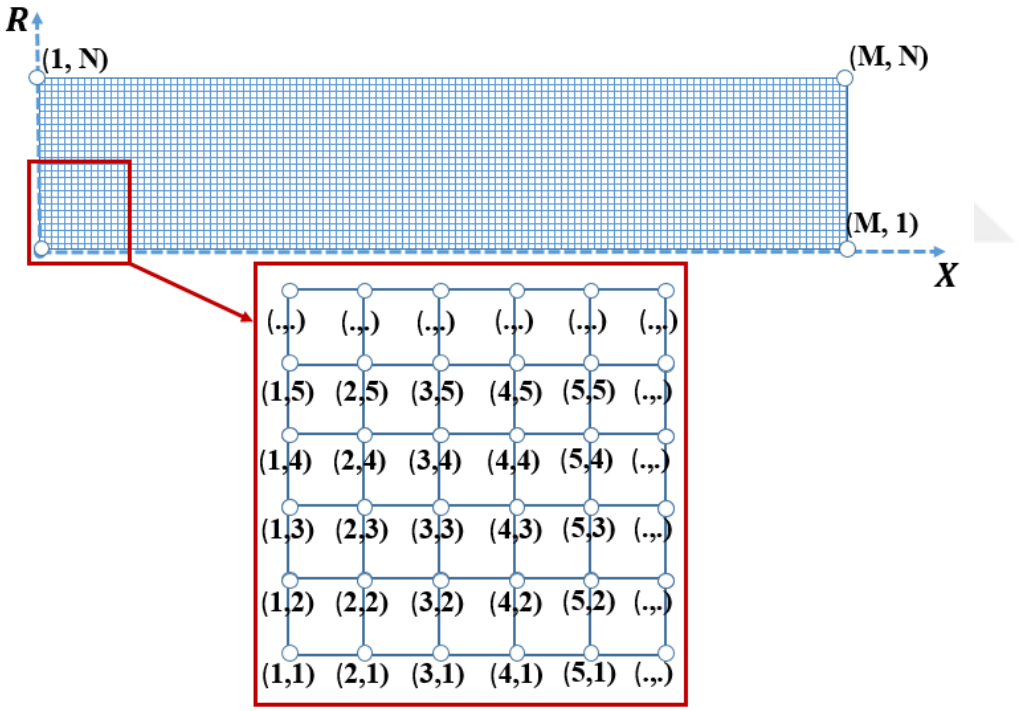


Figure 6.4 Discretized domain and the bottom left stencil for 4th order finite difference scheme.

Table 6.2 Weighting coefficients for axial derivative terms of finite difference scheme.

Node	m-3	m-2	m-1	m	m+1	m+2	m+3
(1,n)	-	-	-	-11/6	3	-3/2	1/3
(2,n)	-	-	-2/6	-3/6	1	-1/6	-
(3,n)- (M-2,n)	-	1/12	-2/3	0	2/3	-1/12	-
(M-1,n)		1/6	-1	3/6	2/6		
(M-1,n)	1/3	3/2	-3	11/6			

Table 6.3 Weighting coefficients for radial derivative terms of finite difference scheme.

Node	n-3	n-2	n-1	n	n+1	n+2	n+3
(m,1)	-	-	-	-11/6	3	-3/2	1/3
(m,2)	-	-	-2/6	-3/6	1	-1/6	-
(m,3)- (m,N-2)	-	1/12	-2/3	0	2/3	-1/12	-
(m, N-1)		1/6	-1	3/6	2/6		
(m, N)	1/3	3/2	-3	11/6			

6.1.4.1 Solver Verification: Wave propagation in an infinite circular duct without particles

First the numerical approach is verified without aerosol against the well-known standard analytical solution given in Eq. (6.2), with various duct modes. The validation of the 3-D code is made by ignoring the particle existence in the medium. This condition is satisfied by again adjusting the volume concentration of the water droplets to a very low number ($\emptyset_{vo} = 10^{-15}$) as if the medium purely consists of air. The decision on the number of grids in axial and radial directions is important. Since the code is now spatially two dimensional, the total number of grids is increased. In the 1-D code, NPPW has been selected to be 40 and the

accuracy of the results are very good. This time in order not to have too long processing times in the solution, NPPW in axial direction is taken as 30. The damping factors σ_x and σ_r have varying values as in the case of 1-D and have a maximum value of 40,000 at the outer boundaries. The selection of the mode is dependent on the radius of the duct and the frequency. In other words, there will be cut-on values for higher order modes. Thus, the frequency of the solution will have different values as the radius of the duct is fixed to 0.2 m in the verification scenarios.

Mode (0,0)

In the first case, mode (0, 0) which corresponds to a plane wave is considered. It has a pressure amplitude of 1 Pa and axial frequency of 1,500 Hz. It has been defined as an incident wave into the PML region (two wavelengths) on the left. The number of grids in radial direction is not necessarily to be high; anyway it has been taken as 15. The pressure distribution in the solution domain is given on the left in Figure 6.5. Similar to the 1-D solution, damping is assigned at the right PML where the waves die out without any reflection in neither axial nor radial directions. Also, the distribution of absolute pressure calculated on $R-\theta$ Plane is shown on the right in Figure 6.5. Although it shows distinct colors in the plot, this can be deceptive as the numbers in the legend display almost the same value.

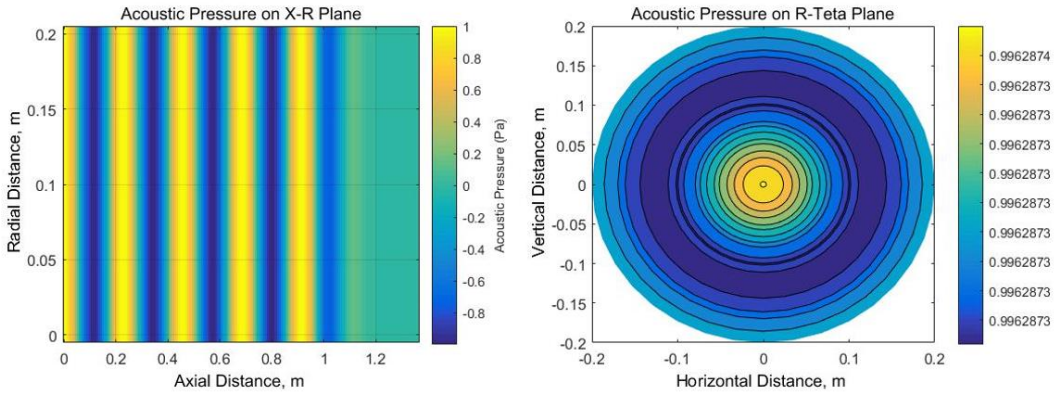


Figure 6.5 Mode number (0, 0) – acoustic pressure plot (f_{ax}=1,500 Hz).

Computational results are checked with the exact results and the corresponding plots are compared in Figure 6.6. As it is clearly seen, except the PML at the right boundary, the computational results match perfectly with the exact solution.

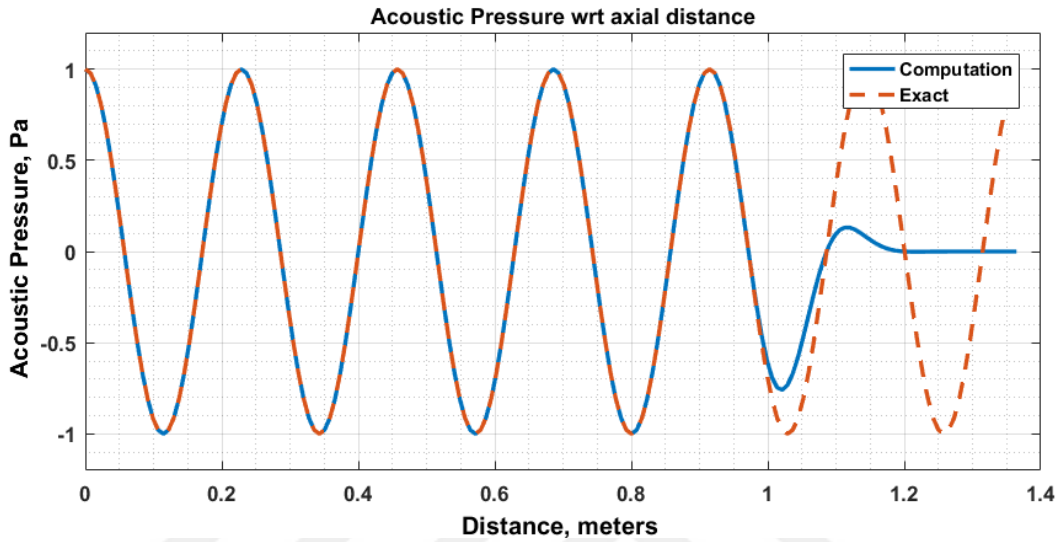


Figure 6.6 Comparison of the pressure perturbations for mode number (0, 0), f_{ax}=1,500 Hz.

Mode (1,0)

In the second case, mode (1, 0) which corresponds to first azimuthal wave is considered. The wave has a maximum pressure amplitude of 0.5819 Pa and axial frequency of 1,500 Hz. The number of grids in radial direction is 15 which seems to be sufficient for the gradient of this mode. The pressure distribution of in the solution domain is given on the left in Figure 6.7. Also, the distribution of absolute pressure which has been calculated on $R-\theta$ Plane is shown on the right in Figure 6.7. R - θ

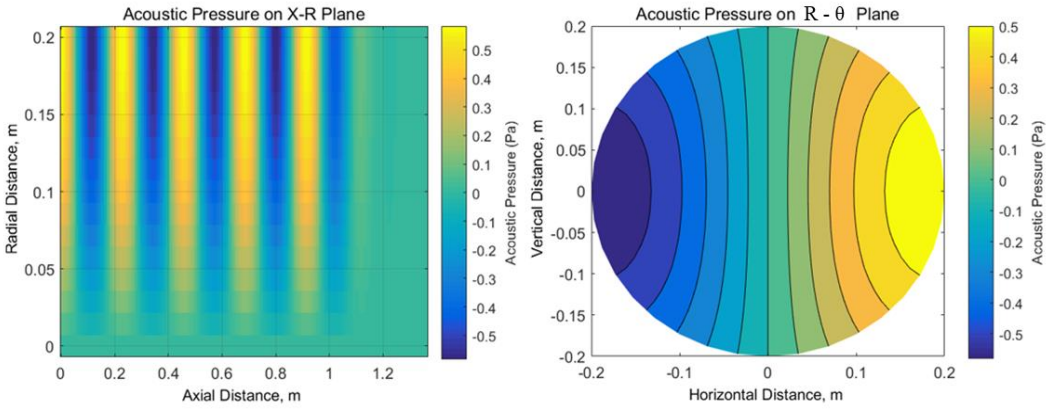


Figure 6.7 Mode number (1, 0) – acoustic pressure plot (f_{ax}=1,500 Hz).

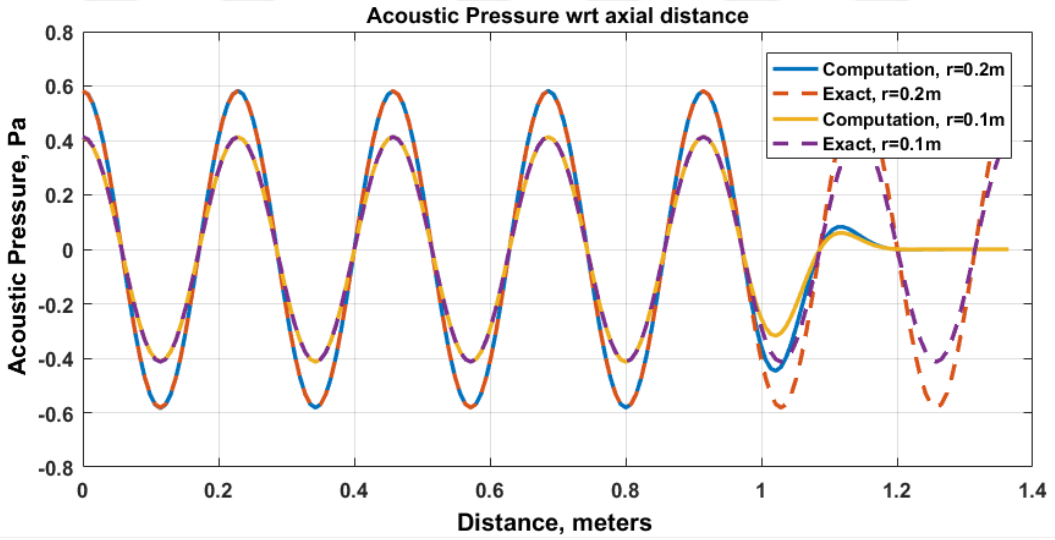


Figure 6.8 Comparison of the pressure perturbations for mode number (1, 0), f_{ax}=1,500 Hz.

Computational accuracy has also been checked with the exact results and the plots of acoustic pressure are presented in Figure 6.8. The agreement between the two can be regarded as almost perfect.

Mode (0,1)

In the third case, mode (0, 1) which corresponds to first radial mode wave is considered. The wave has maximum pressure amplitude of 1 Pa and axial frequency of 1,500 Hz. Again, the number of grids in radial direction is 15, which seem to be sufficient for the gradient of this mode. The pressure distribution in the solution domain is given on the left while the distribution of absolute pressure on $R - \theta$ plane is shown on the right in Figure 6.9.

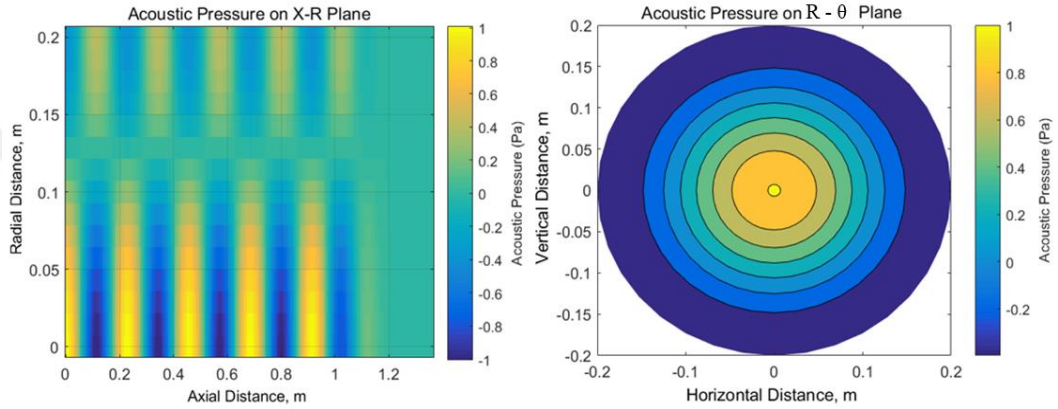


Figure 6.9 Mode number (0, 1) – acoustic pressure plot (f_{ax} =1,500 Hz).

Computational results have been compared with the exact results and the corresponding plots are compared in Figure 6.10. Except the PML region at the right boundary, the computational results match perfectly with the exact solution at $r = 0$ m. and $r = 0.2$ m.

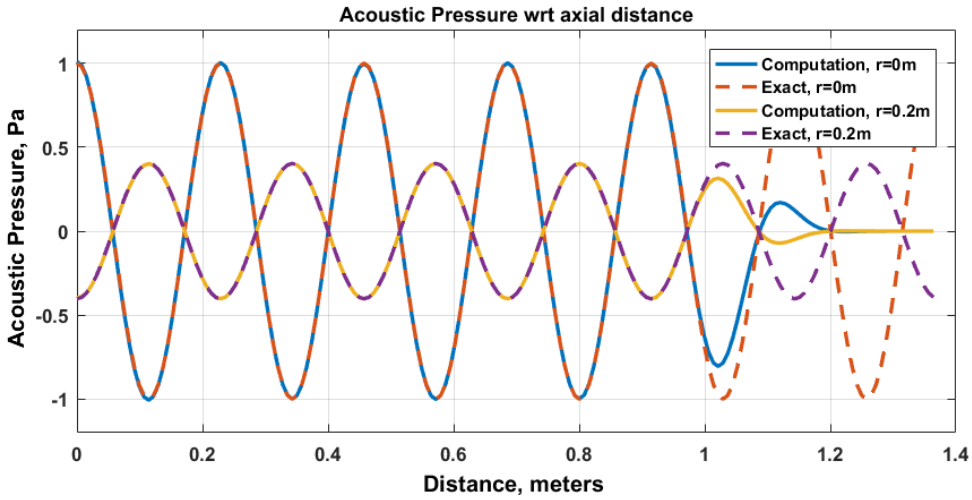


Figure 6.10 Comparison of the pressure perturbations for mode number (0, 1), f_{ax} =1,500 Hz.

Mode (1,1)

In the third case, mode (1, 1) which corresponds to first mixed radial and azimuthal mode wave is considered. The wave has pressure amplitude of 0.58 Pa and axial frequency of 1,500 Hz. The number of grids in radial direction is increased to 24 because there are more and sharper gradients. The pressure distribution in the solution domain is given on the left in Figure 6.11. The distribution of absolute pressure on $R-\theta$ Plane is shown on the right.

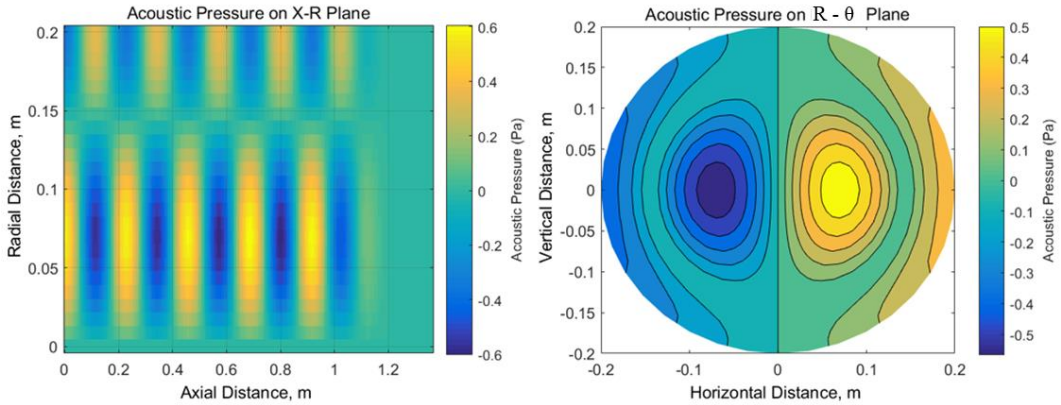


Figure 6.11 Mode (1, 1) – acoustic pressure plot (f_{ax}=1,500 Hz).

As it is seen in Figure 6.12, except the PML at the right boundary, the computational results match almost perfectly with the exact solution at $r = 0.052$ m. and $r = 0.2$ m for duct mode (1,1).

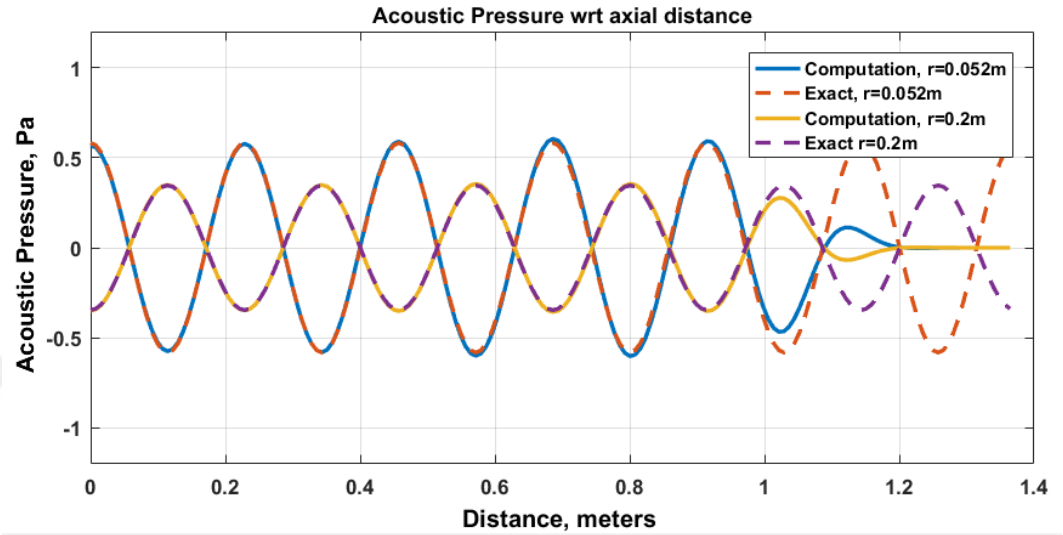


Figure 6.12 Comparison of the pressure perturbations for mode number (1, 1), f_{ax}=1,500 Hz.

Mode (2,0)

Next, mode (2, 0) which corresponds to second azimuthal mode wave is considered. The wave has pressure amplitude of 0.5 Pa and axial frequency of 1,500 Hz. The number of grids in radial direction is kept as 24. The pressure distributions on $X - R$ and on $R - \theta$ Planes, respectively, shown in Figure 6.13.

Computational results are also checked with the exact results and the corresponding plots are compared in Figure 6.14. As it can be observed, with the exception of the PML at the right boundary, the computational results match almost perfectly with the exact solution at $r = 0.2$ m.

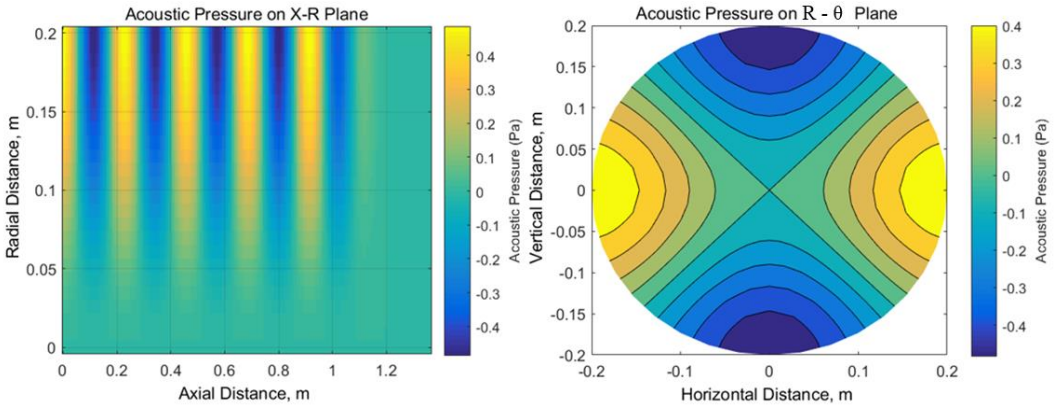


Figure 6.13 Mode number (2, 0) – acoustic pressure plot (f_{ax} =1,500 Hz).

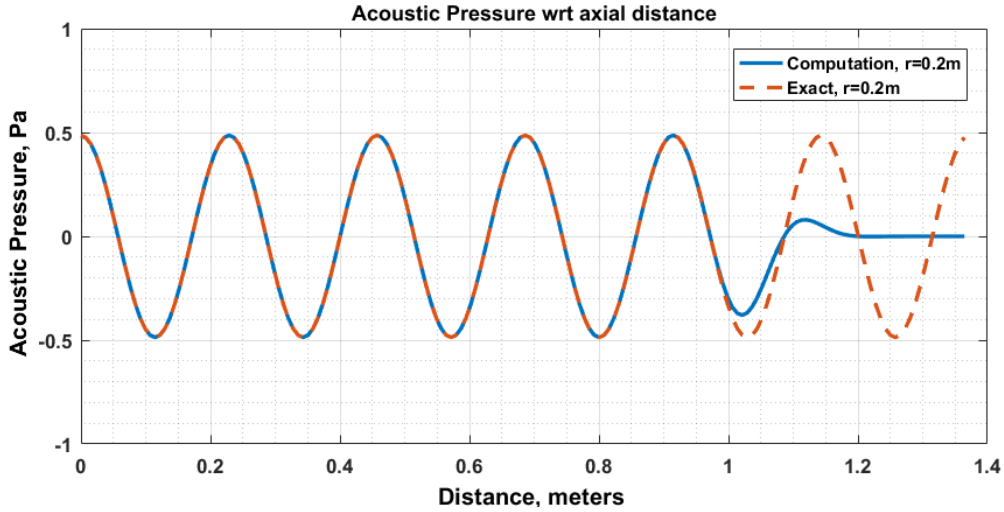


Figure 6.14 Comparison of the pressure perturbations for mode number (0, 2), f_{ax} =1,500 Hz.

Mode (0,2)

Finally, mode (0, 2) which corresponds to second radial mode wave is considered. The wave has a maximum pressure amplitude of 1 Pa and axial frequency of 1,500 Hz. The number of grids in radial direction is as 24. The pressure distribution of in the solution domain is given on the left in Figure 6.15. Also, the distribution of absolute pressure which were calculated on $R-\theta$ Plane at the middle of the axial length is shown on the right in Figure 6.15. Computational

results are also compared with the exact results and the corresponding plots are shown in Figure 6.16. The numerical solution match perfectly with the exact solution at $r = 0$ m. and $r = 0.2$m.

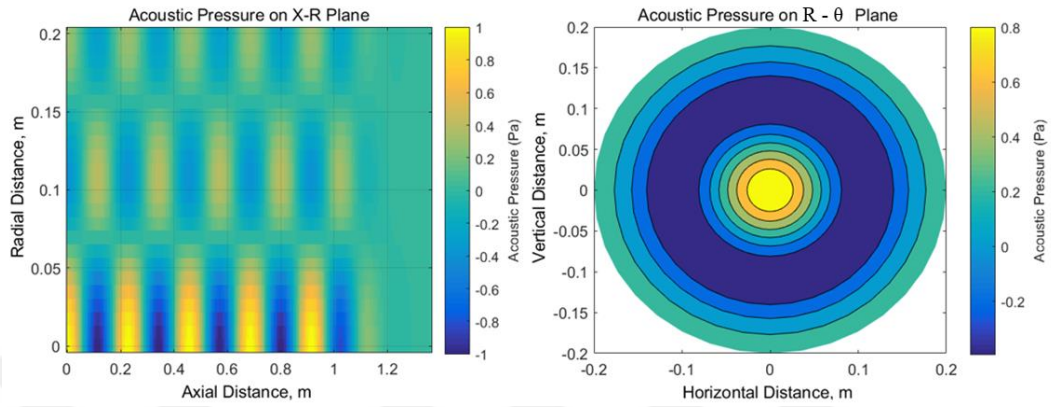


Figure 6.15 Mode number (0, 2) – acoustic pressure plot (f_{ax} =1,500 Hz).

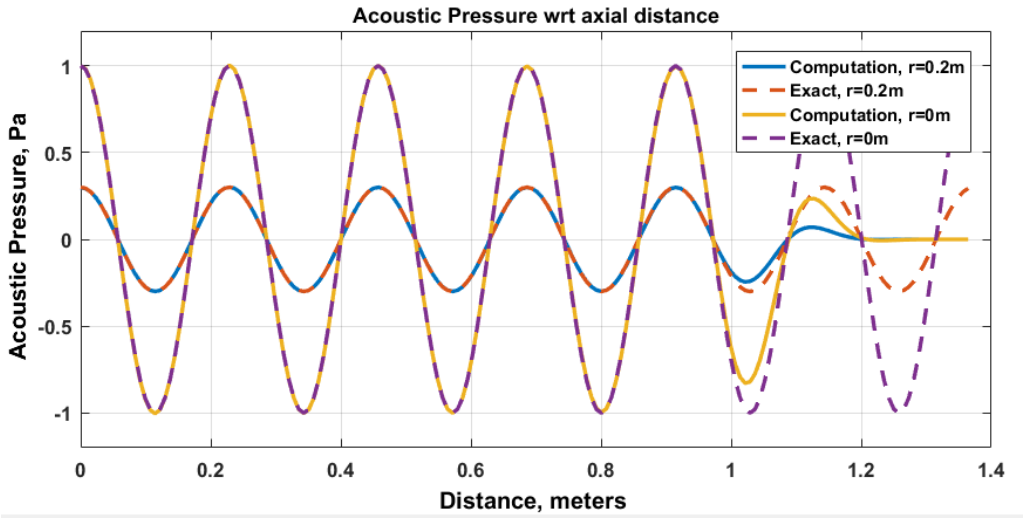


Figure 6.16 Comparison of the pressure perturbations for mode number (0, 2), f_{ax} =1,500 Hz.

6.2 Extension of the 1-D Analytical Solution to 3-D

In order to check the validity of the numerical results for 3-D case, open literature have been searched for existing theoretical or experimental results but there are no results available especially for the case of cylindrical duct. For this reason analytical solution for obtaining the complex wavenumber in the case of an aerosol filled in a cylindrical duct has been developed herein. Likewise, the interaction between the phases (gas and particles) is assumed to be isothermal. In addition to the assumptions given in Chapter 3, the considerations made are as given below:

- The inner surface of the duct walls are fully reflective, meaning there is no energy loss nor energy transmission,
- The motions of the particles in three spatial directions are uncoupled,
- The duct is infinitely long; in other words there is no acoustic reflection from the ends.

The governing equations are as given below. Similar to the simplifications made in the numerical approach, the momentum equations of the particle phase have been used to find the velocity perturbations of the particle phase in terms of the fluids Eq. (6.13) to Eq. (6.15).

$$i\omega\hat{u}_g - \frac{\sigma_m}{\tau_d}\left(\frac{\omega}{1-i\omega\tau_d}\right)\hat{u}_g + \frac{1}{\rho_{go}}\frac{\partial\hat{p}_g}{\partial x} = 0 \tag{6.32}$$

$$i\omega\hat{v}_g - \frac{\sigma_m}{\tau_d}\left(\frac{\omega}{1-i\omega\tau_d}\right)\hat{v}_g + \frac{1}{\rho_{go}}\frac{\partial\hat{p}_g}{\partial r} = 0 \tag{6.33}$$

$$i\omega\hat{w}_g - \frac{\sigma_m}{\tau_d}\left(\frac{\omega}{1-i\omega\tau_d}\right)\hat{w}_g + \frac{1}{\rho_{go}r}\frac{\partial\hat{p}_g}{\partial\theta} = 0 \tag{6.34}$$

$$i\omega\hat{p}_g + \gamma p_{go}\left\{\frac{\partial\hat{u}_g}{\partial x} + \frac{\partial\hat{v}_g}{\partial r} + \frac{\hat{v}_g}{r} + \frac{1}{r}\frac{\partial\hat{w}_g}{\partial\theta}\right\} = 0 \tag{6.35}$$

From Eq. (6.32) to Eq. (6.34), velocity perturbations can be written in terms of pressure perturbation. The spatial derivative in axial direction is taken simply as $ik_{x,m,n}$. The equations become as:

$$\hat{u}_g = \frac{ik_{x,m,n}}{\rho_{go}}\frac{1}{\left[-i\omega + \frac{\sigma_m}{\tau_d}\left(1 - \frac{1}{1-i\omega\tau_d}\right)\right]}\hat{p}_g \tag{6.36}$$

$$\hat{v}_g = \frac{1}{\rho_{go}}\frac{1}{\left[-i\omega + \frac{\sigma_m}{\tau_d}\left(1 - \frac{1}{1-i\omega\tau_d}\right)\right]}\frac{\partial\hat{p}_g}{\partial r} \tag{6.37}$$

$$\hat{w}_g = \frac{1}{\rho_{go}r}\frac{1}{\left[-i\omega + \frac{\sigma_m}{\tau_d}\left(1 - \frac{1}{1-i\omega\tau_d}\right)\right]}\frac{\partial\hat{p}_g}{\partial\theta} \tag{6.38}$$

Insertion of these equations into Eq. (6.35) yields the following equation:

$$-i\omega\hat{p}_g + {c_o}^2 \frac{1}{\left[-i\omega - \frac{\sigma_m}{\tau_d}\left(1 - \frac{1}{1 - i\omega\tau_d}\right)\right]} \left\{ {k_{x,m,n}}^2 + \frac{\partial^2}{\partial r^2} + \frac{1}{r}\frac{\partial}{\partial r} + \frac{1}{r^2}\frac{\partial^2}{\partial \theta^2} \right\} \hat{p}_g = 0 \tag{6.39}$$

Both in the radial and azimuthal directions, mode shapes will remain the same. From the theoretical solution of the wave equation in cylindrical coordinates, it has been shown that the wave number for the duct mode is defined as (Appendix-B) [115]:

$${k_{r,m,n}}^2 = -\left(\frac{\partial^2}{\partial r^2} + \frac{1}{r}\frac{\partial}{\partial r} + \frac{1}{r^2}\frac{\partial^2}{\partial \theta^2}\right) \tag{6.40}$$

By replacing the corresponding terms and making re-arrangements, the simplest form can be obtained as:

$${k_{x,m,n}}^2 = {k_o}^2 \left(1 + \frac{\sigma_m}{1 - i\omega\tau_d}\right) - {k_{r,m,n}}^2 \tag{6.41}$$

In order to have a propagating duct mode, the real part of the R.H.S of Eq. (6.41) should be positive. That means the wavenumber should be greater than the corresponding wavenumber of the duct mode. The term next to ${k_o}^2$ is equal to one if the medium does not contain any particles. In the case of an aerosol σ_m and τ_d are not zero and dependent on the aerosol parameters like concentration, particle diameter, particle density etc. To see how these parameters can affect the characteristics of the duct, the axial wave number in axial direction "k_{axial}*" in the case of an aerosol is plotted against the axial wavenumber "k_{axial}" in the case of air

only for the first azimuthal, radial and hybrid duct modes. The system parameters used in the calculation are tabulated in Table 5.1.

The results for first azimuthal, radial and hybrid duct modes are shown in Figure 6.17, Figure 6.18 and Figure 6.19, respectively. As the volume concentration increases, the wave number is modified with an increase in its value towards the lower end and it may be fixed to a constant value which is dependent of the concentration level and the duct mode. On the other hand, the difference between the two wavenumbers is negligible towards the higher end which means the effect due to presence of particles in the medium gets weaker towards higher frequencies.

If the results are compared for the duct modes, it is obvious that the axial wave number in axial direction "k_{axial}*" in the case of an aerosol is greater for the hybrid mode (1, 1) which means the effect is more pronounced when the duct mode is higher.

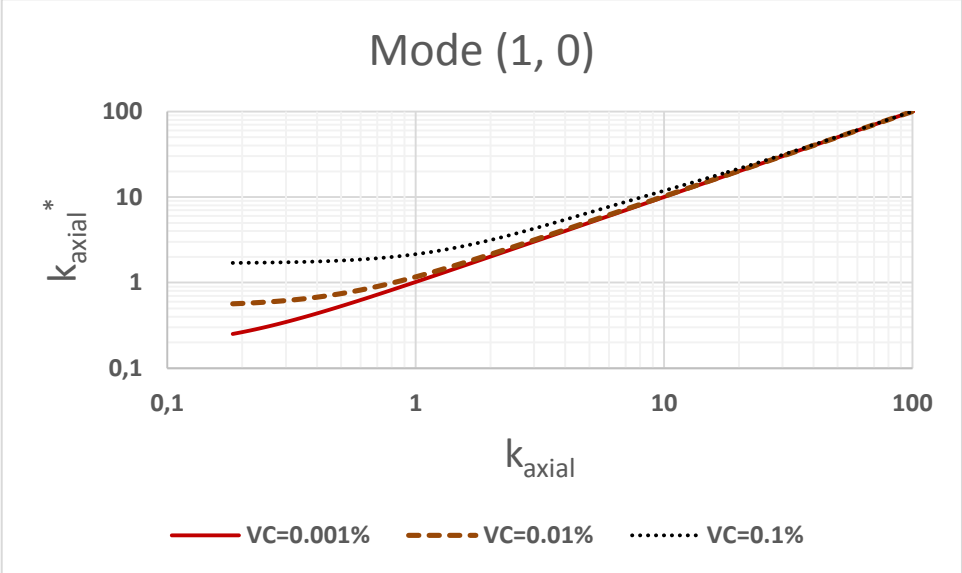


Figure 6.17 Modified wave number versus reference wave number in axial direction for three different volume concentrations: Duct mode (1, 0).

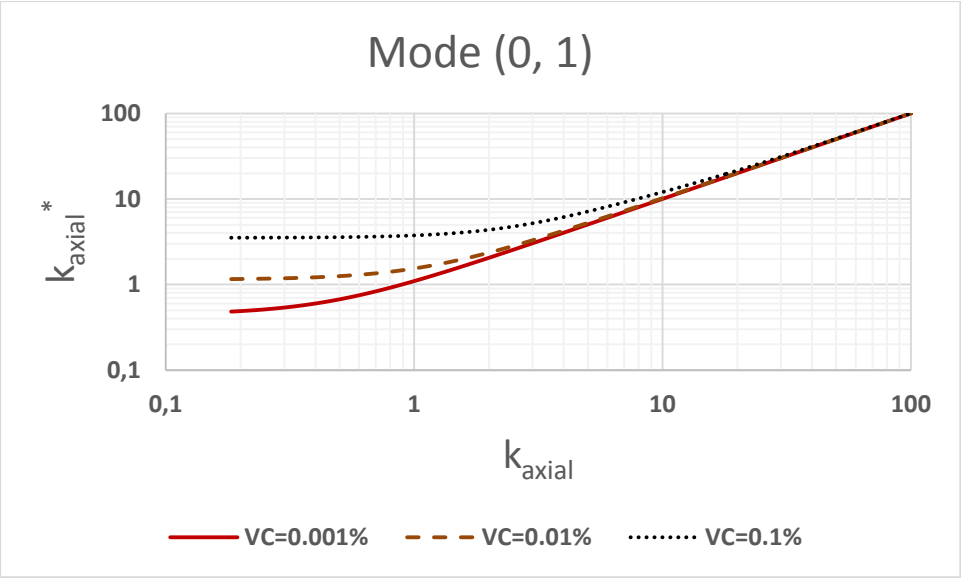


Figure 6.18 Modified wave number versus reference wave number in axial direction for three different volume concentrations: Duct mode (0, 1).

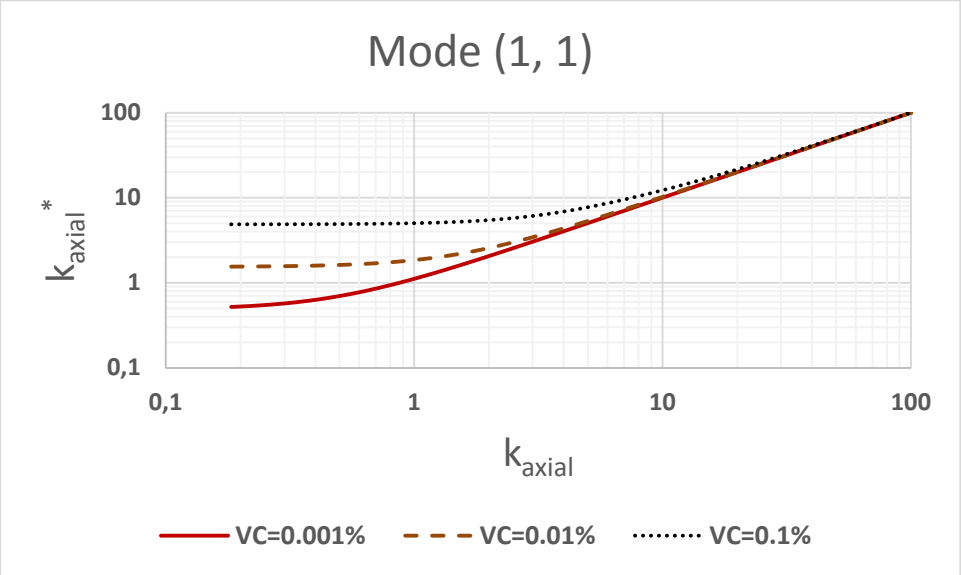


Figure 6.19 Modified wave number versus reference wave number in axial direction for three different volume concentrations: Duct mode (1, 1).

As a second scenario, the results of different average particle radius values of 1μm., 5μm. and 10μm. are shown for first azimuthal, radial and hybrid duct modes in Figure 6.20, Figure 6.21 and Figure 6.22, respectively. The volume concentration level is fixed to 0.1%.

Towards the lower and higher end, each result converges to the same values no matter what the particle size is. However, there are some variations in k_{axial}* in the range between 1< k_{axial}<500. When the particle radius is equal to 10μm, the modified wave number "k_{axial}*" converges to the reference value (no particle case) near the lower end. On the other hand; the convergence to the reference value happens towards the higher end if the particle radius is equal to 1μm. In other words, the effect of having particles is more pronounced and the influenced frequency range gets wider when the particle size gets smaller.

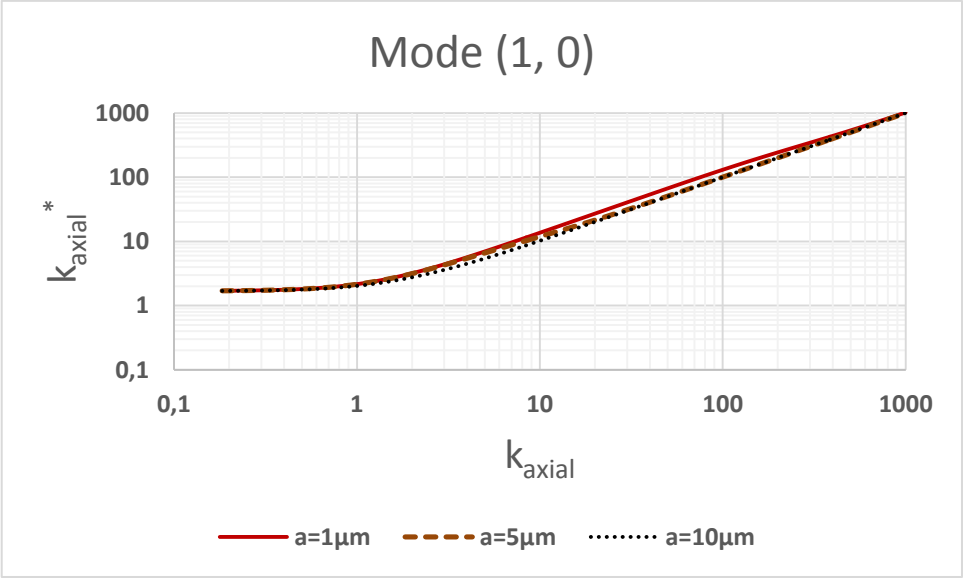


Figure 6.20 Modified wave number versus reference wave number in axial direction for three different particle size: Duct mode (1, 0).

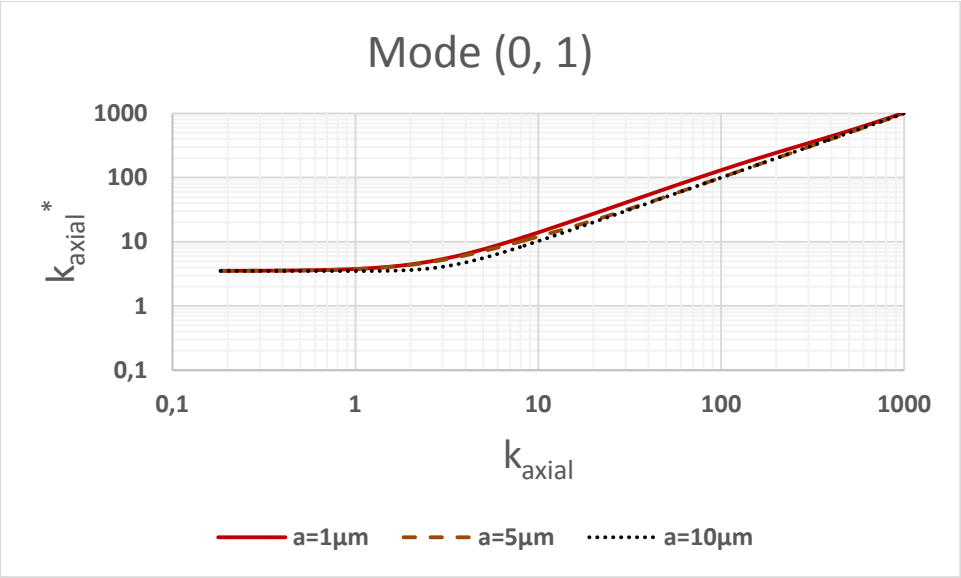


Figure 6.21 Modified wave number versus reference wave number in axial direction for three different particle sizes: Duct mode (0, 1).

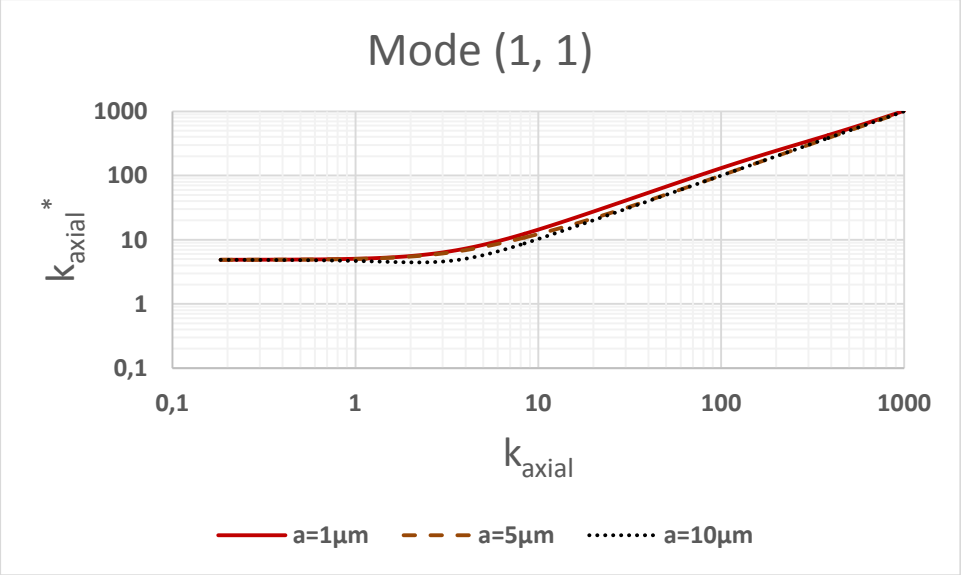


Figure 6.22 Modified wave number versus reference wave number in axial direction for three different particle sizes: Duct mode (1, 1).

As a summary, the aerosol parameters changes the wave number duct mode in the propagation direction which means the cut-off frequency limits of the duct is

affected by the aerosol parameters. These effects are more pronounced when the concentration level is higher and particle diameter is smaller. The change in the wavenumber starts at lower frequencies and generally extends to higher frequencies at decreasing levels and finally vanishes. Eventually, if the medium consist of particles, the cut-off frequency values of the duct has a tendency to decrease, and this effect can be adjusted through aerosol parameters, especially the average particle size.

CHAPTER 7

THREE DIMENSIONAL (AXISYMMETRIC) RESULTS AND COMPARISONS

7.1 Hard Boundary

The first set of result will be shared for the case in which the duct walls are considered as fully reflective; in other words, the wall condition is set to hard boundary.

7.1.1 Comparisons with Analytical Results

While calculating numerical and analytical results, the system is considered to be composed of air and water droplets at 20^{o}C, as specified in Table 5.1. Unlike the 1-D solution, the results will be given for various cases in which the waveform (mode of the duct) will be different. The pressure perturbation in axial direction of the duct is defined as an input and acoustical results are obtained with respect to frequency (axial). The diameter of the duct is set to unit radius of 1m. in the numerical solutions.

Mode (0,0)

In the first case, mode number (0, 0) which corresponds to a plane wave is considered. In Figure 7.1, the attenuation per distance results are given in the frequency range of 10 Hz- 10,000 Hz. Theoretical and numerical results match with each other perfectly for three different volume concentration levels.

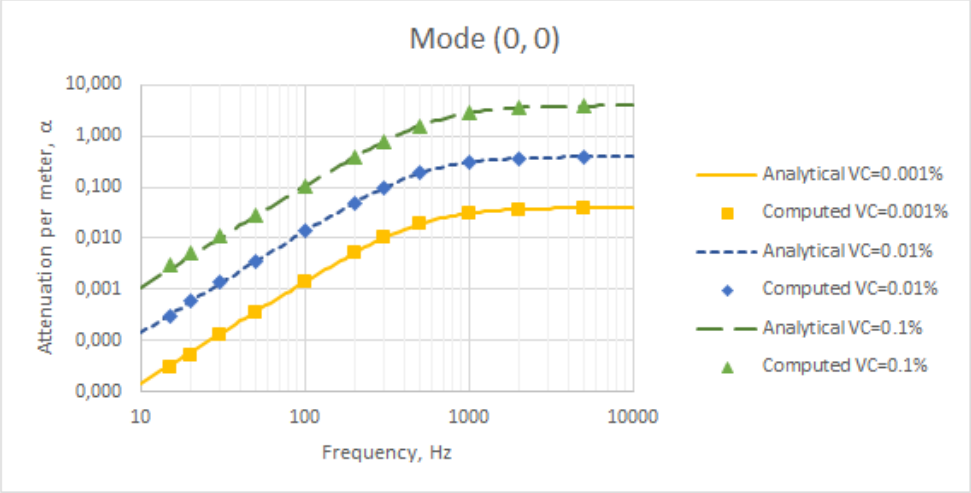


Figure 7.1 Analytical and numerical attenuation results of mode (0, 0).

In Figure 7.2, dispersion results are shown. The agreement between two approaches is excellent. As the NPPW is chosen as 30 by considering the wavelength of the incident wave's axial frequency, there are small errors due to finite precision. Other than that, the results looks the same with the ones obtained in1-D approach.

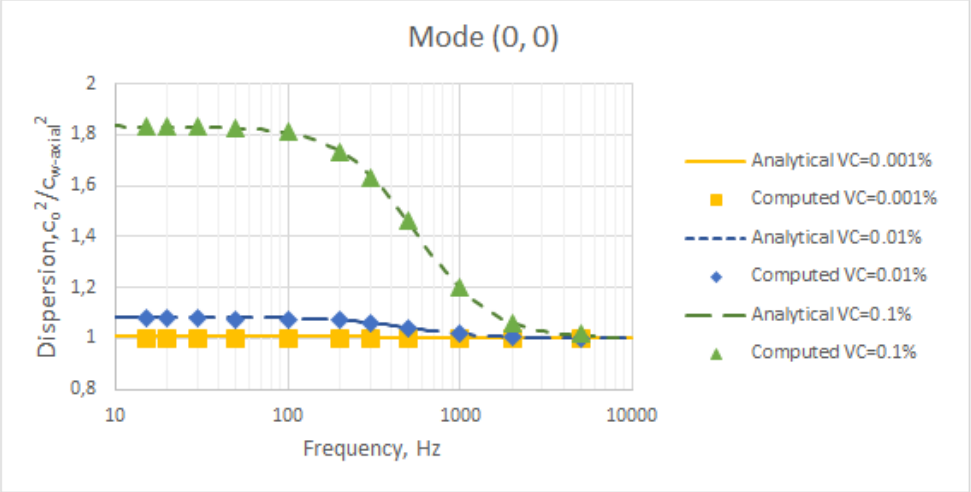


Figure 7.2 Analytical and numerical dispersion results of mode (0, 0).

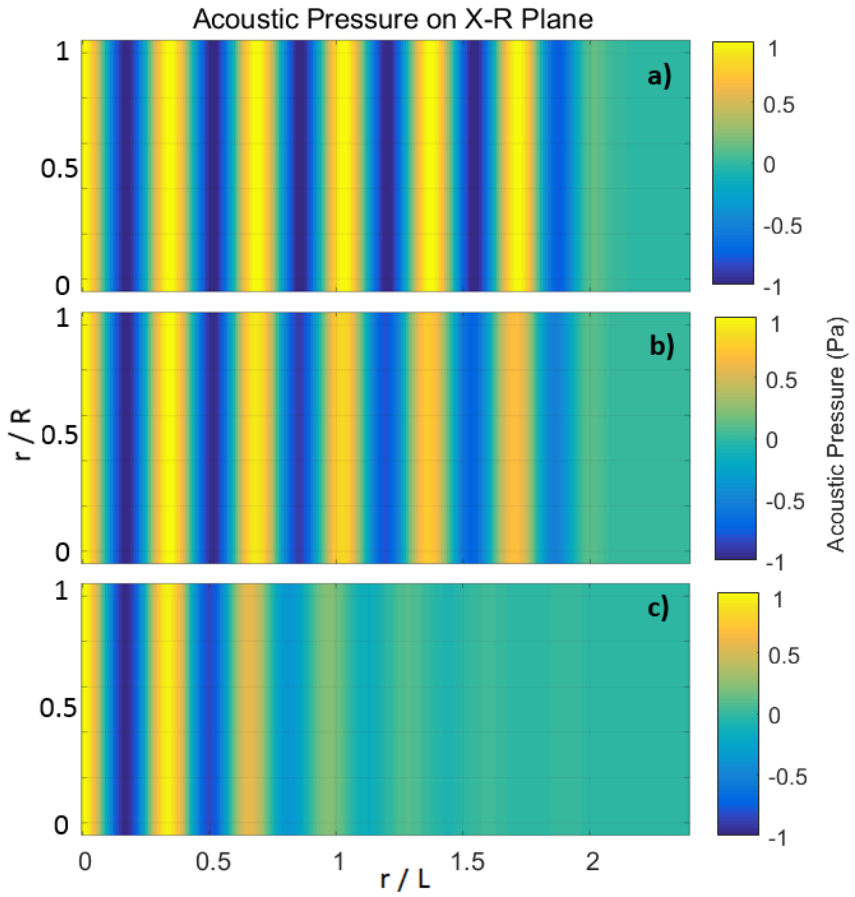


Figure 7.3 Numerical pressure results of mode (0, 0) at 1,000 Hz for volume concentrations: a) 0.001%, b) 0.01% and c) 0.1%.

The contour results in X-R plane for three different levels of concentrations are shown in Figure 7.3. The frequency of the incident wave is 1,000 Hz. The right side of the plots where pressure amplitudes decay to zero and the left side where pressure amplitudes stay constant, corresponding to PML regions. The attenuation and dispersion results have been obtained on these plots by finding the peak of the sequential peaks and making the related calculations. As the level of concentration increases, there is a significant increase in decay rate in axial direction. One can also recognize that dispersion (the change in wavelength) is very significant for the case where volume concentration is equal to 0.1%. On the other hand; there is no decay in amplitude in radial direction as stated in the analytical solution.

Mode (1,0)

In the second case, mode number (1, 0) which corresponds to first azimuthal wave is considered. According to Eq. (6.41), the complex wavenumber is dependent both on the mode number and the concentration parameters. As the frequency of the wave increase after a certain value such as ten times the cut-off frequency, the real component of the wavenumber is only dependent on the aerosol parameters by considering the level of magnitudes. The cut-off frequency of the mode in this configuration is equal to 10.05 Hz. Thus, it is expected to get similar dispersion results as the mode (1, 0) approximately above 100 Hz. On the other hand; the attenuation is supposed to be independent of the mode beyond cut-cut off frequency since the corresponding term is always real.

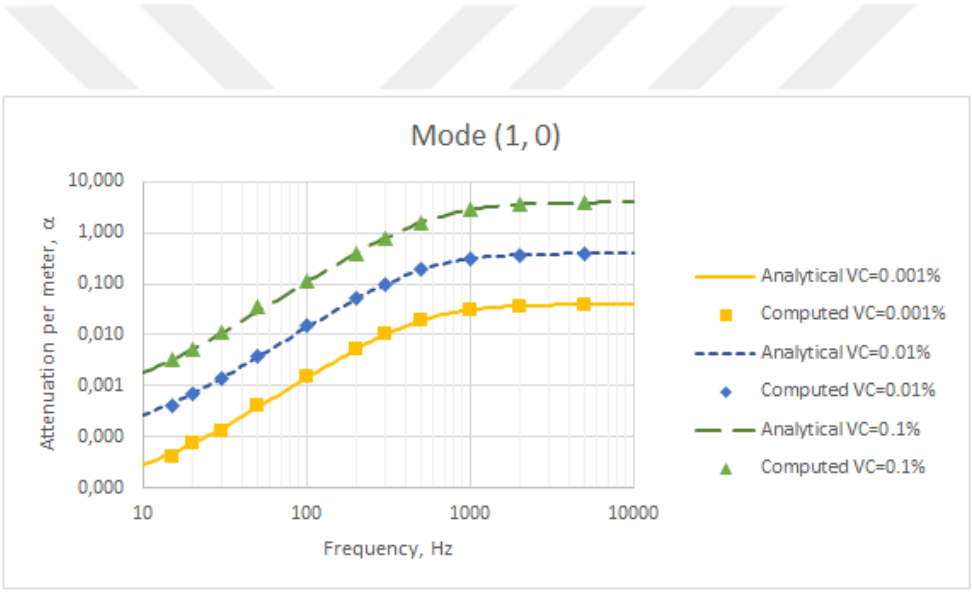


Figure 7.4 Analytical and numerical attenuation results of mode (1, 0).

The attenuation results of the first azimuthal mode (1, 0) for different concentration levels is shown in Figure 7.4. The results are almost the same as the mode (0, 0) as expected.

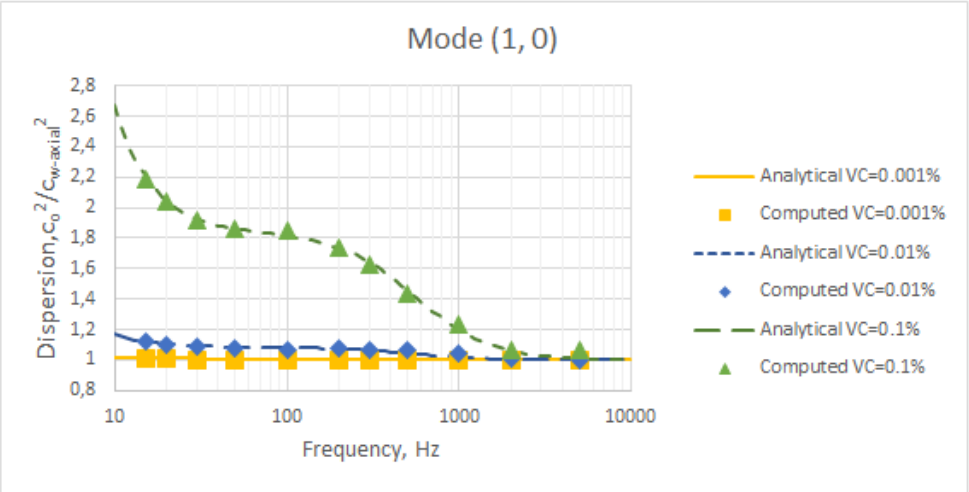


Figure 7.5 Analytical and numerical dispersion results of mode (1, 0).

In Figure 7.5, dispersion results are shown. Note that the x axis corresponds to the axial frequency of the incident pressure perturbation. The theoretical results showing different behavior than mode (0, 0) towards the lower frequency end and it is very significant for volume concentration of %0.1. This is an expected result as the frequency get closer to the cut off value, the complex wave number in axial direction gets dependent on both terms (concentration parameters and duct mode) as given in Eq. (6.41). And since the phase speed is scaled to speed of sound (343 m/s), it tends to go infinity in the limit of cut-off frequency.

The contour results in X-R plane for three different level of concentrations are shown in Figure 7.6. The frequency of the incident wave is 1,000 Hz. Similar to the previous case; as the level of concentration increases, there is a significant increase decay rate in axial direction.

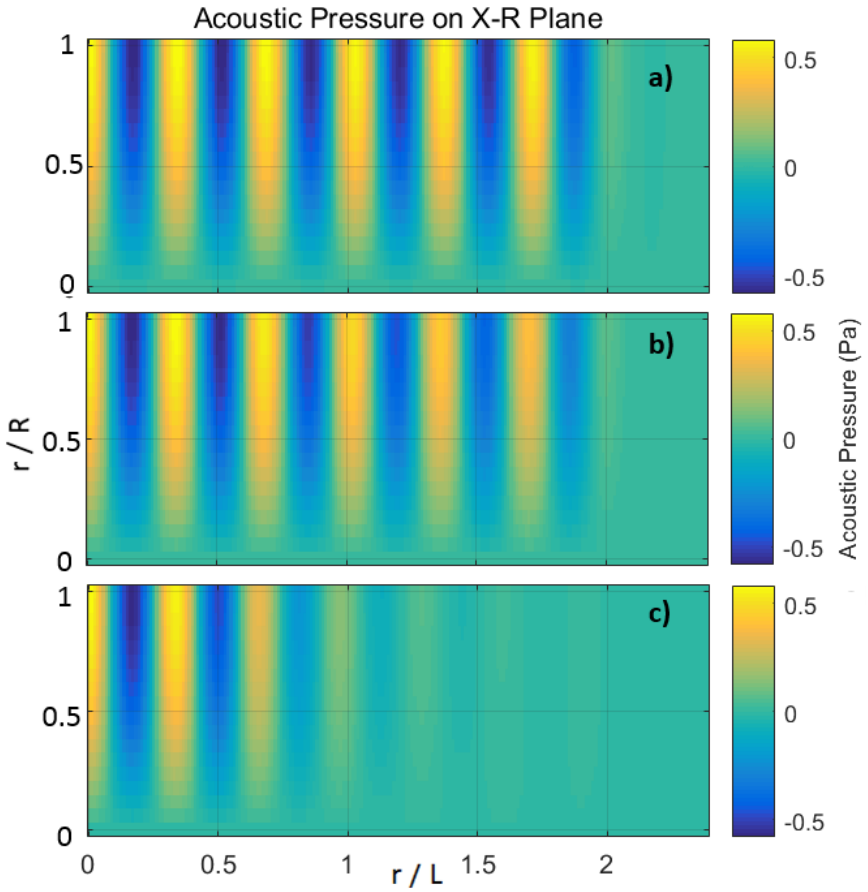


Figure 7.6 Numerical pressure results of mode (1, 0) at 1,000 Hz for volume concentrations: a) 0.001%, b) 0.01% and c) 0.1%.

Mode (0,1)

In the third case, mode number (0, 1) which corresponds to first radial mode wave is considered. The same conditions and explanations given for mode (1, 0) are valid hereby. The cut-off frequency of the mode in this configuration is now equal to 20.9 Hz. Accordingly, the dispersion results will expected to be the same as of the mode (0, 0) approximately above 100 Hz. The attenuation results of the first radial mode (0, 1) for different concentration levels are shown in Figure 7.7.

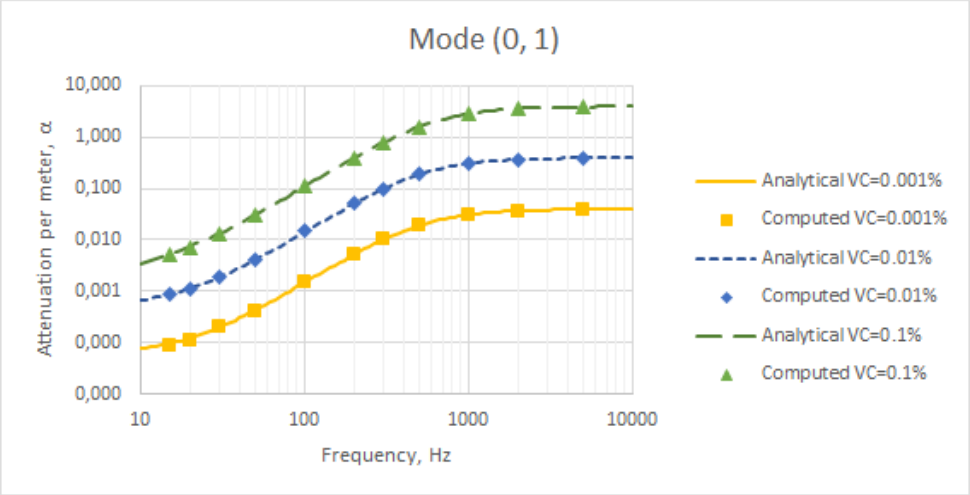


Figure 7.7 Analytical and numerical attenuation results of mode (0, 1).

In Figure 7.8, dispersion results are shown. Note that the x axis corresponds to the axial frequency of the incident pressure perturbation. Especially for volume concentration of 0.1%, the up-bending trend towards the lower frequencies becomes more significant.

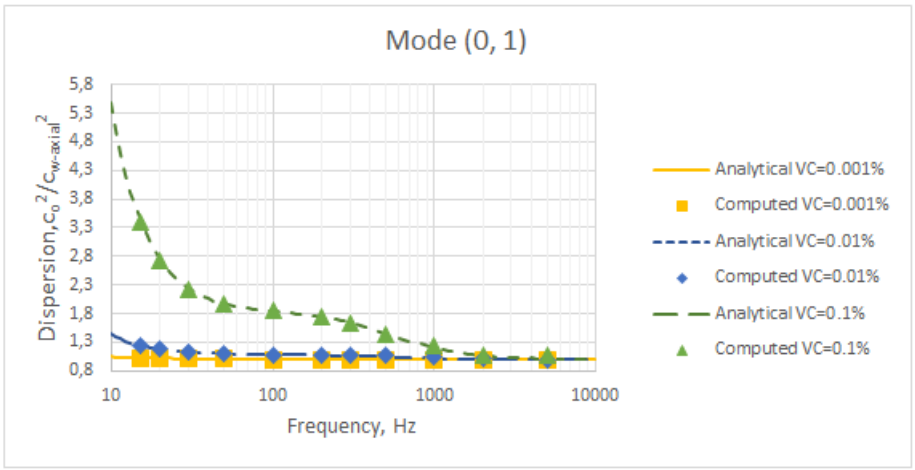


Figure 7.8 Analytical and numerical dispersion results of mode (0, 1).

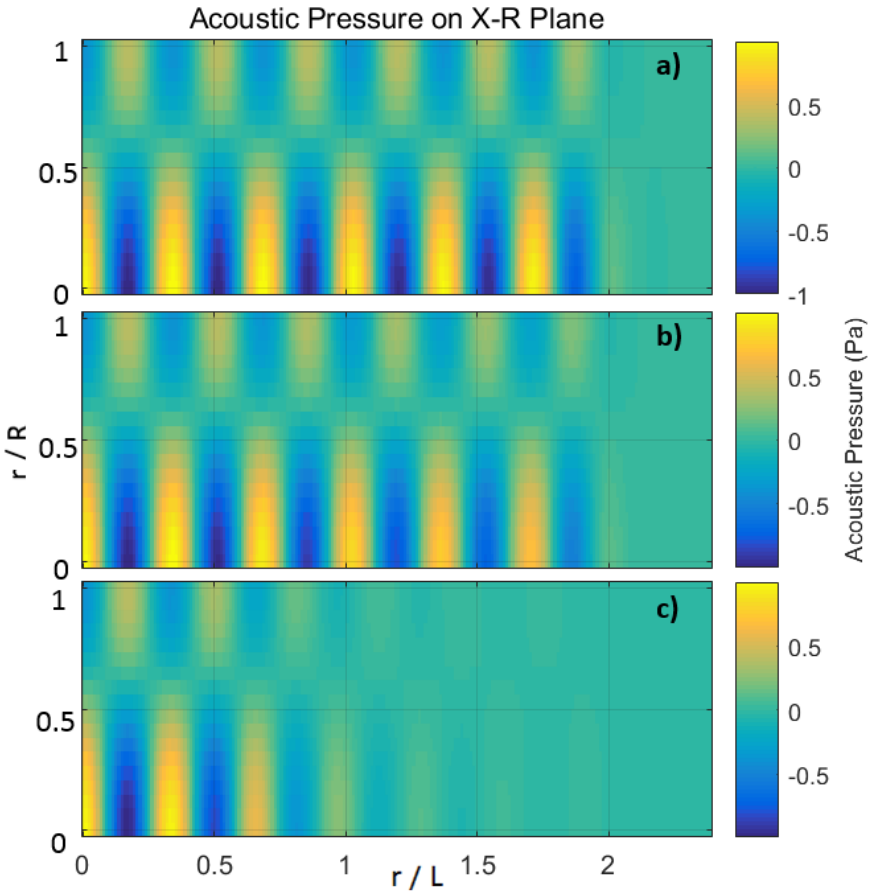


Figure 7.9 Numerical pressure results of mode (0, 1) at 1,000 Hz for volume concentrations: a) 0.001%, b) 0.01% and c) 0.1%.

The contour results in X-R plane for three different levels of concentrations are shown in Figure 7.9. The frequency of the incident wave is again taken equal to 1,000 Hz.

Mode (1,1)

In the last case, mode number (1, 1) which corresponds to first mixed radial and azimuthal (hybrid) mode wave is considered. The same conditions and explanations given for mode (1, 0) are valid hereby. The cut-off frequency of the mode in this configuration is now equal to 29.1 Hz. Accordingly, the dispersion results will be same as of the mode (0, 0) approximately above 100 Hz. The

attenuation results of the hybrid mode (1, 1) for different concentration levels are shown in Figure 7.10.

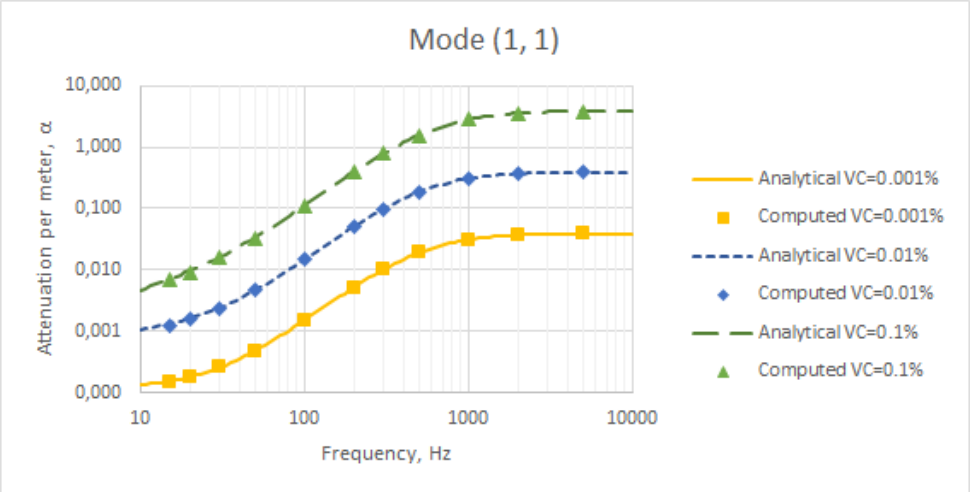


Figure 7.10 Analytical and numerical attenuation results of mode (1, 1).

In Figure 7.11, dispersion results are shown. Note that the -x axis corresponds to the axial frequency of the incident pressure perturbation.

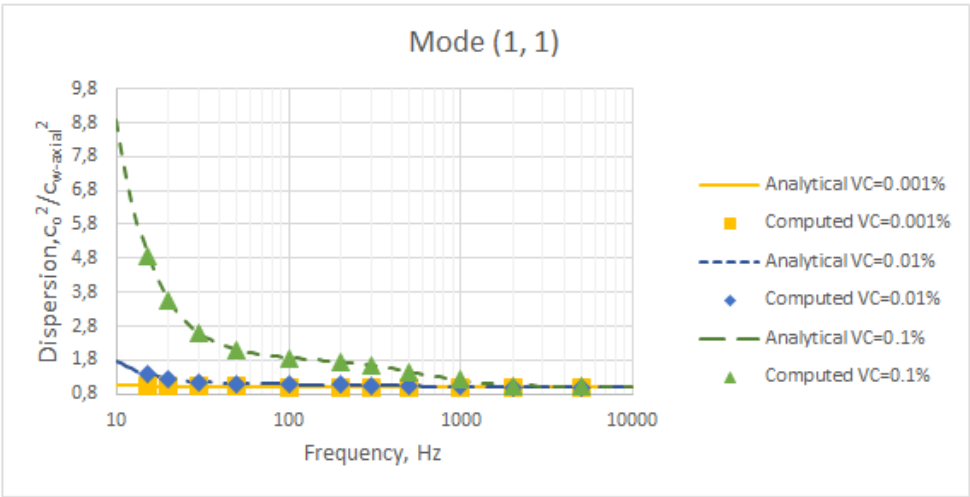


Figure 7.11 Analytical and numerical dispersion results of mode (1, 1).

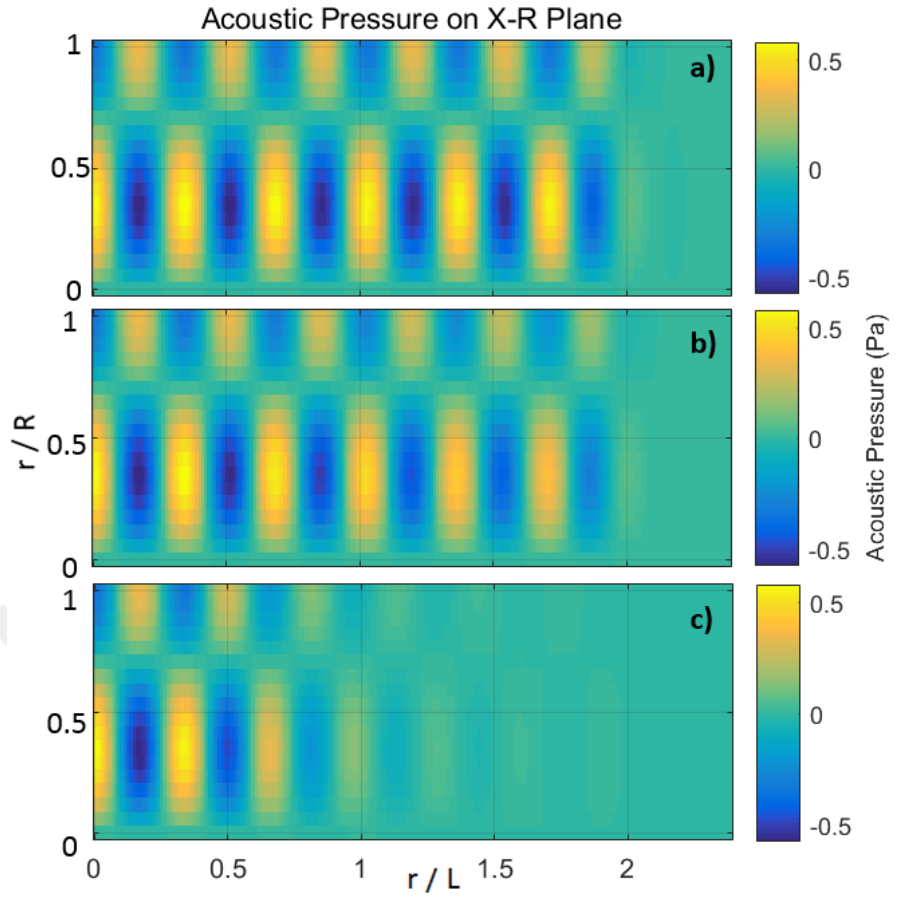


Figure 7.12 Numerical pressure results of mode (1, 1) at 1,000 Hz for volume concentrations: a) 0.001%, b) 0.01% and c) 0.1%.

The contour results for mode (1, 1) in X-R plane for three different levels of concentrations are shown in Figure 7.12. The frequency of the incident wave is 1,000 Hz. Again, the dispersion in the results is more visible to catch even with naked eye when the concentration level is equal to 0.1 %.

7.1.2 Additional Results

As theoretical and numerical results for 3-D case have been crossed checked with each other, additional results can be obtained by analytical approach. Previously, it has been observed that particles can change the cut-off frequencies of the duct and this effect is dependent on duct and aerosol parameters. In order to understand

this clearly, solutions are made by parametrically changing volume concentration and particle radius with respect to axial (propagation) frequency. The aim is to see how these parameters can change the cut-off frequency of the duct. The condition for propagation along the duct is satisfied according to the given formula below:

$$k_o{}^2 \left(1 + \frac{\sigma_m}{1 - i\omega\tau_d}\right) - k_{r,m,n}{}^2 > 0 \tag{7.1}$$

where ω is the frequency in radians per second in axial direction (propagation frequency). It is obvious that the condition is dependent on this frequency as well as the aerosol parameters, the wavenumber of the corresponding duct and the duct mode. The Eq. (7.1) can be re-written by ignoring the imaginary parts (this assumption is valid for dilute suspensions) so as to find the change in the cut-off frequency:

$$\frac{f_{cut-off}}{k_{r,m,n}} \approx Re\left\{\frac{1}{2\pi}\frac{c_o}{\sqrt{1 + \frac{\sigma_m}{1 - i\omega\tau_d}}}\right\} \tag{7.2}$$

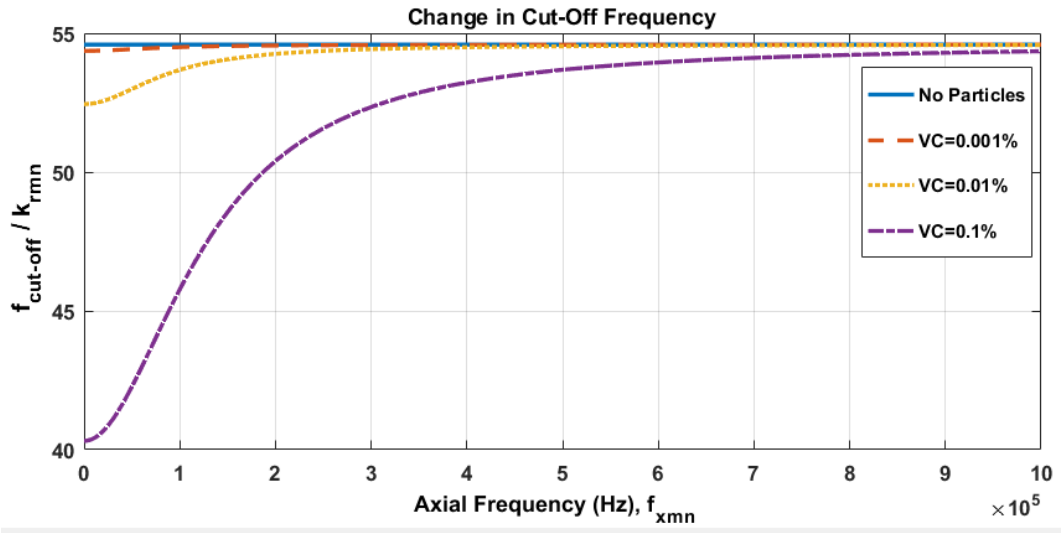


Figure 7.13 The change in the cut-off frequency for different volume concentrations versus axial frequency, linear axis.

In Figure 7.13, the change in the scaled cut-off frequency is plotted against the axial frequency for three different volume concentration levels, as well as for the case with no particles. The system parameters used in the calculation are as given in Table 5.1. The average value of the particle radius is fixed to 1μm. In the higher frequency end, the change is related to the equivalent physical properties (density) of the system and it can be regarded as insignificant up to the order of 0.1% volume concentration. On the other hand, there is significant difference towards the lower frequency end. It is obvious that the change (the decrease) in the cut-off frequency becomes greater as the concentration level increases. In order to investigate the behavior better, the same graph is plotted with logarithmic axis in Figure 7.14. Towards the lower end, the cut-off frequency values converge to single values for each concentration level. For the corresponding particle size, the convergence happens at almost 1,000 Hz for the three concentration levels. It shows that this frequency is probably dependent on the particle size.

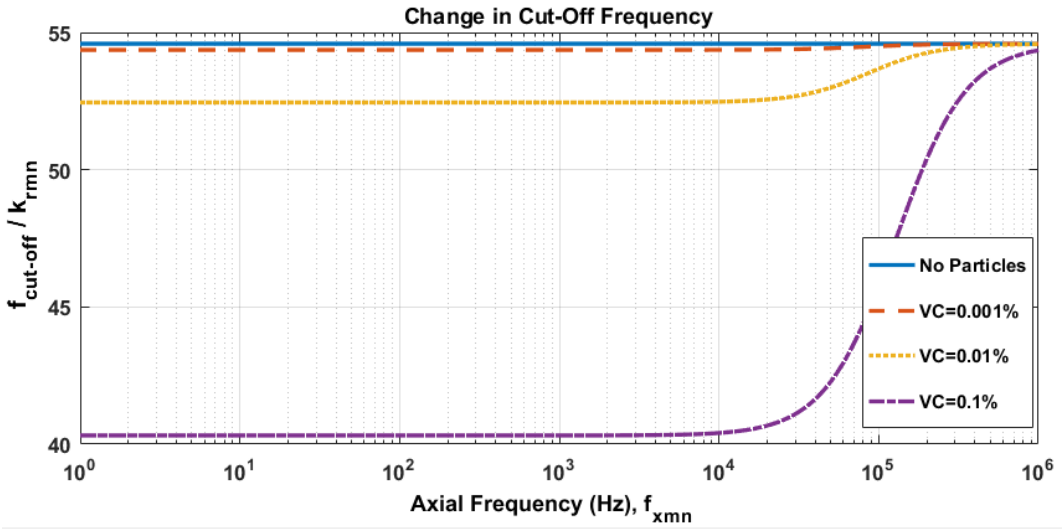


Figure 7.14 The change in the cut-off frequency for different volume concentrations versus axial frequency, logarithmic axis.

In the second set, the volume concentration of the particles (water droplets) is kept constant at VC=0.1%, while the diameters of the particles are changed. The corresponding results are shown in Figure 7.15. The first data again corresponds to the case where the fluid is air only. As the radii of the particles get smaller, the difference in the cut-off frequency values decreases. This change is more recognizable when the radius is equal to 1μm. and the affected frequency range extends up to the higher end.

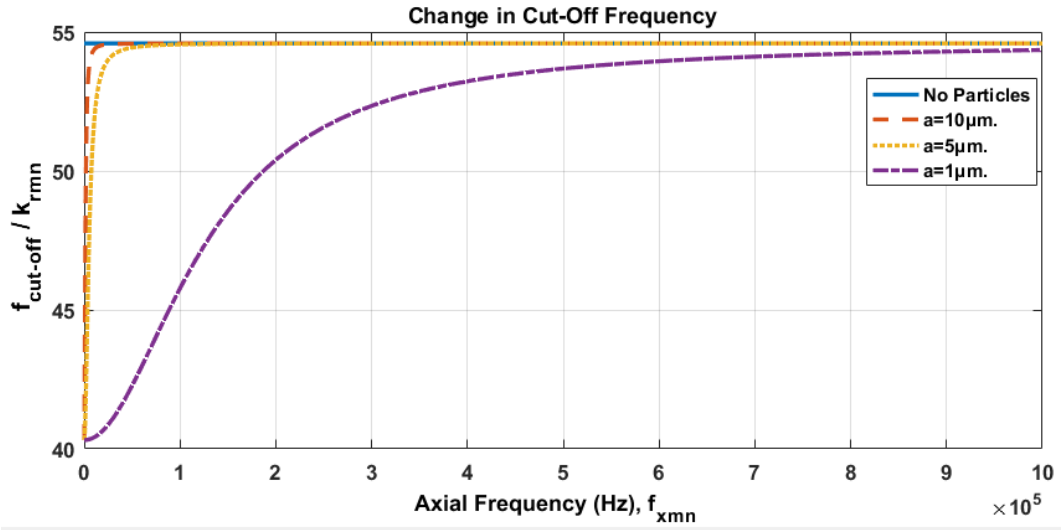


Figure 7.15 The change in the cut-off frequency for different particle radius parameters versus axial frequency, linear axis.

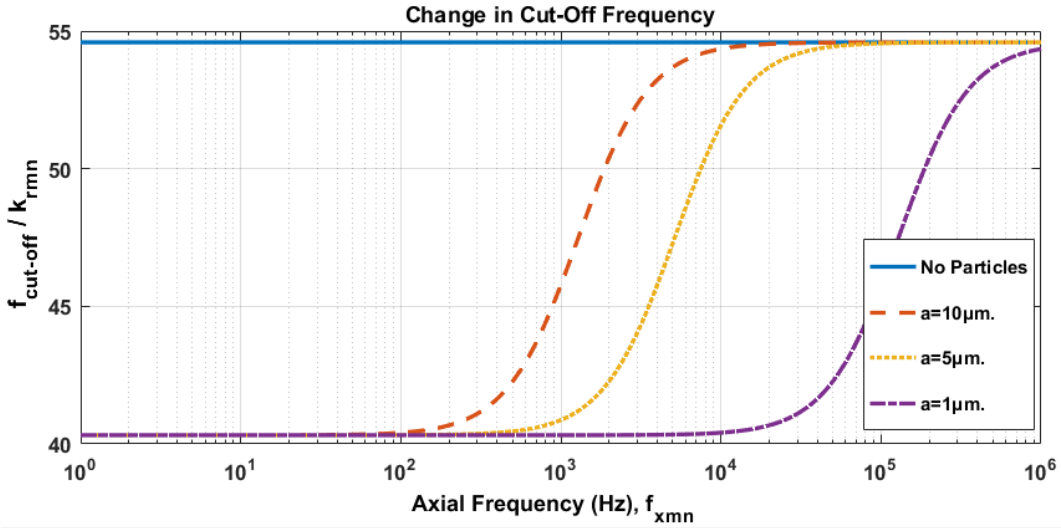


Figure 7.16 The change in the cut-off frequency for different particle radius parameters versus axial frequency, logarithmic axis.

The same plot is redrawn with logarithmic axis in Figure 7.16. The results show that each function converges to a single value towards the lower end, no matter what the particle size is. However; it is clear that the size of the particle shifts the

rate of the convergence behavior in a way that as the size gets bigger, the affected range gets narrower.

As a summary, presence of particles in a medium can change the acoustic modes of the duct. This change is dependent on the volume concentration and the size of the particles. It should be noted that the effect due to particle size is also dependent on the frequency. It is important to remember that these results and deductions are valid for aerosols of dilute concentrations. Thus, if the concentration levels become so high that this condition is not complied, then the predictions made by using the results presented herein will not be valid.

7.2 Impedance Boundary

The boundary condition on the wall may not necessarily be always hard boundary, rather there can be absorptive linings for noise control purposes or the wall is not hard enough. In order to take these effects into consideration and solve the sound propagation problem through an aerosol, the wall boundary condition in the model has been extended. Now, one can assign an impedance value or surface absorption value onto the walls.

7.2.1 Comparisons with a Commercial Code: Purely Air

In order to verify the code's solver capability with impedance surface condition, several comparisons have been made with ANSYS Mechanical® software which has a finite element solver. It has the capability of solving acoustic propagation problems by means of wave equation with several different loading and boundary conditions.

The problem considered here is again sound propagation through a cylindrical duct. The inner wall of the duct is assumed to have absorptive linings. The results have been obtained for the duct modes of (0, 0), (1, 0), (0, 1) and (1, 1). The radius of duct is conveniently taken as 0.5 meters so that the dispersion of the

waves is easier to observe. The frequency of the wave (in axial direction) is defined as 1,000 Hz. The boundary condition on the inlet and the exit of the duct allows the waves to exit the duct without back reflection.

The boundary condition on the wall has been modified in the code in appropriate form so as to define the impedance value. The assumption is that the acoustic velocity v which is in the normal direction to the wall is not zero on the boundary. Thus, we use the definition of impedance Z to relate this normal velocity with the pressure. The corresponding boundary equations are given in Table 7.1.

Table 7.1 Impedance boundary conditions on the wall.

Boundary	$\hat{\boldsymbol{p}}$	$\hat{\boldsymbol{u}}$	$\hat{\boldsymbol{v}}$	$\hat{\boldsymbol{w}}$
Wall	${}^{\partial p}/_{\partial r} = \frac{-i\rho_o\omega}{Z}p$	Extrapolated	$v = {}^{p}/_{Z}$	Extrapolated

In case where acoustic surface absorption coefficient is desired to be defined, then, the relation between normal incident sound absorption and impedance must be known. The standing wave solution of plane wave is as given below [101]:

$$Z = \rho_o c_o \frac{1+R}{1-R} \tag{7.2}$$

where R is the reflection coefficient and it has a relation with the surface absorption coefficient α_{su} as $R = \sqrt{1-\alpha_{su}}$. Thus, if α_s is defined then the corresponding value for the surface impedance can be calculated.

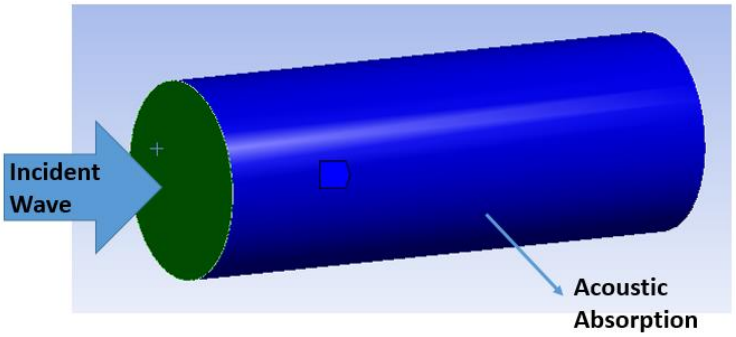


Figure 7.17 Acoustic absorption surface and the location of the incident wave

As shown in Figure 7.17, the surface absorption coefficient α_s has been defined all over the inner surface of the duct and it is equal to 0.9. The incident waves have been introduced into the problem domain from the left side of the duct. The medium is considered as air only at 20°C temperature. The details of the ANSYS® model and the corresponding definitions are given in Appendix-C.

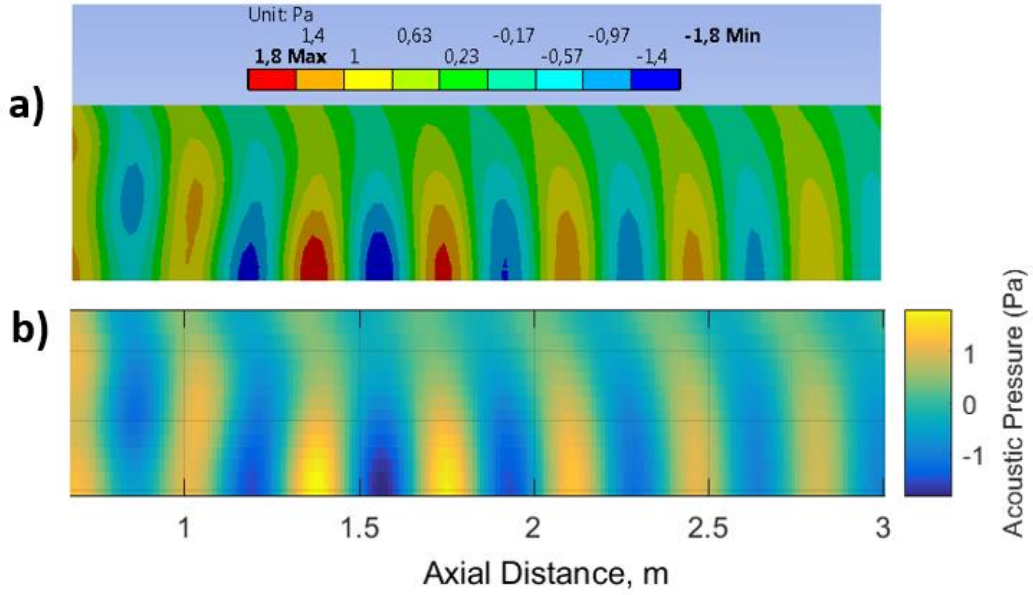


Figure 7.18 Acoustic pressure results in X-R plane of a) ANSYS Mechanical, b) developed code for duct mode (0, 0).

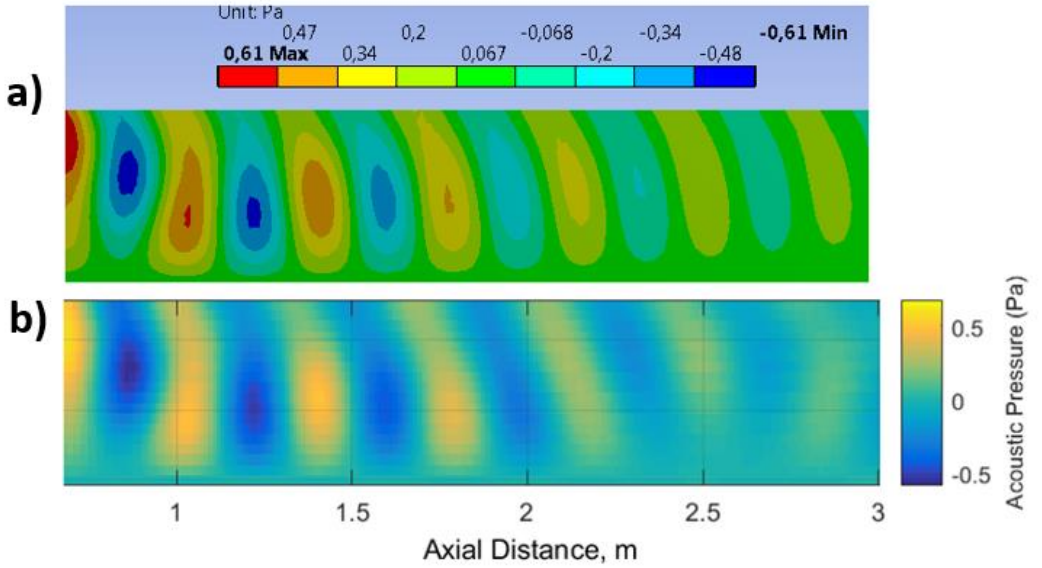


Figure 7.19 Acoustic pressure results in X-R plane of a) ANSYS Mechanical, b) developed code, for the duct mode (1, 0).

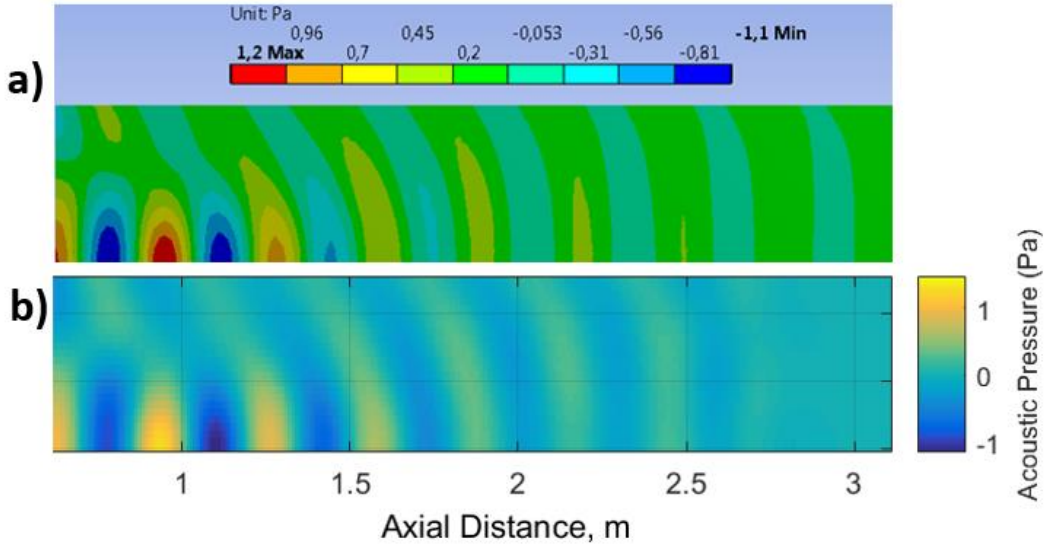


Figure 7.20 Acoustic pressure results in X-R plane of a) ANSYS Mechanical, b) developed code, for the duct mode (0, 1).

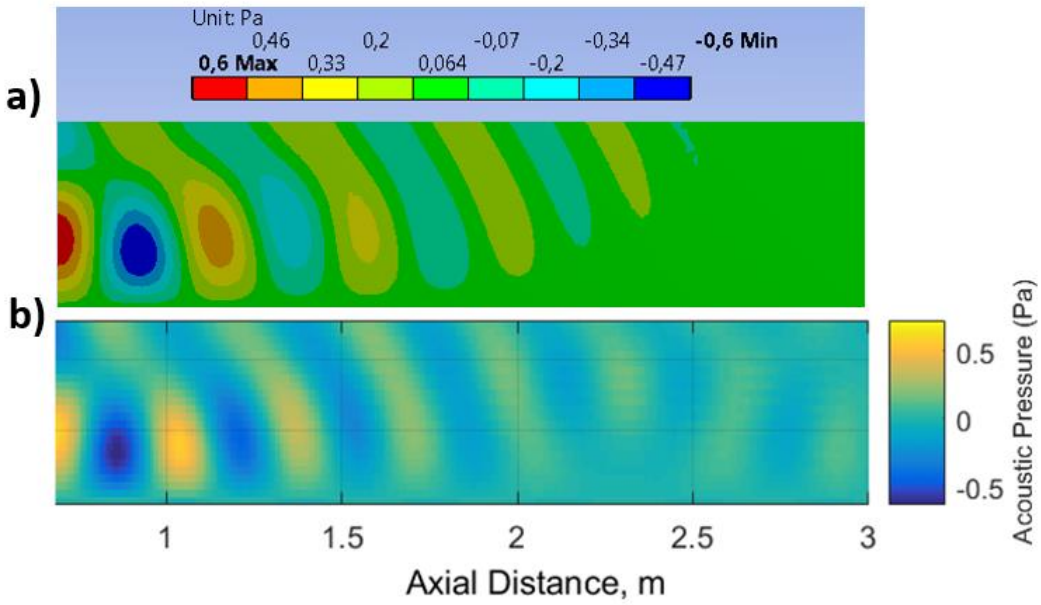


Figure 7.21 Acoustic pressure results in X-R plane of a) ANSYS Mechanical, b) developed code, for the duct mode (1, 1).

Acoustic pressure distribution plots for modes (0, 0), (1, 0), (0, 1) and (1, 1) are given in Figure 7.18, Figure 7.19, Figure 7.20 and Figure 7.21, respectively. The results match with each other very well. Each of the plots shows that due to high valued surface absorption coefficient and wide duct section, the incident acoustic waves are dispersed so much that they lose their initial mode shapes. This situation has been chosen deliberately in order to show that the model has very high performance of capturing the accurate results even in challenging problems.

7.2.2 Aerosol Medium: Water Droplets in an Air

In this section acoustic pressure distribution in the case of an aerosol medium and impedance wall condition will be investigated. Previously, the results of hard boundary condition for the first four duct modes have already been shared. The focus will be on the effect of the acoustic surface absorption boundary condition. The surface absorption coefficient will take values of 0.25, 0.50 and 0.75. The duct radius will be taken as 0.5 meters and the frequency of the incident wave will be 1,000 Hz. The system is considered to be composed of air and water droplets at

20^{o}C, as specified in Table 5.1. The volume concentration is fixed to 0.01% and the average radius of the water droplets is 5 μm.

- **Mode (0, 0)**

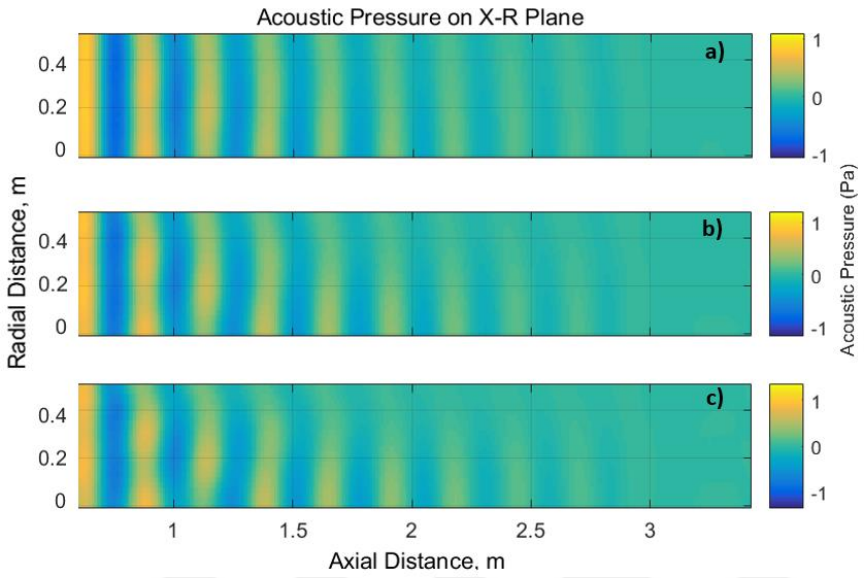


Figure 7.22 Acoustic pressure results in X-R plane of the mode (0, 0) with a)α_{su}=0.25, b) α_{su} =0.50 and α_{su} =0.75.

- **Mode (1, 0)**

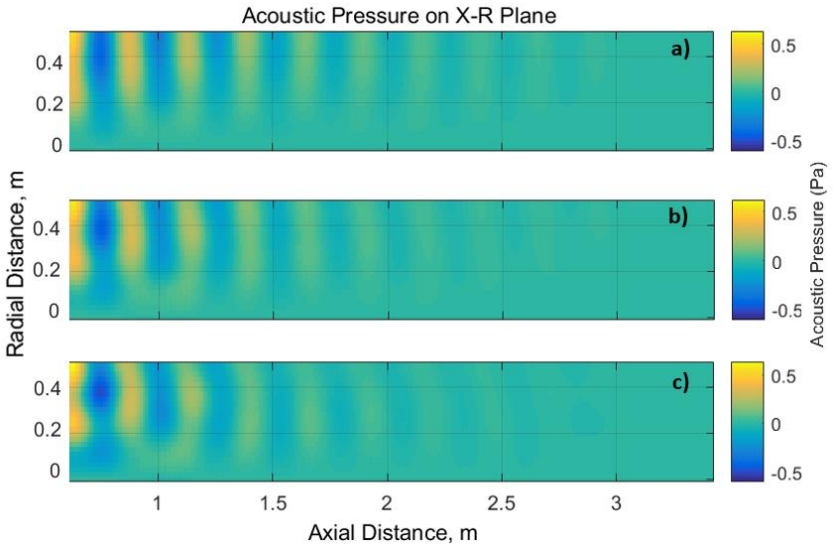


Figure 7.23 Acoustic pressure results in X-R plane of the mode (1, 0) with a)α_{su}=0.25, b) α_{su} =0.50 and c) α_{su} =0.75.

- **Mode (0, 1)**

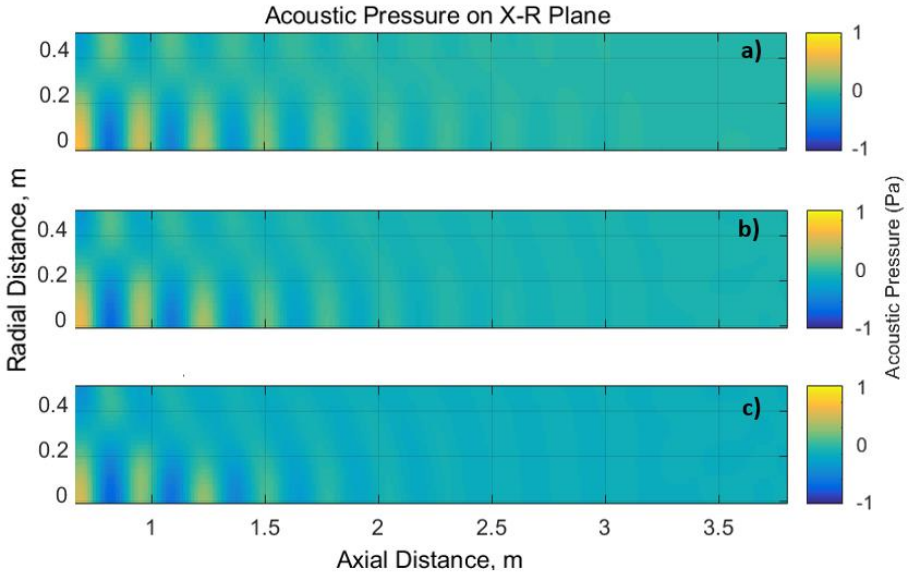


Figure 7.24 Acoustic pressure results in X-R plane of the mode (0, 1) with a)α_{su}=0.25, b) α_{su} =0.50 and c) α_{su} =0.75.

- **Mode (1, 1)**

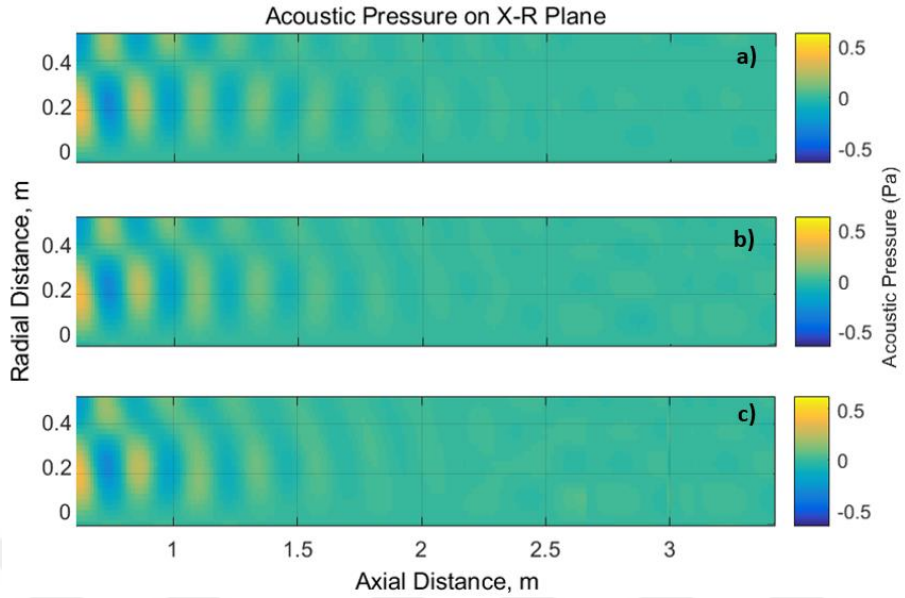


Figure 7.25 Acoustic pressure results in X-R plane of mode (1, 1) with a)α_{su}=0.25, b) α_{su} =0.50 and c) α_{su} =0.75.

Acoustic pressure distribution plots of different surface absorption value for mode (0, 0), (1, 0), (0, 1) and (1, 1) are given in Figure 7.22, Figure 7.23, Figure 7.24 and Figure 7.25, respectively. The common traits for each mode are:

- As the surface absorption coefficient α_{su} is increased, the original waveform of the waves changes more
- As α_{su} is increased, the attenuation is increased; especially the amplitude of the pressure near the duct wall starts to decay firstly.

Although the total attenuation along the duct is thought to be dependent on the size of the duct, in order to estimate whether it is equal to linear summation of the individual attenuations due to water droplets and absorptive wall, the results of attenuations is obtained for different set of conditions for mode (0, 0). The corresponding results are shown in Table 7.2.

Table 7.2 Attenuation per meter for different media and boundary conditions.

Radius=0.5 m.		**Hard Wall**	$\alpha_s = 0.25$	$\alpha_s = 0.50$
Mode (0, 0) 1,000 Hz	**Pure Air**	0	0,023	0,040
	VC=0.001%	0,031	0,054	0,072
	VC=0.01%	0,308	0,337	0,360
	VC=0.1%	2,840	2,887	3,930

Columns starting with α_s correspond to the case where surface absorption is assigned with the indicated values. For $\alpha_s = 0.25$ and $\alpha_s = 0.50$, the total attenuation values are nearly equal to the linear summation of the attenuation due to surface absorption and the attenuation due to particles for low concentration levels, while it is solely equal to the attenuation due to particles for high VC levels.

Consequently, the total attenuation may be predicted for low surface absorption, low VC levels and sufficiently large sectioned duct ($wavelength < duct\ radius$) conditions as;

Total Attenuation $\cong$ Attenuation (due to water droplets + due to surface absorption).

7.3 Summary

In this chapter, the computed 3-D results have firstly been compared with the analytical results and the agreement is excellent. This means that developed approach can be adapted to rather more complex but still axisymmetric problems in the field of engineering like particle characterization in pipes for chemical processes and acoustic agglomeration applications. Next, the validity of the numerical solution for wave propagation in circular duct with impedance wall has been verified with the commercial software ANSYS® in the case of purely air media. Then the particle parameters have been turned on and several acoustic

results have been shared for different duct modes with absorptive duct walls in order to see the capability of the method for such problems.

Other than that, 3-D analytical results which shows effect of aerosol parameters on the acoustics of the cylindrical duct have been shared. These results show that the aerosol parameters create inconstant changes on the acoustic modes of the duct with respect to frequency.

CHAPTER 8

SUMMARY AND CONCLUSION

8.1 Summary

This study aims to develop a numerical model to solve the sound propagation in aerosols and to obtain acoustic absorption and dispersion characteristics of the system. Such media exist in many engineering fields; such as atmospheric sciences, chemical engineering, environmental engineering and biomedical applications. In addition to these, there is also a particular marine engineering application where sea water is injected into hot exhaust lines in order to suppress exhaust noise and decrease exhaust temperature. The air-water mixed medium in the exhaust duct can also be regarded as an aerosol. Predicting acoustic parameters for different geometrical, operational and physical parameters at the design stage is very important.

Several analytical approaches exist in literature, which are capable of calculating these parameters for very basic conditions only. In addition, these approaches are based on many simplifying assumptions. Although some of these approaches yield satisfactory results in limited engineering fields such as atmospheric sciences, a more complete solution for analyses of problems in detail and for accurate predictions of acoustical parameters is needed. This can be achieved through numerical approaches.

Coupled phase theory yielded very successful results (Fig 2.2.) when compared with the experimental data [13]. In addition to its superiority for aerosol acoustics

among other theories as it is based on continuum approach, it has been chosen as the reference theory for developing the numerical model in this thesis.

The reference theory has the solutions for acoustic attenuation and dispersion parameters based on the given conditions and assumptions below;

- Problem is considered as 1-D, thus only plane wave propagation is valid,
- As the problem is 1-D, the solution do not include any boundary conditions,
- The medium is stationary, in other words there is no mean flow effects,
- The theoretical solutions are valid only for dilute aerosols and the ratio of particle mass to gas mass (mass loading) is negligible.

8.1.1 One Dimensional Results

In the first stage, 1-D numerical model has been developed on MATLAB®. The numerical scheme is based on 4^{th} order finite difference spatial discretization. The governing equations have been derived for both gas and a particle phase (water droplets) by assuming each phase occupies its own volume, as the theory depicts. Since the compressibility of water droplets is very low compared to air, they have been assumed as rigid. That means there will be no pressure perturbation for the particle phase, and thus there is no need to write an equation of state. The energy transfer between the phases is assumed to be through momentum and heat exchange. These interaction processes are defined through Stokes' drag law and Fourier's heat conduction law, respectively. Similar to the analytical reference, the numerical results have been obtained for two different cases;

- Sound propagation without thermal effects: The heat transfer between the gas and the particles is ignored, the interaction is only momentum exchange due to viscous drag,
- Sound propagation with thermal effects: Both momentum and heat transfer between the phases are considered.

The numerical results have been compared with the analytical results for each case. There is almost perfect matching for the attenuation and dispersion parameters when the concentration of the particles is as low as 0.001 % at which the mass loading parameter is small enough to be neglected. However; as the concentration level increases up to 0.1 %, the numerical results differ from the analytical ones significantly. This is because the reference analytical solutions are valid for low mass loading parameter. The finite mass loading has effects on the scaled attenuation parameter (attenuation per wavelength) as given;

- The increase in particle volume concentration is not linearly proportional with the peak value of attenuation. In other words, as the concentration level increases, increase in the attenuation value gets smaller.
- The increase in particle volume concentration shifts the frequency of the peak value of the attenuation up to higher frequencies.

On the other hand, an increase in particle concentration level changes the acoustic characteristics of the medium and thus dispersion happens. Compatible with the analytical results, the numerical results show that maximum dispersion exists towards the lower frequency end. However; similar to the results of attenuation parameter, as the particle concentration level increases up to a level that the mass loading becomes finite, the numerical dispersion values differ from the analytical (reference) values. This difference is very significant especially when the thermal effects are included in the solution in addition to the viscous effects.

In the second step, the 1-D code has been upgraded to include mean flow terms in order to include mean flow effect. The existing analytical solution does not include this effect, thus the governing equations in the analytical solution are also extended to cover the effects of mean flow. The corresponding system matrix cannot be reduced into a single analytical solution form. For this reason, Symbolic Math Toolbox™ module of MATLAB® has been adopted for extended analytical solution. According to the plotted results, both numerical and analytical results are identical. The effect of mean flow on the attenuation is obtained as expected, that is when the flow direction is upstream the attenuation values increase and it is

vice versa when the flow direction is upstream. When the scaled attenuation parameter is checked, the results show that the flow shifts the frequency of the maximum attenuation up and down according to the flow direction. This behavior is more pronounced when the thermal effects are included in the model.

The effect of mean flow on dispersion is also obtained as expected, the behavior is similar to the case of pure air. However, the relative percentage change in dispersion is not constant for all frequencies. The frequencies below the relaxation frequency seem to be more affected than the frequencies above it. For low concentration levels, the effect of flow on dispersion is uniform throughout the frequency range; while the effect is amplified towards lower frequencies (than the relaxation frequency) for higher concentration levels. The frequency value which corresponds to the maximum of scaled attenuation "$\hat{\alpha} = \alpha\, c_o/\omega$" shifts towards left or right depending on the direction of the flow. As expected, attenuation values increase when the flow is upstream and they decrease when the flow is downstream to wave propagation direction.

8.1.2 Three Dimensional Results

In the second stage, 1-D numerical model has been extended to 3-D axisymmetric version. The acoustic wave propagation is considered in a circular sectioned duct with axially symmetric system parameters and boundary conditions which makes it possible to handle the problem as axisymmetric. The numerical scheme is again 4^{th} order finite difference spatial discretization. The governing equations are almost the same as the1-D version except there are four additional equations of momentum, two for each phase. Rigid particle assumption is also valid in this case and the energy transfer between the phases is assumed to be isothermal, meaning there will be no energy transfer through heat conduction.

In the first step, the boundary condition is defined as hard surface. Because the existing analytical solution is valid for 1-D, it has been extended to include radial and azimuthal dimensions by means of axisymmetric transformations. Thus, the numerical results can be compared with the extended 3-D analytical results.

Firstly, the numerical model has been verified for purely air medium and several duct modes have been compared with the exact results. Next, particle parameters have been turned on and results have been obtained for different parameter sets. Both results (analytical and numerical) completely match with each other, meaning the code is now ready to solve complex problems for higher order modes with varying system parameters in radial direction also. In addition, the extended analytical solution is used to investigate the effect of particle concentration and size parameters on the cut-off frequencies of the duct for different parameter sets. These results are indeed very interesting in a way that the volume concentration level and particle radius parameters create variable changes on the acoustics of the duct with respect to frequency. Accordingly, if the cut-off frequency of a duct (filled with purely gas) is quite low, then it is more sensitive to particle concentration and tends to shift even down.

In the second step, the 3-D code has been extended to solve the wave propagation with the impedance wall condition. The input for the boundary condition can also be defined as surface absorption coefficient. Firstly, the capability of the code has been verified for purely air medium by comparing the corresponding results obtained from a commercial software. As the results match with each other, the numerical results are then investigated for different particle and surface absorption parameter sets. Quick deduction which predicts the total attenuation as the linear sum of the attenuation due to surface and particle effects, has been made for circular ducts with large radius such that the wavelength is shorter than the radius).

8.2 Conclusions

In the scope of this thesis, both numerical and analytical studies have been made in order to investigate the acoustic wave propagation through an aerosol. Such problems are of great importance in several engineering applications such as noise control applications, particle characterization, acoustic agglomeration and

thermal-acoustic stability control in combustion chambers. Although the solution methods that have been implemented so far in those applications are mostly experimental works, analytical solution methods are also used which can give reasonable results if the related assumptions are not violated. But, there is a need for more advanced solution methods so as to investigate the acoustic effects of different parameters (geometric, physical, and operational) of the problem specific.

Although the reference analytical solution which is called coupled phase theory yields successful results when compared to specific experimental data, it has also limitations. On the other hand, existing commercial acoustic software which are based on different methods like finite element, boundary element or statistical energy analysis, do not have the capability to solve sound propagation problems in suspension like media. Some of the CFD tools may indirectly have such capability while solving fluid flow problems with additional modelling techniques like discrete phase modelling, but they are not suitable in terms solution times since the solution techniques is in time domain. In particular, commercial FEA codes are not capable of solving acoustical attenuation and absorption characteristics of aerosols with relatively higher volume concentrations.

By means of the developed 1-D numerical solution, the attenuation and dispersion results are now can be obtained for finite volume concentrations and mean flow effects. The corresponding results in Chapter 5 have shown that these parameters have significant effects. Taking actual conditions in practice into account, it can be said that both parameters are present and that their effects on acoustical results are to be considered.

Although one of the primary assumptions in the governing theory for the developed method says that the aerosol must be dilute which means the ratio of the volume of the particle phase to the gas phase must not exceed any value which violates the energy interaction models between the phases. But it does not necessarily mean that the volume concentration level has to be of infinitesimal value. For example, when the volume concentration level is as high as 0.1 % in

the case of air with water droplets, the effective density is almost doubled compared to purely air case which results in nonlinear relation between attenuation and dispersion values and the volume concentrations. Similarly, other effective physical parameters can also change. While analytical solution methods fail to consider these changes in the solution, the developed numerical solution has this capability.

In most of the cases, the acoustic problems include convective (mean flow) effects. The existing analytical solutions do not include such convective terms, but the corresponding effect on dispersion and attenuation is rather predicted based on the results for single phase medium. However, results obtained by means of developed numerical and analytical methods this thesis have shown that the phenomena is more complex. The mean flow does not simply affect the sound propagation in conventional manner, but indeed it modifies the energy interaction (momentum transfer through drag) between the phases which is dependent on the size of the particles. The developed method has the capability to account for these effects on the solution. According to the reported results, the amplitude and the direction of the mean flow seems to have significantly different effect on the attenuation and dispersion near the frequency value of dynamic relaxation. As this frequency is of great focus in acoustic agglomeration and particle characterization applications, the effect of mean flow must not be ignored. With these new advancements in the theory, particle size and concentration identifications which are generally based on curve fitting through mathematical models can now be more accurately made, especially in chemical processes.

In most of the related applications such as acoustic agglomeration of fine particle in exhaust lines, noise suppression in wet exhaust systems, suspension (particle) characterization in flow pipes, etc. , the shape of the problem geometry is generally a duct with circular cross section. If the duct mode is a plane wave for the frequency of interest, the variation of aerosol parameters in radial direction is neglected and the duct walls are considered as perfectly reflective in terms of acoustic, then the 1-D solutions can be employed. If any of these conditions are

not satisfied, then there is a need for a 3-D solution. For this purpose, the 1-D numerical method is then upgraded to axisymmetric 3-D version which makes it possible to solve sound propagation in a cylindrical duct with hard or impedance wall boundary conditions. In addition, it has the capability of solving higher order duct modes.

Unlike 1-D case, there is no existing analytical solution for axisymmetric 3-D case. For this reason an analytical solution for obtaining the complex wavenumber in the case of an aerosol filled in a cylindrical duct has been developed herein. The governing equations are the same as those given in numerical approach. Both in the radial and azimuthal directions, mode shapes remain the same as the duct surfaces are assumed to be hard wall. The results of numerical and analytical solutions have been cross checked with each other. Eventually, one can use developed analytical solution if the duct surface is not absorptive and the medium is homogeneous.

For the acoustic applications in ducts, the cut-off frequencies of duct acoustic modes are generally calculated through well-known analytical solutions or numerical tools, both of which utilize the wave equation. If the medium does not consist of a single phase but it is rather a suspension (aerosol), then, sometimes equivalent physical properties are used in the solutions for convenience. However; according to the results given in Chapter 7, the particle parameters (size and concentration) have variable effects on the cut-off frequencies with respect to axial frequency. This is very interesting outcome in a way that the cut-off frequency is dependent on the incident frequency (axial) through the dynamics of the particles.

On the other hand, by means of the axisymmetric 3-D solution, one can solve sound propagation in a duct with impedance boundary conditions. In most of the actual case, there is an absorptive on the surfaces. In addition, the distribution of particles in the domain may not be homogenous as in the case of a combustion chamber of a jet. In order to calculate acoustic modes of the chamber (which is mostly axisymmetric), one should consider as many effects as possible to avoid

thermal-acoustic instability which happens when the frequency of the firing coincides with the chamber modes. When viewed from this aspect, the numerical method can be utilized to avoid such fatal issues.

Consequently, by means of the developed numerical and analytical solutions, one can investigate sound propagation problems in detail encountered in various engineering fields where the medium is regarded as an aerosol and whether there is a mean flow condition, or there are higher order duct modes in the frequency range, or the surface type of the duct is either hard or soft wall.

8.3 Recommendations for future work

This study can be improved by implementing further capabilities:

- The numerical method can be extended to include pressure perturbation variables of particle phase and additional terms so that it can be used to solve the acoustic wave propagation problem in a bubbly liquid. This can especially be attractive for people who are studying underwater acoustics.
- The numerical method can be extended geometrically to solve the acoustic wave propagation in various engineering applications like combustion chambers (acoustical stability), jet engines and rockets (noise propagation through aerosol), acoustic agglomeration applications, etc...
- The numerical method can be diversified to account for different drag laws or heat transfer functions in aerosols.
- The numerical method can be upgraded to include additional mass or energy laws.
- The numerical method can be extended to solve for aerosols with multi numbers of particle phase in the system.
- The solution algorithm can be upgraded and the type of discretization schemes can be tried for best solution times.

REFERENCES

[1] C. J. T. Sewell, “The Extinction of Sound in a Viscous Atmosphere by Small Obstacles of Cylindrical and Spherical Form,” *Philos. Trans. R. Soc. London. Ser. A, Contain. Pap. a Math. or Phys. Character*, vol. 210, no. 459–470, pp. 239–270, 1911.

[2] G. G. Stokes, “On the Effect of the Internal Friction of Fluids on the Motion of Pendulums,” *Math. Phys. Pap.*, vol. 3, pp. 1–122, 1922.

[3] P. S. Epstein, “On the absorption of sound waves in suspensions and emulsions,” Pasadena, California, 1941.

[4] R. J. Urick, “A sound velocity method for determining the compressibility of finely divided substances,” *J. Appl. Phys.*, vol. 18, no. 11, pp. 983–987, 1947.

[5] R. J. Urick, “The Absorption of Sound in Suspensions of Irregular Particles,” *J. Acoust. Soc. Am.*, vol. 20, no. 3, pp. 283–289, 1948.

[6] E. O. Knudsen, J. V. Wilson, and N. S. Anderson, “The Attenuation of Audible Sound in Fog and Smoke,” *J. Acoust. Soc. Am.*, vol. 20, no. 6, 1948.

[7] P. S. Epstein and R. R. Carhart, “The Absorption of Sound in Suspensions and Emulsions. I. Water Fog in Air,” *J. Acoust. Soc. Am.*, vol. 25, no. 3, pp. 553–565, 1953.

[8] B. G. Watters, S. Labate, and L. L. Beranek, “Acoustical Behavior of Some Engine Test Cell Structures,” *J. Acoust. Soc. Am.*, vol. 27, no. 3, pp. 449–456, 1955.

[9] J. W. Zink and L. Delsasso, “Attenuation and dispersion of sound by solid particles suspended in a gas,” *J. Acoust. Soc. Am.*, vol. 30, no. 8, pp. 765–771, 1958.

[10] J. C. F. Chow, “The Attenuation of Acoustic Waves in a Two-Phase Medium,” Rhode Island, 1963.

[11] R. A. Dobbins and S. Temkin, “Measurements of particulate acoustic attenuation,” *AIAA J.*, vol. 2, no. 6, pp. 1106–1111, 1964.

[12] B. T. Chu and J. Chow, “On a macroscopic theory of a two-phase fluid,” New York, 1965.

[13] S. Temkin and R. A. Dobbins, “Measurements of attenuation and dispersion of sound by an aerosol,” *J. Acoust. Soc. Am.*, vol. 40, no. 5, pp.

1016–1024, 1966.

[14] C. M. Harris, “Absorption of Sound in Air versus Humidity and Temperature,” *J. Acoust. Soc. Am.*, vol. 40, no. I, pp. 11–17, 1966.

[15] S. Temkin and R. A. Dobbins, “Attenuation and Dispersion of Sound by particulate-Relaxation Processes,” *J. Acoust. Soc. Am.*, vol. 40, no. May, pp. 317–324, 1966.

[16] J. E. Cole III and R. A. Dobbins, “Propagation of Sound Through Atmospheric fog,” *J. Comput. Acoust.*, vol. 27, pp. 426–434, 1970.

[17] E. P. Mednikov, “Absorption and dispersion of sound in aerosols at large particle velocity amplitudes,” *Sov. Physics--Acoustics*, vol. 15, pp. 507–509, 1970.

[18] F. E. Marble and D. C. Wooten, “Sound Attenuation in a Condensing Vapor,” *Phys. Fluids*, vol. 2657, no. 1970, 1970.

[19] J. E. Cole III and R. A. Dobbins., “Measurements of the Attenuation of Sound by a Warm Air Fog,” *Journal of the Atmospheric Sciences*, vol. 28, no. 2. pp. 202–209, 1971.

[20] J. R. Allegra and S. A. Hawley, “Attenuation of Sound in Suspensions and Emulsions: Theory and Experiments,” *J. Acoust. Soc. Am.*, vol. 51, no. 5B, p. 1545, 1972.

[21] R. C. Mecredy and L. J. Hamilton, “The Effects of Nonequilibrium Transfer Mass and Momentum on Two-Phase Sound Speed,” *Int. J. Heat Mass Transf.*, vol. 15, pp. 61–72, 1972.

[22] F. E. Marble and S. Candel, “Acoustic attenuation by vaporization of liquid droplets. Application to noise reduction in fans and ducts,” *7th Fluid Plasma Dyn. Conf.*, vol. 13, no. 5, pp. 634–639, 1974.

[23] G. A. Davidson and D. S. Scott, “Finite-Amplitude Waveforms in Aerosols,” *Aerosol Sci.*, vol. 5, pp. 55–69, 1974.

[24] M. Jaeschke, W. J. Hiller, and G. E. A. Meier, “Acoustic Damping in a gas micture with suspended submiscroscopic droplets,” *J. Sound Vib.*, vol. 43, no. 3, pp. 467–481, 1975.

[25] G. A. Davidson, “Sound Propagation in Fogs,” *J. Atmos. Sci.*, vol. 32, pp. 2201–2205, 1975.

[26] F. A. Lyman, “Attenuation of High Intensity Sound in a Droplet Laden Gas,” *J. Sound Vib.*, vol. 51, no. 2, pp. 219–235, 1977.

[27] R. A. Alforque, Y. Sawada, and H. Nishihara, “Measurement of Acoustic Velocity and Attenuation in an Air-Water Two-Phase Medium,” *J. Nucl. Sci. Technol.*, vol. 14, no. 2, pp. 156–158, 1977.

[28] F. Lyman and D.-M. Chen, “Acoustic attenuation in a non-uniform gas containing droplets,” *4th Aeroacoustics Conf.*, vol. 16, no. 5, pp. 503–509, 1977.

[29] L. Y. Cheng, D. a. Drew, and R. T. Lahey, “An Analysis of Wave Propagation in Bubbly Two-Component, Two-Phase Flow,” *J. Heat Transfer*, vol. 107, no. May 1985, p. 402, 1985.

[30] R.-J. Wei and J.-R. Wu, “Absorption of sound in water fog composed of submicron droplets,” *J. Acoust. Soc. Am*, vol. 81, no. 5, pp. 1350–1354, 1987.

[31] A. A. Vetter and F. E. C. Oulick, “Acoustical Resonance Measurement of Particle Loading in Gas-Solids Flow,” *J. Eng. Gas Turbines Power*, vol. 109, pp. 331–335, 1987.

[32] a H. Harker and J. a G. Temple, “Velocity and attenuation of ultrasound in suspensions of particles in fluids,” *J. Phys. D. Appl. Phys.*, vol. 21, no. 11, pp. 1576–1588, 1988.

[33] J. S. Tebbutt and R. E. Challis, “Ultrasonic wave propagation in colloidal suspensions and emulsions: a comparison of four models,” *Ultrasonics*, vol. 34, no. 2–5, pp. 363–368, 1996.

[34] R. L. Gibson, “Viscous attenuation of acoustic waves in suspensions,” *J. Acoust. Soc. Am.*, vol. 85, no. 5, p. 1925, 1989.

[35] T. A. Strout, “Attenuation of Sound in High-Concentration Suspensions: Development and Application of an Oscillatory Cell Model,” UNIVERSITY OF MAINE, 1991.

[36] J. M. Evans, “Models for sound propagation in suspensions and emulsions,” The Open University, 1996.

[37] C. J. Hickey, R. Raspet, and W. V Slaton, “Effects of thermal diffusion on sound attenuation in evaporating and Condensing Gas-Vapor Mixtures in Tubes,” *J. Acoust. Soc. Am.*, vol. 107, no. March 1999, pp. 1126–1130, 2000.

[38] J. M. Evans and K. Attenborough, “Sound propagation in concentrated emulsions: comparison of coupled phase model and core-shell model.,” *J. Acoust. Soc. Am.*, vol. 112, no. 5 Pt 1, pp. 1911–1917, 2002.

[39] B. S. D. Richards, T. G. Leighton, and N. R. Brown, “Visco-inertial absorption in dilute suspensions of irregular particles,” in *Orıc. R. Soc. Lond. A*, 2003, pp. 2153–2167.

[40] T. D. Norum, “Reductions in Multi-component Jet Noise by Water Injection,” *10th AIAA/CEAS Aeroacoustics Conf.*, vol. 9, no. Cd, pp. 1–25, 2004.

[41] M. Kandula, “Dispersion of sound in dilute suspensions with nonlinear particle relaxation.,” *J. Acoust. Soc. Am.*, vol. 127, no. 3, pp. 284–290, 2008.

[42] M. Kandula, “Sound propagation in saturated gas-vapor-droplet suspensions considering the effect of transpiration on droplet evaporation,” *Appl. Acoust.*, vol. 73, no. 8, pp. 849–854, 2012.

[43] T. G. Leighton, J. Jiang, and K. Baik, “Demonstration comparing sound wave attenuation inside pipes containing bubbly water and water droplet fog,” *J. Acoust. Soc. Am.*, vol. 131, no. 3, pp. 2413–21, 2012.

[44] D. C. Allgood, G. P. Saunders, and L. A. Langford, “Reduction of Altitude Diffuser Jet Noise Using Water Injection,” *50th AIAA Aerosp. Sci. Meet. Incl. New Horizons Forum Aerosp. Expo.*, no. 680, 2012.

[45] D. Gubaidullin, A. Nikiforov, and E. Utkina, “Acoustic waves in two-fraction mixtures of gas with vapor, droplets and solid particles of different materials and sizes in the presence of phase transitions,” *Fluid Dyn.*, vol. 46, no. 1, pp. 72–79, 2011.

[46] N. Kudryashov and N. Teterev, “Numerical simulation of acoustic wave propagation via a liquid with gas bubbles,” *Proc. - Eur. Conf. Noise Control*, pp. 6001–6005, 2008.

[47] T. A. Group, “Wet Exhaust Systems.” [Online]. Available: http://www.axceswetsystems.com/wet-exhaust-systems/. [Accessed: 03-Feb-2017].

[48] Lord Rayleigh, *The Theory of Sound*, First Amer. New York Dover Publications, 1877.

[49] S. H. O. Moss, “Acoustic measurements of flowing and quasi-static particulate suspensions,” The Open University, 1997.

[50] W. V Slaton, R. Raspet, and C. J. Hickey, “The effect of the physical properties of the tube wall on the attenuation of sound in evaporating and condensing gas–vapor mixtures,” *J. Acoust. Soc. Am.*, vol. 108, no. 5, pp. 2120–2124, 2000.

[51] D. A. Gubaidullin, “Spherical and Cylindrical Low-Amplitude Waves in Polydisperse Fogs with Phase Transitions,” *Fluid Dyn.*, vol. 38, no. 5, pp. 734–741, 2003.

[52] M. Baudoin, J.-L. Thomas, F. Coulouvrat, and D. Lhuillier, “An extended coupled phase theory for the sound propagation in polydisperse concentrated suspensions of rigid particles.,” *J. Acoust. Soc. Am.*, vol. 121, no. 6, pp. 3386–97, 2007.

[53] T. L. Hoffmann, “Environmental implications of acoustic aerosol agglomeration,” *Ultrasonics*, vol. 38, no. 1, pp. 353–357, 2000.

[54] K. P. Hapgood, G. V. Franks, J. S. Curtis, and M. Rhodes, *Introduction to Particle Technology*, 2nd ed. John Wiley & Sons, 2008.

[55] J. J. Rodríguez-Maroto, F. J. Gomez-Moreno, M. Martín-Espigares, A. Bahillo, M. Acha, J. A. Gallego, E. Riera, T. L. Hoffmann, and G. Rodríguez, “Acoustic agglomeration for electrostatic retention of fly-ashes at pilot scale: influence of intensity of sound field at different conditions,” *J. Aerosol Sci.*, vol. 27, no. 96, pp. S621–S622, 1996.

[56] A. Van Wijhe, “Acoustic coagulation of aerosols,” DELFT University of

Technology, 2013.

[57] S. Temkin, “Gasdynamic agglomeration of aerosols. I. Acoustic waves,” *Phys. Fluids*, vol. 6, no. 7, p. 2294, 1994.

[58] I. González, T. L. Hoffmann, and J. A. Gallego, “Precise measurements of particle entrainment in a standing-wave acoustic field between 20 and 3500 Hz,” *J. Aerosol Sci.*, vol. 31, no. 12, pp. 1461–1468, 2000.

[59] E. Riera-Franco de Sarabia, L. Elvira-Segura, I. González-Gómez, J. J. Rodríguez-Maroto, R. Muñoz-Bueno, and J. L. Dorronsoro-Areal, “Investigation of the influence of humidity on the ultrasonic agglomeration of submicron particles in diesel exhausts,” *Ultrasonics*, vol. 41, no. 4, pp. 277–281, 2003.

[60] G. Zhang, J. Liu, J. Zhou, and K. Cen, “Acoustic agglomeration of coal-fired fly ash particles in low frequency sound fields,” *Huagong Xuebao/CIESC J.*, vol. 60, no. 4, pp. 1001–1006, 2009.

[61] D. Zhou, Z. Luo, M. Fang, H. Xu, J. Jiang, Y. Ning, and Z. Shi, “Preliminary experimental study of acoustic agglomeration of coal-fired fine particles,” *Procedia Eng.*, vol. 102, pp. 1261–1270, 2015.

[62] J. Liu, J. Wang, G. Zhang, J. Zhou, and K. Cen, “Frequency comparative study of coal-fired fly ash acoustic agglomeration,” *J. Environ. Sci.*, vol. 23, no. 11, pp. 1845–1851, 2011.

[63] J. Wang, J. Liu, G. Zhang, J. Zhou, and K. Cen, “Orthogonal design process optimization and single factor analysis for bimodal acoustic agglomeration,” *Powder Technol.*, vol. 210, no. 3, pp. 315–322, 2011.

[64] A. R. Noorpoor, A. Sadighzadeh, and H. Habibnejad, “Influence of acoustic waves on deposition and coagulation of fine particles,” *Int. J. Environ. Res.*, vol. 7, no. 1, pp. 131–138, 2013.

[65] S. H. Park and K. W. Lee, “Poster Session II. Aerosol dynamics and transport,” *J. Aerosol Sci.*, vol. 31, pp. S845–S846, 2000.

[66] J. Yan, L. Chen, and L. Yang, “Combined effect of acoustic agglomeration and vapor condensation on fine particles removal,” *Chem. Eng. J.*, vol. 290, pp. 319–327, 2016.

[67] C. Sheng and X. Shen, “Modelling of acoustic agglomeration processes using the direct simulation Monte Carlo method,” *J. Aerosol Sci.*, vol. 37, no. 1, pp. 16–36, 2006.

[68] C. Knoop and U. Fritsching, “Gas/particle interaction in ultrasound agitated gas flow,” *Procedia Eng.*, vol. 42, no. August, pp. 770–781, 2012.

[69] C. Knoop and U. Fritsching, “Dynamic forces on agglomerated particles caused by high-intensity ultrasound,” *Ultrasonics*, vol. 54, no. 3, pp. 763–769, 2014.

[70] W. T. Yuen, S. C. Fu, J. K. C. Kwan, and C. Y. H. Chao, “Aerosol Science and Technology The Use of Nonlinear Acoustics as an Energy- Efficient

Technique for Aerosol Removal The Use of Nonlinear Acoustics as an Energy-Efficient Technique for Aerosol Removal," *Aerosol Sci. Technol.*, vol. 48, no. 9, pp. 907–915, 2014.

[71] W. T. Yuen, S. C. Fu, and Y. H. Chao, "The correlation between acoustic streaming patterns and aerosol removal efficiencies in an acoustic aerosol removal system," *Aerosol Sci. Technol.*, vol. 50, no. 1, pp. 52–62, 2016.

[72] D. Markauskas, A. Maknickas, and R. Kačianauskas, "Simulation of acoustic particle agglomeration in poly-dispersed aerosols," *Procedia Eng.*, vol. 102, pp. 1218–1225, 2015.

[73] D. Markauskas, R. Kačianauskas, and A. Maknickas, "Numerical particle-based analysis of the effects responsible for acoustic particle agglomeration," *Adv. Powder Technol.*, vol. 26, pp. 698–704, 2015.

[74] Z. Qiao, Y. Huang, N. Vincenzo, and W. Dong, "Aerosol manipulation by acoustic tunable phase-control at resonant frequency," *Powder Technol.*, vol. 281, pp. 76–82, 2015.

[75] K. Ohtani, Y. Koike, S. Ueha, and H. Yokoi, "Novel wedge-shaped doubly inclined chamber for the flow-through separation of suspended particles," *Ultrasonics*, vol. 38, no. 1, pp. 647–649, 2000.

[76] E. Zoppelllari and D. Juvé, "Reduction of hot supersonic jet noise by water injection," *Aiaa-98-2204*, 1998.

[77] Y. Marchesse, Y. Gervais, and H. Foulon, "Water injection effects on hot supersonic jet noise," *Comptes Rendus Mec.*, vol. 330, no. 1, pp. 1–8, 2002.

[78] A. Krothapalli, L. Venkatakrishnan, L. Lourenco, B. Greska, and R. Elavarasan, "Turbulence and noise suppression of a high-speed jet by water injection," *J. Fluid Mech.*, vol. 491, pp. 131–159, 2003.

[79] J. K. Ignatius, S. Sankaran, R. A. Kumar, and T. N. V Satyanarayana, "water injection during launch vehicle lift-off," *Int. J. aeroacoustics*, vol. 7, no. 3, pp. 223–241, 2008.

[80] S. Sankaran, J. K. Ignatius, R. Ramkumar, T. N. V. Satyanarayana, S. R. Chakravarthy, and N. R. Panchapakesan, "Suppression of High Mach Number Rocket Jet Noise by Water Injection," *J. Spacecr. Rockets*, vol. 46, no. 6, pp. 1164–1170, 2009.

[81] M. Kandula, "Broadband shock noise reduction in turbulent jets by water injection," *Appl. Acoust.*, vol. 70, no. 7, pp. 1009–1014, 2009.

[82] M. Kandula, "Prediction of Turbulent Jet Mixing Noise Reduction by Water Injection," *AIAA J.*, vol. 46, no. 11, pp. 2714–2722, 2008.

[83] H. P. Rice, M. Fairweather, J. Peakall, T. N. Hunter, B. Mahmoud, and S. R. Biggs, "Measurement of particle concentration in horizontal, multiphase pipe flow using acoustic methods: Limiting concentration and the effect of attenuation," *Chem. Eng. Sci.*, vol. 126, pp. 745–758, 2015.

[84] H. K. Kytömaa, "Theory of sound propagation in suspensions: a guide to

particle size and concentration characterization," *Powder Technol.*, vol. 82, no. 1, pp. 115–121, 1995.

[85] A. A. Vetter, "Sensitivity of the Acoustical Resonance Measurement of Particle Loading in Gas-Solids Flow," vol. 110, no. April 1988, pp. 197–200, 2016.

[86] S. D. Richards, T. G. Leighton, and N. R. Brown, "Sound absorption by suspensions of nonspherical particles: measurements compared with predictions using various particle sizing techniques.," *J. Acoust. Soc. Am.*, vol. 114, no. 4 Pt 1, pp. 1841–1850, 2003.

[87] L.-S. Zhai, N.-D. Jin, Z.-K. Gao, Z.-Y. Wang, and D.-M. Li, "The ultrasonic measurement of high water volume fraction in dispersed oil-in-water flows," *Chem. Eng. Sci.*, vol. 94, no. 0, pp. 271–283, 2013.

[88] M. Guo, Y. Yan, Y. Hu, D. Sun, X. Qian, and X. Han, "On-line measurement of the size distribution of particles in a gas-solid two-phase flow through acoustic sensing and advanced signal analysis," *Flow Meas. Instrum.*, vol. 40, pp. 169–177, 2014.

[89] V. Stolojanu and A. Prakash, "Characterization of slurry systems by ultrasonic techniques," *Chem. Eng. J.*, vol. 84, no. 3, pp. 215–222, 2001.

[90] P. Sayan and J. Ulrich, "The effect of particle size and suspension density on the measurement of ultrasonic velocity in aqueous solutions," *Chem. Eng. Process. Process Intensif.*, vol. 41, no. 3, pp. 281–287, 2002.

[91] J. A. Bamberger and M. S. Greenwood, "Using ultrasonic attenuation to monitor slurry mixing in real time," *Ultrasonics*, vol. 42, no. 1–9, pp. 145–148, 2004.

[92] A. Shukla, A. Prakash, and S. Rohani, "Particles settling studies using ultrasonic techniques," *Powder Technol.*, vol. 177, no. 2, pp. 102–111, 2007.

[93] X. Chen, W. Zhou, X. Cai, M. Su, and H. Liu, "In-line imaging measurements of particle size, velocity and concentration in a particulate two-phase flow," *Particuology*, vol. 13, no. 1, pp. 106–113, 2014.

[94] W. O. Carpenter, B. T. Goodwiller, J. P. Chambers, D. G. Wren, and R. A. Kuhnle, "Acoustic measurement of suspensions of clay and silt particles using single frequency attenuation and backscatter," *Appl. Acoust.*, vol. 85, pp. 123–129, 2014.

[95] H. P. Rice, M. Fairweather, J. Peakall, T. N. Hunter, B. Mahmoud, and S. R. Biggs, "Particle concentration measurement and flow regime identification in multiphase pipe flow using a generalised dual-frequency inversion method," *Procedia Eng.*, vol. 102, pp. 986–995, 2015.

[96] G. W. Wilson and A. E. Hay, "Acoustic backscatter inversion for suspended sediment concentration and size: A new approach using statistical inverse theory," *Cont. Shelf Res.*, vol. 106, pp. 130–139, 2015.

[97] G. T. Yim and T. G. Leighton, “Real-time on-line ultrasonic monitoring for bubbles in ceramic ‘slip’ in pottery pipelines,” *Ultrasonics*, vol. 50, no. 1, pp. 60–67, 2010.

[98] T. A. Hazlehurst, “Acoustic solutions to the particle mixing problem in aqueous dispersions,” University of Leeds, 2015.

[99] S. Temkin, *Suspension Acoustics - An Introduction to the Physics of Suspensions*. 2005.

[100] W. Hinds, *Aerosol Technology - Properties, Behavior, and Measurement of Airborne Particles*, Second Edi., vol. 2. 1999.

[101] S. Temkin, *Elements of Acoustics*. John Wiley & Sons, 1981.

[102] L. E. Kinsler, A. R. Frey, A. B. Coppens, and J. V Sanders, *Fundamentals of Acoustics*, 4th Editio., vol. 1. John Wiley & Sons, 1999.

[103] Q.-H. Liu and J. Tao, “The perfectly matched layer for acoustic waves,” *J. Acoust. Soc. Am.*, vol. 102, no. 4, pp. 2072–2082, 1997.

[104] F. Q. Hu, “A Perfectly Matched Layer absorbing boundary condition for linearized Euler equations with a non-uniform mean flow,” *J. Comput. Phys.*, vol. 208, no. 2, pp. 469–492, 2005.

[105] Y. Özyörük and B. Tester, “Assessment of a frequency-domain linearised Euler solver for turbofan aft radiation predictions and comparison with measurements,” *Procedia Eng.*, vol. 1, no. 6, pp. 153–162, 2010.

[106] Y. Özyörük, “Algorithmic improvements to a frequency-domain linearized Euler solver for turbomachinery noise radiation,” in *16th AIAA/CEAS Aeroacoustics Conference*, 2010, p. 3718.

[107] Y. Özyörük, B. Tester, and Y. Ozyoruk, “Effects of mean flow and temperature on acoustic liner performance in dual stream flow ducts,” *15th AIAA/CEAS Aeroacoustics Conf.*, no. 3166, 2009.

[108] C. K. W. Tam and J. C. Webb, “Dispersion-relation-preserving finite difference schemes for computational acoustics,” *J. Comput. Phys.*, no. 107, pp. 262–281, 1993.

[109] C. Bogey and C. Bailly, “A family of low dispersive and low dissipative explicit schemes for flow and noise computations,” *J. Comput. Phys.*, vol. 194, no. 1, pp. 194–214, 2004.

[110] J. C. Kok, “A symmetry and dispersion-relation preserving high-order scheme for aeroacoustics and aerodynamics,” *Eccomas Cfd*, vol. 4, pp. 5–8, 2006.

[111] J. B. B. R. Vichnevetsky, *Fourier Analysis of Numerical Approximations of Hyperbolic Equations*. Philadelphia: S.I.A.M, 1982.

[112] Y. Özyörük, “Numerical prediction of aft radiation of turbofan tones through exhaust jets,” *J. Sound Vib.*, vol. 325, no. 1–2, pp. 122–144, 2009.

[113] MathWorks, “Symbolic Math Toolbox User’s Guide,” 2015.

[114] E. Arslan, Y. Özyörük, and M. Çalişkan, “Numerical Analysis of One-Dimensional Sound Propagation Through a Duct Containing Water Droplets,” *J. Comp. Acous.*, vol. 25, no. 1, 2017.

[115] M.L.Munjal, *Acoustics of Ducts and Mufflers With Application to Exhaust and Ventilation System Design*. John Wiley & Sons, 1987.

APPENDIX A

MATERIAL PROPERTIES

Table A.1 Material properties of air

Temperature - t - (^oC) (deg F)	Density - ρ - (kg/m^3) (slugs/cu.ft)	Specific Heat - c_p - (kJ/(kg K)) (Btu/lb F)	Thermal Conductivity - k - ($W/(m\ K)$)	Kinematic Viscosity - ν - $x\ 10^{-6}$ (m^2/s)	Expansion Coefficient - b - $x\ 10^{-3}$ ($1/K$)	Prandtl's Number - P_r -
-150	2.793	1.026	0.0116	3.08	8.21	0.76
-100	1.980	1.009	0.0160	5.95	5.82	0.74
-50	1.534	1.005	0.0204	9.55	4.51	0.725
0	1.293	1.005	0.0243	13.30	3.67	0.715
20	1.205	1.005	0.0257	15.11	3.43	0.713
40	1.127	1.005	0.0271	16.97	3.20	0.711
60	1.067	1.009	0.0285	18.90	3.00	0.709
80	1.000	1.009	0.0299	20.94	2.83	0.708
100	0.946	1.009	0.0314	23.06	2.68	0.703
120	0.898	1.013	0.0328	25.23	2.55	0.70
140	0.854	1.013	0.0343	27.55	2.43	0.695
160	0.815	1.017	0.0358	29.85	2.32	0.69
180	0.779	1.022	0.0372	32.29	2.21	0.69
200	0.746	1.026	0.0386	34.63	2.11	0.685
250	0.675	1.034	0.0421	41.17	1.91	0.68
300	0.616	1.047	0.0454	47.85	1.75	0.68
350	0.566	1.055	0.0485	55.05	1.61	0.68
400	0.524	1.068	0.0515	62.53	1.49	0.68

Temperature - t - (^oC)	Speed of Sound - c - (m/s)
-40	306.2
0	331.4
5	334.4
10	337.4
15	340.4
20	343.3
25	346.3
30	349.1
40	354.7
50	360.3
60	365.7
70	371.2
80	376.6
90	381.7
100	386.9
200	434.5
300	476.3
400	514.1
500	548.8
1000	694.8

Table A.2 Material properties of water

Temperature - t - (^oC) (deg F)	Absolute pressure - p - (kN/m^2) (psia)	Density - ρ - (kg/m^3) (slugs/cu.ft)	Specific volume - v - ($10^{-3}\ m^3/kg$)	Specific Heat - c_p - (kJ/(kg K)) (Btu/lb F)	Specific Entropy - e - (kJ/(kg K))
0 (Ice)		916.8			
0.01	0.6	999.8	1.00	4.217	0
4 (maximum density)	0.9	1000.0		4.205	
5	0.9	1000.0	1.00	4.202	0.075
10	1.2	999.8	1.00	4.192	0.150
15	1.7	999.2	1.00	4.1855[1)]	0.223
20	2.3	998.3	1.00	4.182	0.296
25	3.2	997.1	1.00	4.180	0.367
30	4.3	995.7	1.00	4.178	0.438
35	5.6	994.1	1.01	4.178	0.505
40	7.7	992.3	1.01	4.179	0.581
45	9.6	990.2	1.01	4.181	0.637
50	12.5	988	1.01	4.182	0.707
55	15.7	986	1.01	4.183	0.767
60	20.0	983	1.02	4.185	0.832
65	25.0	980	1.02	4.188	0.893
70	31.3	978	1.02	4.191	0.966
75	38.6	975	1.03	4.194	1.016
80	47.5	972	1.03	4.198	1.076
85	57.8	968	1.03	4.203	1.134
90	70.0	965	1.04	4.208	1.192
95	84.5	962	1.04	4.213	1.250
100	101.33	958	1.04	4.219	1.307

APPENDIX B

SOLUTION OF WAVE EQUATION IN CIRCULAR DUCTS

The wave equation in three dimensional form is:

$$\frac{1}{{c_o}^2}\frac{\partial^2 p'}{\partial t^2} = \nabla^2 p' \tag{B.1}$$

In cylindrical coordinates ∇^2 is in the form as given below;

$$\nabla^2 = \frac{1}{r}\frac{\partial}{\partial r}\left(r\frac{d}{dr}\right) + \frac{1}{r^2}\frac{\partial^2}{\partial \theta^2} + \frac{\partial^2}{\partial x^2} \tag{B.2}$$

where r represents the radial coordinate, θ represents the azimuthal coordinate and x represents the axial coordinate. By inserting Eq. (B.2) into Eq. (B.1), one can come up with the equation as follows;

$$\frac{\partial^2 p'}{\partial r^2} + \frac{1}{r}\frac{\partial p'}{\partial r} + \frac{1}{r^2}\frac{\partial^2 p'}{\partial \theta^2} + \frac{\partial^2 p'}{\partial x^2} - \frac{1}{{c_o}^2}\frac{\partial^2 p'}{\partial t^2} = 0 \tag{B.3}$$

If the solution is assumed to be harmonic, then the solution for acoustic pressure can be written by using the separation of variables method as;

$$p'_{(r,\theta,z,t)} = R_{(r)}\emptyset_{(\theta)}X_{(x)}e^{-i\omega t} \tag{B.4}$$

If the Eq. (B.4) is plugged into Eq. (B.3), one can get three different differential equations as given below:

$$\frac{\partial^2 X}{\partial x^2} + X\,{k_x}^2 = 0 \tag{B.5}$$

$$\frac{\partial^2 \emptyset}{\partial \theta^2} + \emptyset\,{k_\theta}^2 = 0 \qquad \text{(Azimuthal symmetry)} \tag{B.6}$$

$$\frac{\partial^2 R}{\partial r^2} + \frac{1}{r}\frac{\partial R}{\partial r} + R\left(k^2 - {k_x}^2 - \frac{{k_\theta}^2}{r^2}\right) = 0 \tag{B.7}$$

And by dispersion relation;

$$k^2 = {k_z}^2 + {k_r}^2 + \frac{{k_\theta}^2}{r^2} \tag{B.8}$$

If it is assumed to have an azimuthal symmetric solution, then $k_\theta = 0$. Then Eq. (B.8) becomes;

$$k^2 = {k_z}^2 + {k_r}^2 \tag{B.9}$$

The solution to the first equation (axial direction) in Eq. (B.5) will be simply as;

$$Z_{(z)} = Ae^{-ikz} + Be^{+ikz} \tag{B.10}$$

The third differential equation in Eq. (B.7) is also named as Bessel Equation and the solution form is as given below;

$$R_{(r)} = C.J_{m(k_r*r)} + D.N_{m(k_r*r)} \tag{B.11}$$

where $J_{m(k_r*r)}$ is the Bessel function and $N_{m(k_r*r)}$ is the Neumann function. The boundary conditions for this problem are; particle velocity is zero on the hard walls of the duct ($v' = 0$ at r = r_{duct}) and the pressure field is bounded everywhere in the domain. According to the second information, the constant D in Eq. (B.11) must be zero so that the Neumann function vanishes. By means of the first boundary condition, the equation can be written as;

$$\left|\frac{\partial\left(J_{m(k_{rmn}*r)}\right)}{dr}\right|_{r=r_{duct}} = 0 \tag{B.12}$$

This can only be satisfied with specific values of J_m and k_r with discrete values of n which corresponds to the root of Bessel functions. The general form of the combined solution is to be got as follows;

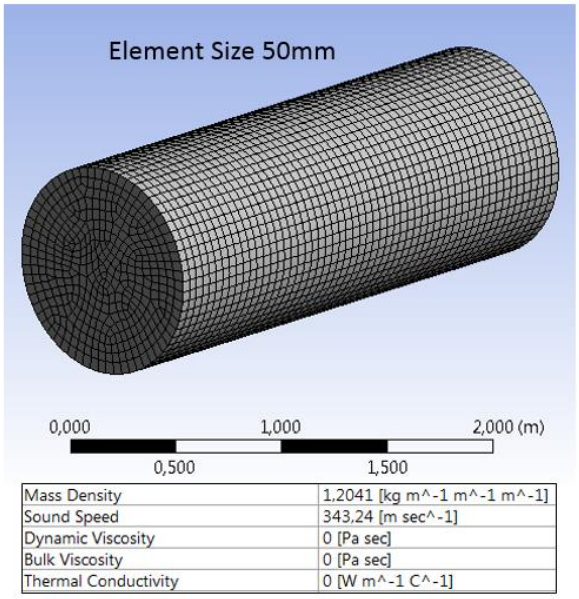
$$p'_{(r,\theta,x,t)} = \sum_{m=0}^{\infty}\sum_{n=1}^{\infty} J_{m(k_{r,m,n}r)} e^{im\theta} e^{i\omega t} \times \left(A_{m,n}e^{-ik_{x,m,n}x} + B_{m,n}e^{+ik_{x,m,n}x}\right) \tag{B.13}$$

and;

$$k_{x,m,n} = \sqrt{\left({k_0}^2 - {k_{r,m,n}}^2\right)} \qquad \text{(B.14)}$$

APPENDIX C

ACOUSTIC MODEL DEFINITIONS IN ANSYS MECHANICAL



Mass Density	1,2041 [kg m^-1 m^-1 m^-1]
Sound Speed	343,24 [m sec^-1]
Dynamic Viscosity	0 [Pa sec]
Bulk Viscosity	0 [Pa sec]
Thermal Conductivity	0 [W m^-1 C^-1]

Figure c.1 Finite element model and material properties

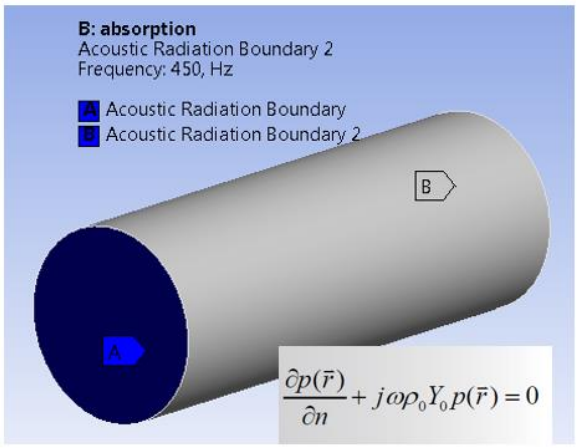
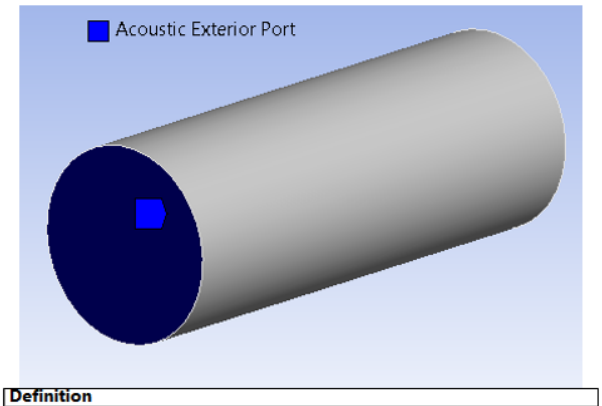


Figure c.2 Non-reflective boundary condition, radiation boundary



Definition	
Port Number	1
Wave Type	Circular Duct
Radius	0,5 [m]
Mode Index For Pressure Variation Along The Radii	1
Mode Index For Pressure Variation Along The Azimuth	0
Coordinate System Number	12
Pressure	1 [Pa]
Phase Angle	0 [°]

Figure c.3 Incident acoustic wave definition

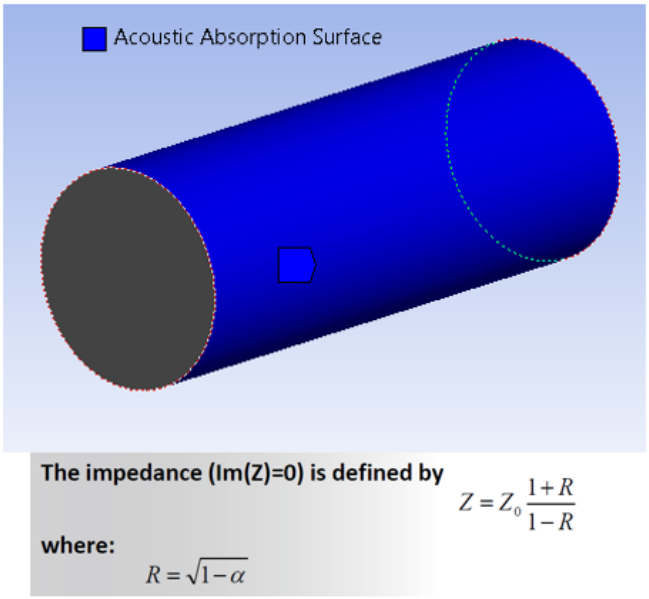


Figure c.4 Acoustic absorption surface definition

CURRICULUM VITAE

PERSONAL INFORMATION

Surname, Name: Arslan, Ersen
Nationality: Turkish (TC)
Date and Place of Birth: 14.06.1986 - Bursa
Marital Status: Married
Phone: 0 555 510 69 85
e-mail: arslanersen@gmail.com

EDUCATION

Degree	Institution	Year of Graduation
MS	METU Mechanical Engineering	2010
BS	Dokuz Eylül Uni. Mech. Engineering	2008
High School	Milli Piyango Anatolian High School, Bursa	2004

WORK EXPERIENCE

Year	Place	Enrollment
2013-Present	FİGES Engineering	Team Manager
2010-2013	FİGES Engineering	Application Engineer
2009-2010	TOFAS, NVH Department	Research Assistant

FOREIGN LANGUAGES

Advanced English, Basic German

PUBLICATIONS

E. Arslan, M. Calışkan, Y. Özyörük "*Investigation of Three Dimensional Axisymmetric Sound Propagation in a Duct with Aerosol"*, Journal of Sound and Vibration, Status: In Submission.

E. Arslan, M. Calışkan, Y. Özyörük "*Numerical study of mean flow effect on sound propagation through an aerosol"*, Proceedings of Meetings on Acoustics, Accepted: 11 April 2017.

E. Arslan, Y. Özyörük, M. Calışkan, "*Numerical study of mean flow effect on sound propagation through an aerosol"*, 5th Joint Meeting of the Acoustical Society of America and the Acoustical Society of Japan, Honolulu, Hawaii, 2016.

E. Arslan, Y. Özyörük, M. Calışkan, "*Numerical Analysis of One Dimensional Sound Propagation through a Duct Containing Water Droplets"*, Journal of Computational Acoustics, Vol No:25, Issue No:01.

E. Arslan, Y. Özyörük, M. Calışkan**.,** *"Implementation of finite difference method in frequency domain for solving 1-D sound propagation problem in air containing water droplets"*, 12th International Conference on Theoretical and Computational Acoustics, Hangzhou, China, 2015.

E. Arslan, Y. Özyörük, M. Calışkan. "*İçinde Su Damlacıkları Bulunan havadaki Ses Yayılım Probleminin Çözülmesinde Bir Boyutlu Sonlu Farklar Yönteminin Uygulanması*" 11. Ulusal Akustik Kongresi ve Sergisi, İstanbul, 19-29 Ekim, 2015

S. Kopuz, **E. Arslan** "*Büyük Hacimli Dizel Makine Egzoz Sistemi Tasarımı*" 7. Otomotiv Teknolojileri Kongresi, Bursa, 26-27 Mayıs, 2014.

E. Arslan, M. Çalışkan, A. Özkan, C. Bilir, T. Küçük**.,** "*Sınırlı Boyutlardaki Yarı-yankısız Bir Odada Araç Geçiş Gürültüsünün Standartlara Uygun Ölçüm Yöntemleri*" 5. Otomotiv Teknolojileri Kongresi, Bursa, 6-8 Haziran, 2010.

HOBBIES

Video Games, Classical Music